AD-A047 071 AEROSPACE SYSTEMS INC BURLINGTON MASS F/G 5/8
PILOT MODELING FOR MANNED SIMULATION. VOLUME I.(U)
DEC 76 R E CURRY, W C HOFFMAN, L R YOUNG F33615-75-C-3069
UNCLASSIFIED ASI-TR-76-29-VOL-1 AFFDL-TR-76-124-VOL-1 NL

1 OF 2
ADA047071

AD A047071

AFFDL-TR-76-124
Volume I

2 B.S.

PILOT MODELING FOR MANNED SIMULATION

AEROSPACE SYSTEMS, INC.
BURLINGTON, MASSACHUSETTS 01803

DDC
RECEIVED
NOV 21 1977
F

DECEMBER 1976

FINAL REPORT APRIL 1975 - JUNE 1976

Approved for public release; distribution unlimited

AD No.
DDC FILE COPY

AIR FORCE FLIGHT DYNAMICS LABORATORY
AIR FORCE WRIGHT AERONAUTICAL LABORATORIES
AIR FORCE SYSTEMS COMMAND
WRIGHT-PATTERSON AIR FORCE BASE, OHIO 45433

NOTICE

When Government drawings, specifications, or other data are used for any purpose other than in connection with a definitely related Government procurement operation, the United States Government thereby incurs no responsibility nor any obligation whatsoever; and the fact that the government may have formulated, furnished, or in any way supplied the said drawings, specifications, or other data, is not to be regarded by implication or otherwise as in any manner licensing the holder or any other person or corporation, or conveying any rights or permission to manufacture, use, or sell any patented invention that may in any way be related thereto.

This report has been reviewed by the Information Office (OI) and is releasable to the National Technical Information Services (NTIS). At NTIS, it will be available to the General Public, including foreign nations.

This technical report has been reviewed and is approved for publication.

R. O Anderson

RONALD O. ANDERSON, Chief
Systems Dynamics Branch

FOR THE COMMANDER

Larry M. Hadley

LARRY M. HADLEY, Lt Col, USAF
Chief, Flight Control Division

Copies of this report should not be returned unless return is required by security considerations, contractual obligations, or notice on a specific document.

AIR FORCE - 16 MARCH 77 - 350

Unclassified

SECURITY CLASSIFICATION OF THIS PAGE (When Data Entered)

(19) REPORT DOCUMENTATION PAGE

READ INSTRUCTIONS BEFORE COMPLETING FORM

(18) 1. REPORT NUMBER: AFFDL-TR-76-124-VOL-1

2. GOVT ACCESSION NO.

3. RECIPIENT'S CATALOG NUMBER

(6) 4. TITLE (and Subtitle): PILOT MODELING FOR MANNED SIMULATION. Volume I.

(9) 5. TYPE OF REPORT & PERIOD COVERED: Final Report. Apr 75 - Feb 76.

6. PERFORMING ORG. REPORT NUMBER: (14) ASI-TR-76-29-Vol-1

7. AUTHOR(s): Curry, R.E.; Hoffman, W.C.; Young, L.R.

8. CONTRACT OR GRANT NUMBER(s): (15) F33615-75-C-3069

9. PERFORMING ORGANIZATION NAME AND ADDRESS: Aerospace Systems, Inc., One Vine Brook Park, Burlington, MA 01803

10. PROGRAM ELEMENT, PROJECT, TASK AREA & WORK UNIT NUMBERS

11. CONTROLLING OFFICE NAME AND ADDRESS: Air Force Flight Dynamics Laboratory (FGD), Air Force Systems Command, Wright-Patterson AFB, Ohio 45433

(11) 12. REPORT DATE: December 1976

13. NUMBER OF PAGES: 186

14. MONITORING AGENCY NAME & ADDRESS (if different from Controlling Office)

(10) Renwick E. Curry, William C. Hoffman, Lawrence R. Young

15. SECURITY CLASS. (of this report): Unclassified

15a. DECLASSIFICATION/DOWNGRADING SCHEDULE

16. DISTRIBUTION STATEMENT (of this Report): Approved for public release; distribution unlimited.

(12) 184 p.

17. DISTRIBUTION STATEMENT (of the abstract entered in Block 20, if different from Report)

18. SUPPLEMENTARY NOTES

19. KEY WORDS (Continue on reverse side if necessary and identify by block number)

Pilot Model
Manned Simulation
Motion Effects
Visual Effects
Vestibular System
Optimal Control Theory
Manual Control

20. ABSTRACT (Continue on reverse side if necessary and identify by block number)

The optimal control model of the pilot has been extended to incorporate motion as well as visual cues so that it can be used to compare fixed-base, moving-base and VFR/IFR differences in simulator systems. The motion cues are included by adding the semi-circular canal and otolith dynamics to the state vector, with the vestibular firing rates available as additional inputs to the Kalman filter/predictor. The psycho-physical thresholds are modeled as dead-zone elements. Details of the visual and motion cue extensions to the model are described and comparisons of

DD FORM 1 JAN 73 1473 EDITION OF 1 NOV 65 IS OBSOLETE

Unclassified

SECURITY CLASSIFICATION OF THIS PAGE (When Data Entered)

389704

1B

20. Abstract (Continued)

predicted and experimental results are presented.

FOREWORD

This report was prepared by Aerospace Systems, Inc. (ASI), Burlington, Massachusetts, for the Air Force Systems Command under Contract No. F33615-75-C-3069. The report documents the results of research performed during the period April 1975 to February 1976. The study was sponsored by the Air Force Flight Dynamics Laboratory (AFFDL), Flight Control Division, Systems Dynamics Branch. Mr. John Stone and Mr. Daniel L. Kugel served as Technical Monitors on the contract.

The effort was directed by Mr. John Zvara, President and Technical Director of ASI. Mr. William C. Hoffman served as Project Engineer. Dr. Renwick E. Curry of the MIT Department of Aeronautics and Astronautics and the MIT Man-Vehicle Laboratory, and Dr. Laurence R. Young, Director of the MIT Man-Vehicle Laboratory, contributed to the study as principal consultants. Miss Kristine Doyle and other members of the ASI technical staff assisted in the development and validation of the computer model.

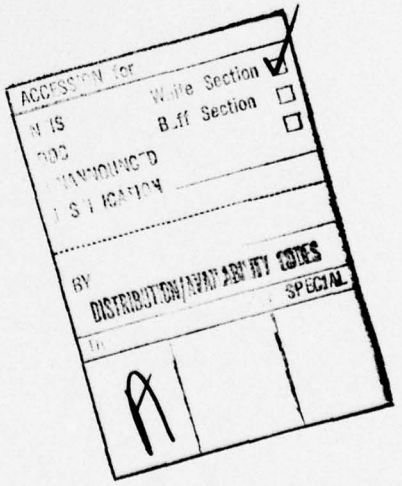

TABLE OF CONTENTS

Section			Page
I	INTRODUCTION		1
II	SUMMARY OF PREVIOUS RESEARCH		4
	2.1	General Capabilities	4
	2.2	Motion Effects on the Pilot Model	7
	2.3	Simulator Requirements for Motion Cues	15
	2.4	Direct Effects of Simulator Motion on Pilot Performance, Independent of Motion Cues Utilized in Feedback	17
III	COMPONENTS OF THE PILOT MODEL		17
	3.1	Introduction	19
	3.2	The Optimal Control Model of the Pilot	20
	3.3	Workload and Scanning Models	23
	3.4	Motion Cues: State Space Formulation of the Vestibular Sensors	26
		3.4.1 Semicircular Canals	26
		3.4.2 Otoliths	28
	3.5	VMC/IMC Cues	28
	3.6	Summary of the Pilot Model	29
		3.6.1 Controlled Element Dynamics: Matrices A,B,E	29
		3.6.2 Cost Functional Weightings	29
		3.6.3 Controller Time Delay	32
		3.6.4 Processor Driving Noise	33
		3.6.5 Additive Motor Noise	33
		3.6.6 Observation Thresholds	33

PRECEDING PAGE BLANK-NOT FILMED

TABLE OF CONTENTS (Continued)

Section			Page
	3.6.7	Observation Noise Ratios	34
	3.6.8	Attention Allocation	34
	3.6.9	Summary	35
IV	MODEL DEVELOPMENT		37
	4.1	Model Parameters for Motion Cues	37
	4.1.1	Description of the Experiment	37
	4.2	Application of the Motion Cue Model to VTOL Hovering	58
	4.2.1	Description of the Experiment	58
	4.2.2	Model Parameters	58
	4.2.3	Model Results	79
	4.3	Model Parameters for VMC Cues	89
	4.3.1	Experimental Description	90
	4.4	Application of the Model with Motion and VMC Cues	96
	4.4.1	Description of the Experiment	97
	4.4.2	Model Parameters	97
	4.4.3	Model Results	101
V	MODEL APPLICATION		108
	5.1	2 Degree-of-Freedom Roll Control Task	108
	5.1.1	Experiment Description	108
	5.1.2	Model Results	114
	5.2	Pilot Performance in Low Visibility Approach	121
	5.2.1	Experiment Description	121

TABLE OF CONTENTS (Continued)

Section			Page
	5.2.2	Model Description	124
	5.2.3	Model Results	129
	SUMMARY, CONCLUSIONS, AND RECOMMENDATIONS		134
	6.1	Summary and Conclusions	134
	6.2	Recommendations for Additional Research	139
APPENDIX			
A	LITERATURE SURVEY ON PILOT MODELING FOR MANNED SIMULATION		141
	A.1	Simulators or Simulation	142
	A.2	Pilot Performance	144
	A.3	Pilot Models	145
	A.4	Vestibular System	146
	A.5	Motion	147
	A.6	Displays	148
	A.7	Scanning	148
	A.8	Workload	148
B	OPTIMAL CONTROL MODEL OF THE PILOT		149
	B.1	Basic Formulation	149
	B.2	Multi-Axis Tasks	155
	B.3	Attention Allocation Using the Optimal Control Model	156
	References		162
	References		163

LIST OF FIGURES

Figure No.		Page
1	Optimal Control Model of Human Response	21
2	Required Attentional Workload vs System Performance	25
3	Comparison of Model Predictions with Change in Weighting Coefficients - Visual Only	31
4	Block Diagram of Shirley's Roll Tracking Experiment	38
5	RMS Tracking Error: Comparison of Model Predictions with Shirley's Experimental Data	51
6a	Comparison of Model Describing Functions with Shirley's Experimental Data. ($Y_c = 1/s(s+4)$)	52
6b	Comparison of Model Describing Functions with Shirley's Experimental Data. ($Y_c = 1/s(.02s + 1)$)	53
	Comparison of Model Describing Functions with Shirley's Experimental Data. ($Y_c = 1/s^2$)	54
6d	Comparison of Model Describing Functions with Shirley's Experimental Data. ($Y_c = 15/(s^2 + 3s + 15)$)	55
6e	Comparison of Model Describing Functions with Shirley's Experimental Data. ($Y_c = 10/(s^2 + 10)$)	56
7	Display Panel Arrangement (Reference 23)	63
8	Longitudinal Performance vs Workload	83
9	Lateral Performance vs Workload	84
10	Vertical Performance vs Workload	84
11	Preliminary Predictions of Total Task Performance (Circles) Compared to Range of Means of Three Subjects	85
12	Correlation of Observed Dwell Fractions with Fractions of Attention-Configuration Differences	88
13	Instrument Display for IMC Experiments	91
14	Contact-Analog Display for VMC Experiments	92

LIST OF FIGURES (Continued)

Figure No.		Page
15	Effect of Attitude Rate Threshold on Pilot Describing Function	95
16	Effect of Attitude Rate Cost Weighting on Pilot Describing Function	95
17	Block Diagram of Control Tasks	98
18	Describing Function Comparison with Motion Cues	104
19	Describing Function Comparison with VMC Cues	105
20	Simulation Schematic Diagram for 2-DOF Roll Control Task	110
21	Comparison of Fixed-Base and Moving Base Results for $K/s(s+1)$	115
22	Comparison of Fixed-Base and Moving-Base Results for $K/s(s+10)$	116
23	Comparison of Fixed-Base and Moving-Base Results for K/s^2	117
24	Comparison of RMS Errors for Fixed-Base and Moving Base	118
25	$K/s(s+10)$ Results with Dillow Filter	119
26	Effect of Lateral Position Washout Variations	120
27	Effect of Roll Washout Variations	122
28	Instrument Panel Layout for Low-Visibility Approach Simulator	123
29	Collins FD-109 Pitch Axis Flight Director	130
B-1	Optimal Control Model of Human Operator	149

LIST OF TABLES

Table		Page
1	Correspondence of Real World and Model Components	36
2	Calculation of Motion System Gain	39
3	Roll Control Tasks from Shirley	44
4a	System Matrices for Shirley's Plant $1/s(s+4)$	45
4b	System Matrices for Shirley's Plant $1/s(.02s+1)$	46
4c	System Matrices for Shirley's Plant $1/s^2$	47
4d	System Matrices for Shirley's Plant $15/(s^2+3s+15)$	48
4e	System Matrices for Shirley's Plant $10/(s^2+10)$	49
5	Control-Rate Weighting Coefficients for Shirley's Cases	50
6	Vehicle Aerodynamic Parameters	60
7	Control Sensitivities	61
8	Vehicle Configurations	62
9	State-Variable Assignment for VTOL Hovering Task	64
10a	RS&M System Matrices - Longitudinal, Good, FB	65
10b	RS&M System Matrices - Longitudinal, Good, MBA	66
10c	RS&M System Matrices - Longitudinal, Good, MBL	67
10d	RS&M System Matrices - Longitudinal, Bad, FB	68
10e	RS&M System Matrices - Longitudinal, Bad, MBA	69
10f	RS&M System Matrices - Longitudinal, Bad, MBL	70
11a	RS&M System Matrices - Lateral, Good, FB	71
11b	RS&M System Matrices - Lateral, Good, MBA	72
11c	RS&M System Matrices - Lateral, Good, MBL	73
11d	RS&M System Matrices - Lateral, Bad, FB	74

LIST OF TABLES (Continued)

Table		Page
11e	RS&M System Matrices - Lateral, Bad, MBA	75
11f	RS&M System Matrices - Lateral, Bad, MBL	76
12a	RS&M System Matrices - Vertical, Good, MB	77
12b	RS&M System Matrices - Vertical, Good, FB	77
13	Display Gains, Weighting Coefficients and Indifference Thresholds	78
14a	Longitudinal Performance vs Workload	80
14b	Lateral Performance vs Workload	81
14c	Vertical Performance vs Workload	82
15a	Fraction of Attention Allocation by Motion and Dynamics	87
15b	Predicted Attention Allocation by Motion and Configuration	87
16a	System Matrices for Newell-Smith K/s(s-1)	93
16b	Model Parameters for IMC Tracking	93
17	System Matrices for Newell-Smith Configuration C	102
18	System Matrices for Newell-Smith Configuration D	103
19	Display Weights and Thresholds	106
20	Pilot-Selected Gains	109
21	State Variable Assignment for 2 Degree-of-Freedom Roll Control Task	112
22	Displayed Variables	112
23	System Matrices for 2 Degree-of-Freedom Roll Control Task	113
24	C-135B Longitudinal Data	125
25	State Variable Assignments for C-135B Simulation	126
26	Equations of Motion for C-135B Model	127
27	Display Variable Equations for C-135B Simulation	131

LIST OF TABLES (Continued)

Table		Page
28	Display Variables - Weights and Thresholds	132
29	RMS Errors for Low-Visibility Approach	133

LIST OF SYMBOLS

a	inverse plant response time constant
A	matrix for system response
AFR(s)	Laplace transform equation for the afferent firing rate of a semicircular canal
B	matrix for system response
c	stick deflection
d	disturbance input
D	control distribution matrix for observations
e	error between input and output
E	matrix for system response
$E\{\}$	expected value of $\{\}$
f	specific force
f_{att}	control attention on attitude task
f_c	portion of total attention devoted to control task (control task workload)
f_{c_i}	fraction of attention allocated to i^{th} display variable (=1, full attention; =0, no attention)
f_o	fraction of attention lost in switching from one display to another
f_{other}	fraction of attention allocated to other side tasks demanding attention from the pilot
f_{pos}	control attention on position task
f_{tot}	total fraction of attention
f_x	control attention on position
f_θ	control attention on altitude
FB	fixed-base
g	acceleration of gravity

g	cost functional weighting (>0) (Appendix B)
$\bar{i}^2$	mean square value of the filter output
J	quadratic cost functional of system performance
K	scaling factor
K_c	plant gain
K_{dis}	scaling factor (error converted to distance)
$K_{\dot{h}}$	altitude rate gain - flight director parameter
$K_{I_{\dot{h}}}$	altitude rate synchronizer gain - flight director parameter
K_{mat}	scaling factor (error converted to roll angle)
K_{stick}	scaling factor (error converted to a voltage by a gain)
K_ϵ	glideslope deviation gain - flight director parameter
l	distance from roll axis to the otoliths
l_s	actual pilot displacement in simulator
l_z	simulated pilot displacement along z axis
L	control gain
L^*	optimal gains
L_m^*	gain on $\hat{u}_m$
L_p, L_v, L_{δ_a}	aerodynamic stability derivatives
MBA	moving-base, angular motion only
MBL	moving-base, linear and angular cues
M_q, M_u, M_{δ_e}	aerodynamic stability derivatives
N	describing function for the dead zone element
$p(t)$	Kalman filter output
p_y	inverse time constant of position washout
p_ϕ	roll washout parameter
q_i	cost functional weighting (≥ 0)
Q_r	weighting on control rate

Q_u	weighting on control displacement
Q_x	weighting on state variables
Q_y	weighting on display variables
rISE	relative Integral Squared Error
Res	residue of fourth order pole
s	Laplace variables
t	time
$T_h^{\cdot}$	altitude rate lag - flight director parameter
T_N	neuromuscular time constant
T_θ	pitch washout lag - flight director parameter
u	control vector
u(t)	control input vector
$u_c(t)$	"commanded" control input
$u_c(\cdot)$	feedback control
u_g	longitudinal gust disturbance
$u_m(t)$	motor noise
$\hat{u}_m(t)$	best estimate of $u_m(t)$
v_g	lateral gust disturbance
$V_u(t)$	white motor noise component
V_y	noise covariance matrix
$V_y(t)$	perceptual observation noise component
$V^0_{y_i}$	power spectral density of the observation noise of the i^{th} display variable when attention is limited to that display variable alone
w(t)	random external disturbances (e.g., turbulence, wind gusts)
W	noise power
x	state vector
x(t)	vehicle state vector

$\hat{x}(t)$	current state estimate of system state x(t) based on observed data
$x_1(t)$	input i(t)
X_u	aerodynamic stability derivative
$y(t)$	displayed information vector
y_i	commanded lateral position
$y_p(t)$	perceived displayed quantities
$y_p(\sigma)$	observed data
$y_p(\cdot)$	perceived information
y_s	actual lateral position of simulator cab
$Y_c(s)$	roll control of arbitrary second-order system
Y_v	aerodynamic stability derivative
Y_y	position washout and equalization transfer function
Y_ϕ	transfer function of roll angle washout circuit
z	vertical displacement
Z_w, Z'_w	aerodynamic stability derivatives
α_i	half width of dead zone element
δ_a	roll control input
δ_c	collective control input
δ_e	pitch control input
θ	pitch angle
ρ_i	multiplicative noise/signal ratio
$\sigma_{(\,)}$	standard deviation of error in ( )
$\sigma^2_{(\,)}$	noise variance of ( )
σ_e	standard deviation of tracking error
σ_i	standard deviation of i^{th} displayed quantity
Σ	error covariance matrix

τ	perceptual time delay
τ_N	time constant
$\nu_m(t)$	Gaussian white noise level with autocovariance
ϕ	roll angle
ϕ_i	commanded roll angle
ϕ_m	model output roll angle
ϕ_s	actual roll angle of simulator cab
$\Phi_{ii}(s)$	spectrum of (approximate) input signal
ω_o	break frequency of the filter
$\dot{\omega}(s)$	angular acceleration
$( )'$	transpose of $( )$
$(\dot{})$	$d( )/dt$
$( )_{max}$	maximum permissible value of $( )$
$( )_{oto}$	refers to otolith
$( )_{scc}$	refers to semicircular canal

SECTION I

INTRODUCTION

Manned aircraft engineering simulations are finding increased usage for research and development to reduce expensive in-flight testing. Industry and Government organizations are developing multiple degree-of-freedom moving base simulation facilities which represent a significant capital investment. For efficient utilization of this equipment, methods must be developed to plan and analyze simulation programs properly. Realistic pilot models will be one of the foundations of these methods.

Control theory pilot models which accurately predict pilot performance would lead to more efficient planning, execution, and analysis of manned simulations of aerospace vehicles. However, despite the considerable development of control theoretical models for the pilot, they have still fallen short of adequate description of pilot behavior for realistic multi-input, multi-loop tasks. In particular, for these models to be used as effective tools in simulator scheduling and pre-experimental analysis, they require elaboration to account for the effects of motion cues, instrument and external visual cues, and display scanning.

The Air Force Flight Dynamics Laboratory (AFFDL) has initiated a three-phase program to extend existing pilot modeling technology to more realistic pilot models for application to engineering simulation. In support of this program, Aerospace Systems, Inc. (ASI) has completed a research program on Phase 1. Specifically, this effort has attempted to:

- Assess past pilot models.
- Postulate an extended multivariable pilot model for a multi-axis, multi-input, multi-output task with motion, visual and scanning effects.

- Demonstrate the technical accuracy of the pilot model with respect to experimental data for a particular aircraft and pilot control task.
- Document the data used, the analysis methods, and the use of the pilot model postulated.

Phases II and III, which are not part of the present investigation, will include the following:

Phase II: Pilot Model Verification: The Phase I pilot model will be verified against a wide range of experimental data for various tasks. This effort will be developed through a coordinated AFFDL and contractual program.

Phase III: Simulation Analysis: The verified pilot model will be incorporated into a unified methodology for simulation planning and analysis.

The objective of the present effort was to develop a multi-variable pilot model which can predict pilot behavior in realistic multi-loop, multi-input, multi-output aircraft tasks and which also describes the effects of motion cues, visual cues, and instrument scanning. The general pilot model developed during this work should improve simulation analysis and planning, increase simulation efficiency, and lower simulator operating costs. Furthermore, aircraft display and control system design, which depend heavily on pilot models, will benefit from the results of this effort.

Our approach to the development and validation of the pilot model is to use data published in the open literature. One of the difficulties inherent in this method is the inability to obtain experimental details which might resolve any discrepancies between model predictions and experimental data. (There have been instances where such differences have lead to a discovery of anomalies in the experimental set up rather than in the model.) On the other hand, a model developed and validated on data from several sources may prove to be particularly robust although detailed predictions for any one set of data may not be as precise as when the data and the model come from the same source.

Section 2 of this report presents a survey and assessment of past pilot models for supporting manned simulation studies. The components of the extended pilot model are described in Section 3, and the development of this model is discussed in Section 4. Section 5 presents the results of applying the model to two previous experimental simulation studies. Conclusions and recommendations for additional research are contained in Section 6. Details of a comprehensive literature survey are provided in Appendix A. The analytical formulation of the optimal control pilot model is summarized in Appendix B. A user's guide to the computer program, Program PIREP, which implements the theoretical pilot model, is provided as a separately-bound document for the user's convenience.

SECTION II

SUMMARY OF PREVIOUS RESEARCH

This section presents an overview of the previous literature concerning pilot models for manned simulation. We assume that the reader is generally familiar with the manual control literature and with the functions of the vestibular system for spatial orientation. (Those desiring background reading in manual control are referred to References 1 and 2. A summary of vestibular functions is available in Reference 3.) Appendix A contains a compilation of all pertinent citations obtained during a comprehensive literature survey that was conducted early in this study.

2.1 GENERAL CAPABILITIES

Studies of human operator behavior that have been performed to date have yielded a sizable data base from which we may infer general, quantitative relationships between pilot model parameters and parameters of the control environment. We can, therefore, use existing pilot-vehicle models to predict system performance and pilot behavior for a wide variety of control systems and display configurations. Quasi-linear models of pilot-vehicle systems have been developed to a high degree. In these models, the pilot is represented by a linear response element (the pilot-describing function) plus a "remnant" term (to account for the portion of his output that cannot be accounted for by the describing function). Model parameters are most readily interpreted when the vehicle dynamics are linear and when the statistics of the control environment are stationary. The describing function may then be interpreted as the deterministic linearized portion of the pilot's strategy, with the remnant representing the random non-linear and time-varying aspects of the pilot's control. If instrument scanning is required, the pilot's monitoring strategy (and possibly his control strategy) will be time-varying. Quasi-linear pilot-vehicle models may be usefully applied to situations of this type as

well, but measurements of pilot remnant will reflect the time-varying nature of the pilot's strategy as well as truly "random" behavior.

Quasi-linear models fall into two basic categories: the frequency-domain representation (Reference 1) and the state-variable (or "optimal-control") model (Reference 2). Both representations allow one to predict pilot describing functions and measures of overall system performance such as mean-squared system error. There are, however, considerable differences in the computational techniques employed by these two types of models.

Both kinds of pilot models contain elements that may be identified with specific physiological or psychophysical functions. The frequency-domain models, for example, often include specific representations of the neuromuscular system. On the other hand, the state-variable model represents the pilot's estimation and control strategies as distinct elements. Frequency-domain and state-variable pilot-vehicle models have both been used to explore the aspects of pilot behavior and system performance described below.

- Total System Performance. For situations in which the vehicle dynamics can be quasi-linearized and the mission requirements represented in a suitable mathematical form, analytical models may be used to predict overall system performance. Thus, these models can be used to determine the extent to which mission requirements can be met with a given display configuration. By noting the effects on system performance of changes in one or more display parameters, one can (1) determine the information requirements of the system, (2) determine improvements associated with display quickening and predictions, and (3) compare the relative merits of command information versus error information. Considerable modeling success has been obtained in this regard, and the model can now be applied with reasonable confidence to the problem of predicting overall system performance and how performance changes with modifications to the display.

- Pilot Response Behavior. The input-output behavior of the pilot (i.e., the combined perceptual, central-processing, and control behavior) is predictable. The response strategy is usually presented in the form of a describing function or set of describing

functions. Comparison of predicted behavior with response strategies measured in "conventional" flight-control situations will indicate whether or not an unusual response strategy is demanded by the system under investigation. Considerable success has been obtained in predicting pilot-describing functions in a variety of control situations.

- The Pilot's Estimation Strategy. The pilot's estimation strategy can be predicted for situations in which the pilot acts as a monitor only. A model of this sort is quite valuable in predicting system transients that occur when the mode of control switches from automatic to manual.

- Pilot Workload. Models have been developed which appear capable of predicting scanning workload, i.e., the fraction of attention that the pilot will devote to the various displays (References 4, 5). Models have been applied to systems containing physically separated displays as well as those in which a single multi-element display has been used. In addition, a model has been developed to predict central-processing workload, i.e., the amount of attention that must be devoted to the task as a whole in order for mission requirements to be achieved (References 5, 6).

- Instrument-Related "Noise." The state-variable model contains a set of parameters associated with perceptual noise. To some extent, these parameters may be adjusted to account for the effects of random disturbances inherent in the display hardware (such as sensor and meter noise). They may also be used to represent resolution limitations of the human's visual system and random response behavior arising from human signal/noise limitations (References 7 and 8).

- Handling Qualities. Pilot-vehicle analysis has been applied extensively to the study of vehicle handling characteristics (References 9 and 10). Several approaches have been explored. Although none has achieved universal application, some general observations can be made. The pilot's rating of a vehicle's handling qualities is influenced by the nature of the open-loop response characteristics of the vehicle, by the closed-loop system performance that can be achieved in various task situations, and by the nature of the response strategy required of the pilot. It has been found, for example, that pilot ratings worsen as tracking error increases and as the lead that must be generated by the pilot increases. Some success has been achieved in modeling the relationship between pilot rating, pilot lead, and system performance. Since pilot-vehicle models are capable of representing both the informational characteristics of the display and the perceptual limitations of the human, these models should prove useful in exploring the relationship between display parameters and vehicle handling qualities.

- Effects of System Failure. By investigating the effects of sudden changes in the display and system parameters on pilot behavior and system performance, one can predict the ability of the pilot to recover from a failure condition. Accordingly, the suitability of the display configuration in a situation of this sort can be evaluated (Reference 11).

- Sensitivity to Pilot Strategy. The sensitivity of closed-loop system performance to changes in the pilot's response strategy can be predicted. For example, one can explore the effects of a constant bias in one or more of the pilot's response parameters, or one can examine the effects of an increase in the magnitude of random fluctuations in these parameters. Although this aspect of the model's predictive capability cannot readily be verified experimentally (since the pilot will usually attempt to select the appropriate response strategy with a minimum of random response activity), predictions of this sort should prove useful in the evaluation of system controllability and pilot acceptance.

2.2 MOTION EFFECTS ON THE PILOT MODEL

The effects of vehicle motion upon the pilot's control in flight or in moving base simulation has been a subject of serious investigation for at least 30 years (Reference 12). An accurate methematical description of the influence of motion on pilot control is a requisite for use of the analytical pilot model in pre-flight and pre-simulation systems studies, and is also necessary in the planning and interpretation of aircraft piloted simulation programs, fixed-base or moving-base. The increase in recent years in the capabilities and numbers of moving base simulators for research purposes has intensified the effort to quantify the contribution of motion to the pilot control model. Similarities and differences between flight and fixed-base simulator results have been treated along the following major lines:

- The additional lead generation produced by the pilot as a result of attitude motion sensing through his vestibular system, in flight and moving-base simulators.

- The decrement in piloting performance, in flight or with motion simulation, resulting from the direct effects of sustained acceleration and vibration upon the pilot's ability to read instruments and perform fine motor control.

- The effects of vehicle motion on a pilot's perceived orientation in space, the resulting motion illusions associated with this perception, and the consequent incidence of inappropriate control and aircraft accidents associated with disorientation.

In some cases the thrust of the research on motion cues has been to use physiological models of motion sensors to express changes in the pilot control law and the resulting system performance. This has been the approach taken in References 13 - 15, all of which use describing function models for the human operator and emphasize the empirical description of motion effects on control.

In parallel with this effort, there has been a major development in mathematical models for the processing of motion cues by the vestibular system, to produce models for human perception of attitude and position on the basis of vestibular cues alone, and even more recently on the basis of combined visual and vestibular cues. The latest versions of the vestibular models have been formulated in state space notation, and are based upon the use of Kalman filter techniques for treatment of vestibular measures of pilot orientation (Reference 16). They are appropriate for incorporation in the optimum control model of the human operator.

In 1967, Young reviewed the results of 21 previous investigations (Reference 13) on comparison of pilot performance and pilot opinion in tasks which compared motion cues (simulator flight) with ground-based fixed tests. The conclusions were as follows:

- When vehicle dynamics are removed from the acceptable region, motion cues become more helpful to the pilot. Easily controlled vehicles do not require additional cues. Marginally stable or unstable vehicles, however, may require more lead compensation than is comfortably generated by pilots on the basis of instruments and consequently the rate sensing elements of the vestibular system prove valuable in giving early indications of attitude changes.

- Motion cues are more helpful with unstable dynamics than with lightly damped oscillatory vehicles. As noted by others, the motion accompanying high-frequency vehicle oscillations may shake the pilot about in the cockpit making precise control and accurate reading of instruments difficult.

- Moving-base simulation yields closer agreement with flight experience than fixed-base simulation, especially in marginally stable or difficult vehicles. For most applications, simulation of vehicle angular motions is more important than translation simulation. Stabilization requires attitude control prior to control of position, thus emphasizing rotational motions. Normal accelerations, from centrifuge simulations, do not appear as important as angular cues except under high g conditions, and the spurious motions associated with closed-loop centrifuge simulation often cloud the pilot stabilization picture.

In 1968 Shirley (Reference 17) completed the most comprehensive investigation carried out to that time on the effects of motion cues on the pilot model. Limiting himself to motion about the roll axis, Shirley compared the effects of fixed-base versus moving-base simulation on 40 different controlled elements. The range of plant dynamics investigated covers approximations to almost all lateral control transfer functions encountered in flight vehicles. Shirley's results show the differences in human operator amplitude and phase angle over the frequency range tested for roll motion cues only, in combination with IFR visual cues, and finally for visual cues only. In addition to the gain and phase for the pilot describing function as a function of frequency, the remnant power spectrum and the measure of performance (mean relative integral square error) is given. These data form an important source for validation of models which incorporate motion cues. The study shows how roll motion cues permit the human operator to increase his cross-over frequency by permitting higher gain tracking as a result of reduced phase lag.

The results of a number of moving-based, and fixed-based simulator experiments in roll indicate that subjects can take advantage of roll information sensed by the semicircular canals and the otoliths to augment and substitute for visual

information in the higher frequency range of vehicle motion, but that this information cannot be substituted for visual information in accurate attitude or position control in a quasi-static situation (References 18 - 21).

In order to distinguish the effect of linear acceleration (sensed primarily by the otoliths) from the effects of angular acceleration (sensed primarily by the semicircular canals), Dinsdale (Reference 22) investigated the relative effects of roll and yaw in manual control utilizing one of the 40 cases of Shirley's study (K/s^2). By examining the describing functions for both otolith and canal stimulation, he concluded that the otolith contributes an important portion of the motion stabilization effects.

Stapleford, Peters and Alex (Reference 15) experimented with the effects of motion cues on the pilot describing function in a set of roll control tasks with variable lateral acceleration, and were able to identify separately the visual and motion paths in terms of effects on pilot describing function. Their conclusions were in general agreement with those of Shirley. They found that the visual path embodies higher gain and less phase lead with motion than without, presumably as a result of the use of vestibular inputs to obtain roll velocity and acceleration information. They proposed models for the utilization of vestibular information based on then available mathematical descriptions of these sensors: simplification of the semicircular canal path to be a first-order lag or even a pure time delay of 0.1 second, and of the utricular path to be treated independently as a first order lag. Although these give the correct direction of effect on pilot describing function and cross-over frequency, they are inadequate for a pilot model intended to include the effects of motion quantitatively.

In a related study (Reference 23), Ringland, Stapleford and Magdaleno experimented with a multi-axis VTOL hovering task, with various amounts of motion

involved. This study demonstrated once again the beneficial effect of roll motion and the often confusing and decremental effect of linear acceleration in these tasks. The results point out the need to consider the interaction between linear and angular acceleration motion cues on the pilot, both in terms of his perception of orientation and his resulting control movements.

The performance effects of motion found in the Stapleford, et al. study (Reference 15) showed not only performance increase but a reduction in the remnant component of the mean square error relative to fixed base values. Ringland, et al. (Reference 23) found, in addition to the motion cue effects on the describing function discussed above, a change in the pilot's scanning behavior relative to fixed-base conditions. In brief, the presence of motion cues permits the pilot to spend more time concentrating on outer loop position control (in terms of percentage of instrument scan time), since higher frequency roll motion can be sensed by the semicircular canals and otoliths to help in inner loop stabilization. These results are consistent with those found earlier by Benjamin (Reference 21) in fixed-base and motion-based helicopter control studies. Ringland, et al. (Reference 23) verified a large difference in describing function data between VMC (Visual Meteorological Conditions) and IMC (Instrument Meteorological Conditions). This difference is apparent in describing function measures, scan frequency, and pilot ratings.

Smaller differences in pilot function behavior between ground simulation and motion (for this case, in-flight testing) were found by Newell (Reference 24) and Newell and Smith (Reference 25). Newell's describing function data illustrates some of the differences between moving-base simulation and flight. Of more practical interest in Reference 24 is the difference documented between IMC and VMC for both flight and ground conditions. VMC permit consistently larger amplitude ratios for the pilot and larger tracking errors. One must be cautious in direct comparison of these

IMC and VMC in-flight measurements of pilot describing functions, however, since they were measured in one case by injecting input as a disturbance, and in the other by injecting it as a command. In the latter situation, only response, but not input were sensed as motion cues. Qualitatively similar results in comparison of roll tracking in flight and ground simulation were found by Smith (Reference 26). A summary of several of the earlier comparisons of in-flight and simulator control for both longitudinal and lateral dynamics was given by Newell and Pietrzak (Reference 27).

In a set of experiments comparing various types of simulation and flight using VTOL hover as the task, Sinacori (Reference 28) verified that the presence of motion cues led to the generation of additional lead by the pilot and a marked decrement in the tendency to overcontrol. The smoothness of flight which is present for cases involving motion, and often absent in the fixed-based situation, has been noted by many authors and may be an important result of the additional lead compensation. Alternatively, it may be due to a hesitancy on the part of the pilots to generate large accelerations in a moving-base simulator or in flight, as opposed to their lack of such inhibitation in a fixed-base simulation where the vehicle accelerations are not sensed directly. Unfortunately Sinacori's data includes information on performance and stick movement spectral analysis but no pilot describing functions.

Further support for the idea that accelerations are directly sensed, and minimized, was provided by Rolfe et al. (Reference 29). By concentrating on the longitudinal control characteristics they found that when pitch motion was present in a moving-base simulator, the control activity was close to that in flight; whereas in its absence, there was a tendency for excessive stick control to be used, especially in initiating and completing a turn. In addition to noting the tendency toward smoother control in flight and with motion cues, they note the tendency of pilots to avoid

movements which would contribute to a negative g's situation. Similar conclusions were drawn by Ringland, et al. (Reference 30). This is furthermore in agreement with the effects of motion on pilot control strategies found by Douvillier, et al., Flaxman, and Huddleston (References 31 - 33).

Bergeron (Reference 34) noted, in a study of pitch and roll axis control, that in at least some cases where motion has relatively little effect on single axis control, it has a significant effect on both the pilot describing function and the resulting system error for multi-axis control. This presumably follows from the effect of motion in allowing the pilot to improve his sharing of attention between two tasks. In an earlier study of two-axis tracking with motion, Bergeron and Adams (Reference 35) noted a reduction in the variability of the measured human operator parameters when motion cues were provided. This effect may again be attributable to the ability of the subject to more easily control tracking tasks in two separated axes when vestibular cues can be used to augment visual cues and alter scan patterns.

Some substantial work of relevance to the question of motion effects on pilot models was published during the period of our research. Dillow et al. (Reference 36) extended the optimal control model for processing roll motion cues in two ways. They made roll acceleration and its derivative observable, and then placed weightings on roll acceleration, as well as roll angle and rate in the cost function to be minimized. Thresholds were assumed for roll and its first three derivatives. The model extension was tested against Shirley's data for a number of first, second and third order plants, under fixed-base and motion-base conditions. Using RMS roll error divided by RMS input as the sole performance measure (rather than pilot describing functions), Reference 36 demonstrated a high degree of agreement between analytical results and Shirley's experimental findings.

The most directly applicable new data we uncovered was by Junker et al. (Reference 37), and a companion paper by Repperger and Junker (Reference 38). These papers treat tasks very similar to those investigated by Shirley and used in our model development, namely the separate role played by visual and motion cues in a roll tracking task. The three plant dynamics used were progressively of higher order and more difficult to control, requiring more lead generation on the part of the pilot. The addition of roll motion cues and the associated possibilities for lead generation resulted in the largest amount of performance increment and pilot model influence for the plants in which lead was most needed. The results for several subjects were given in terms of RMS errors, pilot transfer function frequency response, and values of pilot model gain, and locations of one zero and two poles for each plant with and without motion.

Interestingly, in contrast to Junker et al.'s results, Shirley found that along the real axis of plant poles, for control stick gain held constant, the motion cues were of most help for the lower order plants. One must look into the details of the experiment to find the basis for the difference. Shirley's experiments were strictly compensatory tracking, in which the command roll angle was always zero, and the subject rolled the simulator back to level to overcome the disturbances. He identified the total Y_p for the case of visual cues only, motion only, and vision plus motion. Junker et al. on the other hand, used a roll tracking task in which the pilot rolled the simulator to track a commanded roll angle, the error being displayed on the instrument. Thus for the latter experiments, the visual tracking loop was strictly compensatory, but the motion feedback provided large angle actual response information. This implied a pursuit aspect to the motion feedback, and meant that the actual angular rates and positions sensed were much larger than for the Shirley experiments. The presence of large simulator roll angles could provide the additional stimuli to make the motion sensors more effective in improving performance than was the case for the Shirley experiments with high order systems.

Of particular value in Reference 37 is the separate identification of a motion cue transfer function acting on linear acceleration (gravitational component) information, and another acting on angular acceleration. The utricular information, based on specific force, is low-pass filtered and utilized primarily for quasi-static position sensing. (Junker et al. found no lead generation in the linear acceleration pathway.) On the other hand, the semicircular canals, detecting angular acceleration, are used extensively for roll angle lead generation when they are stimulated. (Junker et al. find that the angular acceleration path transfer function changes from low pass to high pass with motion cues in the higher order plants.)

In addition to the pilot model results, Junker and Replogle (Reference 39) also demonstrate the increased effectiveness of roll motion cues in reducing task learning time and improving tracking performance for tasks having large roll motion and requiring lead, using a plant of K/s^2.

2.3 SIMULATOR REQUIREMENTS FOR MOTION CUES

In addition to the research directed precisely at the question of motion cue effects on pilot performance, there has been considerable interest in determining the adequacy and importance of simulator motion and the development of optimum washout circuits for a given simulator configuration. A review of the factors in simulator design which relate to motion and visual cues is given by Matheny et al. (Reference 40). They generally support the view of the pilot motion cue utilization discussed above. For attitudinal changes, motions will be sensed first through the vestibular senses. The visual senses are generally relied upon to corroborate or substantiate the information received by the motion senses, although in some systems the rate of movement is such that the visual senses are able to detect the fact of movement before the motion senses.

In an experimental study of factors in flight simulation aimed at the required fidelity of motion cues, Klier and Gage (Reference 41) studied a simplified air-to-air combat tracking task in a moving base simulator with pitch, roll and heave degrees of freedom. Using various cut-off frequencies for simulator motion, they found the best performance in terms of time-on-target and RMS error, with a 0 to 2.5 Hz bandwidth. Performance dropped as the bandwidth was increased or decreased from this level. The results obtained by Klier and Gage support the idea that motion cues lead to vestibular generation of lead with good tracking at frequencies below 2 Hz, but that at higher frequencies the presence of vibration, which cannot be damped out by the pilot, serves only to degrade vision and interfere with his ability to track. In another study using two-axis movement control in a moving-base and a similar flight base simulation for pilot training, Jacobs et al. (Reference 42) verified the importance of simulator motion in pilot steering performance, and found an important interaction between simulator motion and preference for specific display formats.

In summarizing the state of art in this area, Staples (Reference 43) pointed out the importance for proper vestibular modeling and its use in simulator wash-out design. In his discussion of Staples' paper, Bray (Reference 44) noted that large differences in the pilot's estimation of spatial orientation can result from their motion-visual interaction, and that lack of motion cues causes a much larger decrement in performance for those subjects classified (on a rod and frame test) as "frame-oriented" than for those who were not frame-oriented. This discussion further emphasizes the importance of systematic investigation of visual-vestibular interaction and spatial orientation, both in terms of how the pilot feels, and the way he will react in a situation tending to produce false motion illusions. Some of the same thoughts are expressed by Lew and Dyda (Reference 45) in a discussion of the pros and cons of ground-based simulation and comparison with flight for landing training.

Sinacori (Reference 46) discusses the need for realistic, distortion-free visual displays in a VFR moving-base simulation. He also lays out the goals of their motion drive system in pitch, roll and yaw to provide the following:

1. Provide semicircular canal stimulation at frequencies where the stimulus corresponds nearly to perceived angular velocity, i.e., 0.2 to 10 rad/sec.

2. Provide utricular stimulation at low frequencies only, i.e., up to 0.25 rad/sec.

3. Minimize false stimulation of the vestibular organs and maintain low frequency postural reflexes.

2.4 DIRECT EFFECTS OF SIMULATOR MOTION ON PILOT PERFORMANCE, INDEPENDENT OF MOTION CUES UTILIZED IN FEEDBACK

It is well known that, in addition to the beneficial effect of simulator or flight motion on improving performance, aiding pilot rating, and leading to smoother controls, the presence of vehicle motion in itself can lead to decrements in performance, especially when the motion is sustained high acceleration or of high frequency vibration. Some of the high acceleration effects on the pilot describing function were reviewed by Sadoff and Dolkas (Reference 47). Recent investigations of the effect of vehicle vibration on pilot describing functions were reviewed at the Tenth Annual Manual Control Conference (References 48 and 49).

Possibly less well known as a direct effect of motion on pilot performance are experiments performed by Guedry and colleagues at Pensacola. Benson and Guedry (Reference 50) demonstrate conclusively the effect of rotary vehicle motion in decreasing the performance on an unrelated tracking task as mediated through the oscillatory movement of the eyes called nystagmus. Larger performance decrements are associated with larger values of nystagmus in both the pitch and yaw axes. Gilson, Benson, and Guedry (Reference 51) in the same year show that as instrument illumination is increased

to reduce the level of nystagmus during vehicle rotation, the interference with tracking is diminished. Both of these contributions lead to the conclusion that an important direct effect of motion on pilot control is mediated through the development of nystagmus and its resulting impairment of visual acuity. This can be represented in the human operator model as an increase in observation noise.

SECTION III

COMPONENTS OF THE PILOT MODEL

This section discusses the principal components of the pilot model formulated for manned simulation applications. The optimal control model of the human operator is selected as the foundation for this extended model. Workload and scanning effects are described, followed by a discussion of motion cues and the vestibular sensors. The differences between visual and instrument flight conditions are then explained. Finally, a summary of the extended pilot model is presented for convenient reference.

3.1 INTRODUCTION

As discussed in Section 2, there are two basic types of pilot models: describing function models and state space models. The first type, which is formulated in the frequency domain, originated with classical control theory. It has been developed to control various single- and multi-loop system configurations. The second type of pilot model, which is formulated in the time domain, was developed from modern control and estimation theory. It, too, is applicable to a variety of system configurations. These approaches to pilot modeling have been effectively applied in the fields of aircraft flying qualities, pilot-vehicle control system integration, and display synthesis.

The optimal control model of the human operator has been selected in this research effort for the following reasons:

- The model more easily handles multi-input and multi-output control tasks.
- The model provides an empirically verified measure of workload which is related to attention rather than eye movement behavior. As such, it will also work at the level of displayed information or the level of detailed display format for both integrated and separate instrument displays.

- The optimal control model of the human operator is more adaptable to calculating the time varying statistical behavior (over the ensemble of trajectories) due to nonstationary statistics arising from the geometric and kinematic relationships of the guidance and navigation systems.

In the remainder of this section we briefly outline the baseline optimal control model of the pilot, discuss the extensions which incorporate scanning and attention allocation, motion cues, and VMC/IMC (Visual Meteorological Conditions/ Instrument Meteorological Conditions) cues. Lastly, we summarize the parameters of the models, guidelines on how to choose the parameters, and what effects are represented by the parameters.

3.2 THE OPTIMAL CONTROL MODEL OF THE PILOT

This section briefly reviews the important elements of the optimal control model of the pilot in describing human performance for fixed-base IMC (instrument meteorological conditions). These conditions are the ones for which the model has been well validated in the past. A more complete analytical description, including the relevant equations of the model, is contained in Appendix B.

A block diagram of the model is presented in Figure 1, which shows the information flow and the interaction of the pilot with the controlled element. The displayed information $y(t)$ passes through the threshold element (either a psychophysical threshold or an indifference threshold). Perceptual observation noise $v_y(t)$ is added to this quantity, which then passes through the perceptual time delay τ. The perceived displayed quantities $y_p(t)$ are the inputs to the core of the model, which consists of a Kalman filter to account for the controlled element dynamics and the observation noise, and a predictor to compensate for time delay. The current state estimate $\hat{x}(t)$ is combined linearly to provide a commanded control signal. To this control signal is added a white motor noise component $v_u(t)$ with the sum passing through a neuromuscular/

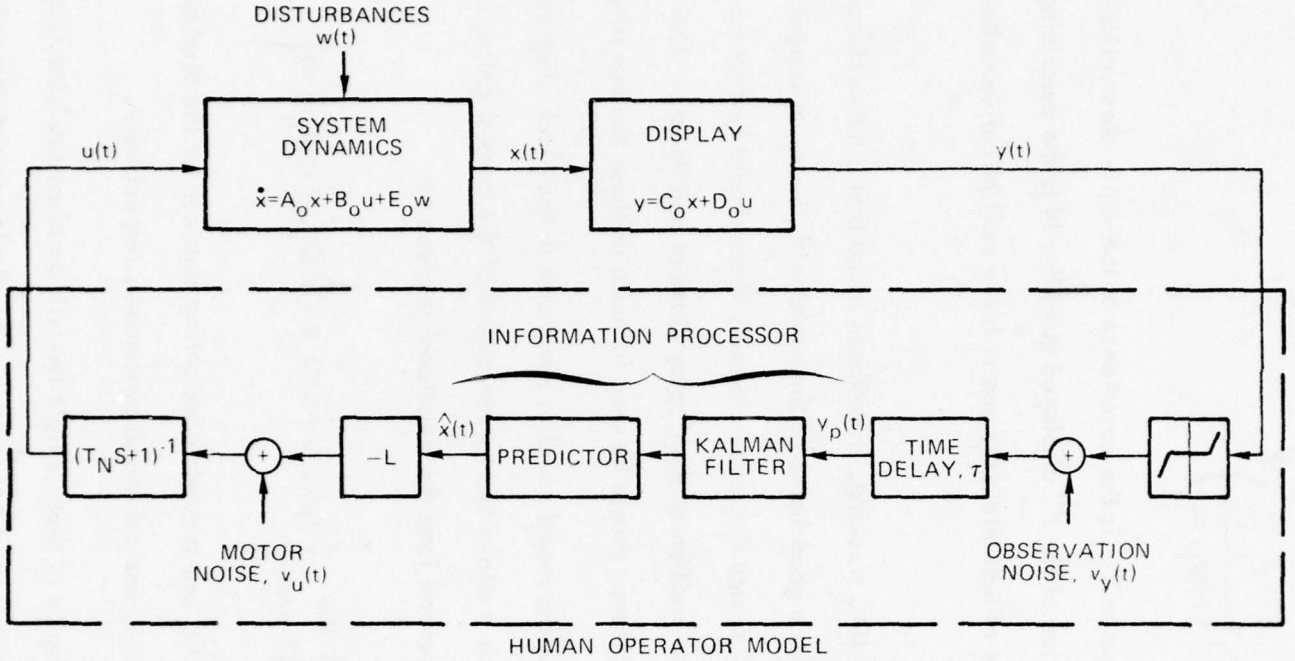

Figure 1. Optimal Control Model of Human Response.

manipulator first-order lag. For a single displayed quantity, the covariance of the observation noise depends on several important parameters and has the form

$$V_{y_i} = \rho_i \left(\frac{\sigma_i}{N(\sigma_i, \alpha_i)} \right)^2 \tag{1}$$

where in the above expression V_{y_i} is the covariance of the white observation noise; σ_i is the standard deviation of the i^{th} displayed quantity; N is the describing function for the dead zone element of half width α_i; and ρ_i is the multiplicative noise/signal ratio.

For fixed-base IMC tracking, it has been found that a noise/signal ratio of -20 dB (or 0.01 π) provides a good match of the model with the experimental data. It has also been found that for each displayed element, there should be two inputs to the model corresponding to the position of the display element and its rate. The above relationship on noise covariance should be used for each of these Kalman filter inputs.

One element of the model which is not shown in the block diagram is the quadratic functional which is minimized by the choice of the control gains, L, shown in Figure 1. In its most general form the functional is given by

$$J = E \left\{ \lim_{T \to \infty} \int_0^T [y'Q_y y + x'Q_x x + \dot{u}'Q_r \dot{u} + u'Q_u u] \, dt \right\} \tag{2}$$

where Q_y, Q_x, Q_r, and Q_u are symmetric weighting matrices for the display variables, state variables, control rate, and control displacement, respectively.

The specific choice of these weightings will be discussed later, but in practice it has usually been found sufficient to weight the display deviations and control rate only, with the weights on control rate chosen to provide a neuromuscular time

constant (T_N in Figure 1) consistent with the manipulator (with a value of T_N = 0.1 - 0.2 second being typical).

3.3 WORKLOAD AND SCANNING MODELS

Estimates of pilot workload developed to date have been of two major types: visual scanning workload (Reference 4) or task interference workload (Reference 6). Both have been well documented and verified in experimental situations. There are several reasons why we elect the task interference workload model in this study.

- Its formulation is consistent with the optimal control model of the pilot
- It will predict time variations and workload level in non-stationary conditions
- It may be used either at the information requirements level or the display format level of detail
- It contains flexibility to accommodate side task workloads.

We feel this last item is of particular importance in predicting pilot workload models for the purpose of simulator resource allocation. Many of the pilot model applications to date have concentrated solely on the continuous control tasks. However, it is known that there are many side tasks of a discrete nature (e.g., communications, frequency changes, equipment adjustments, etc.) which are not usually accounted for in most modeling efforts, but which can be of great importance. The visual scanning method of measuring pilot workload appears not to have the advantages listed above because it is based on time averaged (stationary) statistics, and the scanning behavior is too detailed a metric when working at the information requirements level of detail (References 51-54).

We let the total fraction of attention (nominally 1.0) be composed of the additive terms

$$f_{tot} = f_c + f_o + f_{other} \tag{3}$$

where

$$f_c = \sum_i f_{c_i} \tag{4}$$

In the above equation, f_c is that portion of the total attention devoted to the control task (control task workload); f_{c_i} is the fraction of attention allocated to the i^{th} display variable for control; f_o is the fraction of attention lost in switching from one display to another, or from control task to side task; and f_{other} is the fraction of attention allocated to the other side tasks demanding attention from the pilot.

The effect of any given allocation of control task workload among the display variables (i.e., specifying the individual f_{c_i}) has an effect on performance as follows. The task interference measure of workload indicates that for a modification of the covariance of observation noise of each input, a Kalman filter in the pilot is necessary (References 6, 55-57):

$$V_{y_i} = \frac{V^0_{y_i}}{f_{c_i}} = \frac{\rho_i}{f_{c_i}} \left[\frac{\sigma_i}{N(\sigma_i, \alpha_i)} \right]^2 \tag{5}$$

where $V^0_{y_i}$ is the power spectral density of the observation noise of the i^{th} display variable when attention is limited to that display variable alone (Equation (1)), and f_{c_i} is the fraction of attention allocated to the i^{th} display variable. This workload measure has the correct interpretation at the limiting values of full attention ($f_{c_i} = 1$) and no attention ($f_{c_i} = 0$).

Using this model, we may determine the attentional workload requirements as a function of system performance as follows. Assume a given value of fraction of attention on the control task workload f_c. Then determine the f_{c_i} within the constraint of Equation (4)

to minimize the quadratic performance index (see Appendix B). There are the optimal allocations of attention between display variables for a specified fraction of attention allocated to the control task. From the RMS performance calculations, we also know the system performance J. If this process is performed for several different values of f_c, then we may draw the curve of control-task workload required to accomplish the given level of system performance (J) as shown in Figure 2. The solid curve represents the control task workload, and the dashed curve represents the effect of adding the fraction of attention for transitions and the fraction of attention required for other tasks. This dashed line represents the total required fraction of attention for the pilot and represents the performance workload tradeoffs. Note that the pilot is working at full capacity to maintain the cost function at or below J_1.

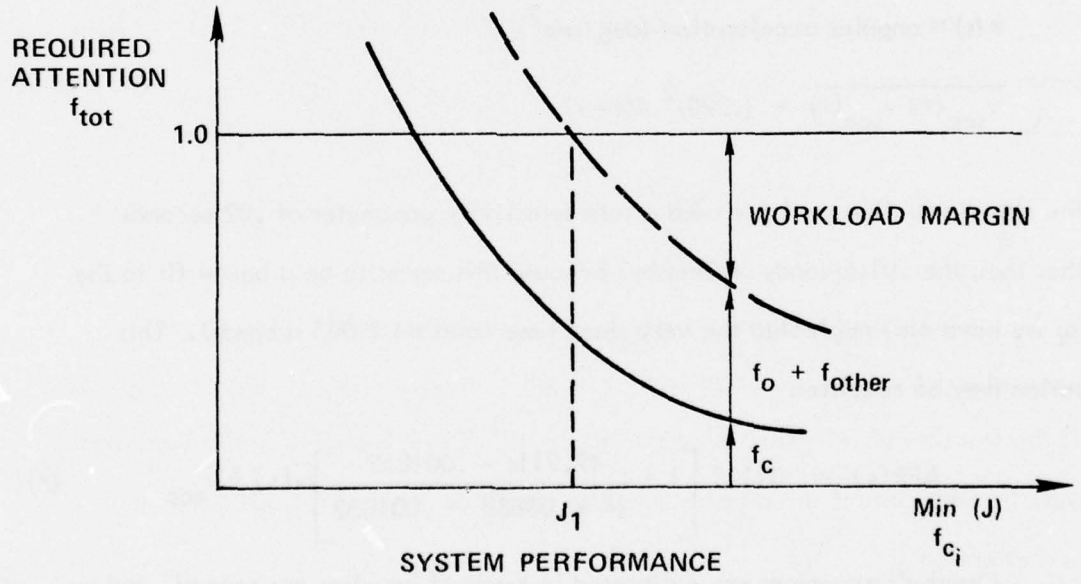

Figure 2. Required Attentional Workload vs System Performance.

3.4 MOTION CUES: STATE SPACE FORMULATION OF THE VESTIBULAR SENSORS

In this section we formulate the equations to be used in the optimal control model of the pilot to represent the vestibular sensors. It consists of two sections: the development of the semicircular canal equations, and the development of the otolith equations.

3.4.1 SEMICIRCULAR CANALS

In Equation (3.9) of Ormsby's thesis (Reference 16), the Laplace transform equation for the afferent firing rate of a semicircular canal is given by

$$\underset{\text{(impulses/second)}}{\text{AFR}(s)} = \frac{300s\,(.02s + 1)}{(18s + 1)\,(30s + 1)}\dot{\omega}(s) + v_{scc}(s) \tag{6}$$

where the input angular acceleration and additive noise satisfying

$\dot{\omega}(s)$ = angular acceleration (deg/sec^2)

$$\overline{v_{scc}(t)\,v_{scc}(\tau)} = (.223)^2\,\delta(t-\tau)$$

In the above equation we have used a rate sensitivity parameter of .02 seconds (rather than the .01 seconds of Ormsby) because this seems to be a better fit to the data; we have also neglected the very short time constant (.005 seconds). This equation may be rewritten

$$\text{AFR}(s) = .01111\left[1 + \frac{49.911s - .001852}{s^2 + .08888 + .001852}\right]\dot{\omega}(s) + v_{scc} \tag{7}$$

Ormsby's equations are calibrated in terms of impulses per second, and we prefer to scale the output in units of angular acceleration. To do this, we use the

fact that near the psychophysical threshold (taken to be $0.19^{\circ}/sec^2$), the ratio of signal to noise variance is approximately $(1.36)^2$ to provide the probability of correct detection of .75. Thus, in the scaled equation the noise variance, $\sigma_{v'}^2$, in units of (degrees/second^2) is given by

$$\frac{\sigma_{v'}^2}{(.19^{\circ}/sec^2)^2} = \left(\frac{1}{1.36}\right)^2 \tag{8}$$

Using the fact that the output will be scaled by the factor K, then we have the relation

$$\sigma_{v'}^2 = K^2 \sigma_{v_{scc}}^2 \tag{9}$$

where

$$K = \frac{0.19^{\circ}/sec^2}{(1.36)\,(.223)\ ips}$$

Thus we are finally led to the following state equations and measurement equations for the semicircular canals

$$\begin{aligned} \dot{x}_{scc1} &= x_{scc2} \\ \dot{x}_{scc2} &= -.001852\, x_{scc1} - .08888\, x_{scc2} + \dot{\omega} \end{aligned} \tag{10}$$

$$\begin{aligned} y_{scc}\ (deg/sec^2) = {} & -1.289 \times 10^{-5}\, x_{scc1} \quad 4\, x_{scc2} \\ & + 0.00696\, \dot{\omega} + v_{scc} \end{aligned} \tag{11}$$

3.4.2 OTOLITHS

The state equations and measurement equations for the otolith are taken from Ormsby's thesis (Reference 16) and are given by

$$\dot{x}_{oto} = -.2\, x_{oto} + .2\, f \tag{12}$$

$$y_{oto} = -46.1\, x_{oto} + 91.1\, f + v_{oto} \tag{13}$$

where f is the specific force. We again are faced with the output equation in units of impulses per second. Ormsby uses the scale factor such that 45 impulses per second corresponds to a steady state stimulation of 1g . Thus we may rescale the output equation to be

$$y_{oto}\ (\text{in g's}) = -1.024\, x_{oto} + 2.024\, f + v_{oto} \tag{14}$$

$$\overline{v_{oto}(t)\, v_{oto}(\tau)} = (.003267\ g)^2 \sec \delta\,(t - \tau) \tag{15}$$

3.5 VMC/IMC CUES

One of the goals of this research effort is to account for outside-the-window visual cues and their effects on pilot behavior in comparison to the normal instrument (IMC) cues. This study was limited to the effect on attitude control performance, and did not consider the more complicated position control task such as occurs during the final phase of landing (i.e., near flare height and below). The effect of full field visual cues has been measured in flight and in ground-based simulation using a wide angle contact analog display (Reference 25). The effects of the wide field display manifested themselves in higher pilot describing function gains when

compared to the IMC tracking tasks, both with and without motion. These effects might be accounted for in the model by decreasing the noise/signal ratio on attitude measurement, especially attitude rate; by decreasing the threshold upon the corresponding measurements; and by decreasing the weight on the attitude rate in the quadratic cost functional. All of the e would have the effect of increasing pilot gain (although to varying degrees) and it is one of the purposes of our investigation to determine the most appropriate way to model the VMC cues.

3.6 SUMMARY OF THE PILOT MODEL

In this section we review the parameters of the optimum control model and briefly describe how one chooses the parameters to represent the situation under study. The outline of this discussion will closely follow the description of the program input contained in Volume 2 of the report.

3.6.1 CONTROLLED ELEMENT DYNAMICS: MATRICES A, B, E

These matrices for the system response (See Appendix B) describe the dynamical characteristics of the element being controlled and any shaping filters required to describe the spectral characteristics of the disturbance input. In the use of the model to describe motion cues, these matrices should also reflect the vestibular dynamics discussed in Section 3.4.

3.6.2 COST FUNCTIONAL WEIGHTINGS

The cost functional weighting matrices contain only diagonal elements in the usual application of the optimal control model of the human operator. In addition, it has generally been found sufficient to ignore weightings on the state Q_x and on the control displacement Q_u. The weightings on the displayed quantities Q_y and a control rate weight Q_r are discussed next

We have generally obtained excellent results from the model by weighting the position of the displayed variables inversely proportional to the square of the maximum allowable displacement. When dealing with a specific display format layout, this generally corresponds to full scale on the display. When dealing with the model at a more general level, this would correspond to a maximum display value appropriate to specified mission requirements. Recall that the optimum control model of the pilot requires two inputs for each displayed quantity: its position and its rate. While the discussion above describes how to choose the weight on the position of the display element, there has previously been little guidance available for selecting the weight for the rate of a displayed quantity.

In many applications the maximum value of a position or attitude variable is easy to determine from the mission requirements, hence its weighting coefficient in the quadratic cost functional is relatively straightforward, i.e., the coefficient is $(y_{max})^{-2}$. There is no corresponding interpretation on the rate of change of that variable in many instances, so it is subject to some uncertainty. Figure 3 shows the change in RMS error predicted by the model as a function of $(y_{max}/\dot{y}_{max})^2$ for several of the plants treated by Shirley (Reference 17). The abscissa has units of seconds^2, and its interpretation led to our final choice of the weighting coefficients. As shown in Figure 3, this can lead to significant changes in the performance predictions of the model. To place a realistic value on the weighting of the rate term, consider that if the minimization process is doing a reasonable job, we would expect

$$\left|\frac{y}{y_{max}}\right| \approx \left|\frac{\dot{y}}{\dot{y}_{max}}\right| \tag{16}$$

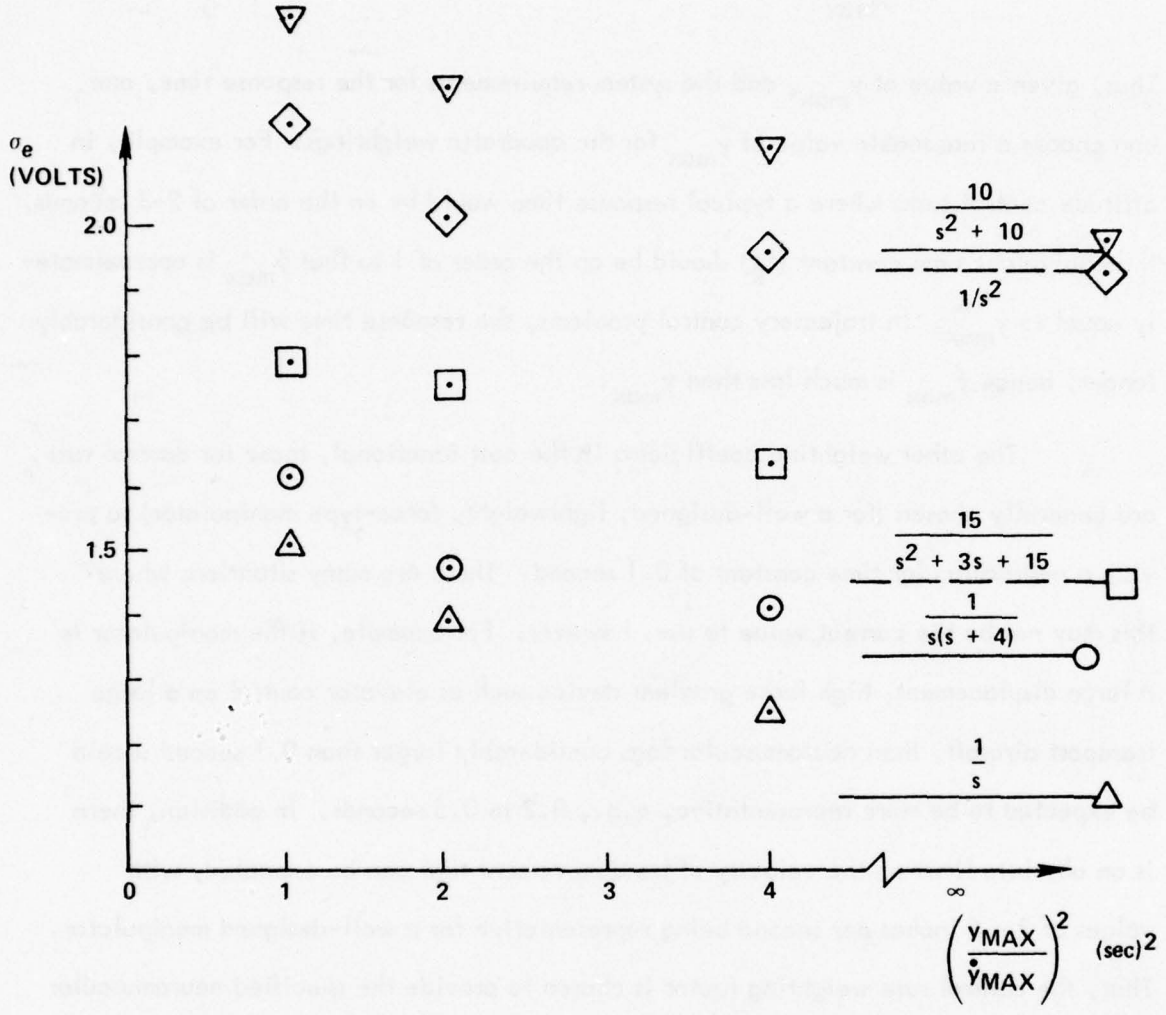

Figure 3. Comparison of Model Predictions with Change in Weighting Coefficients - Visual Only.

If this ratio remains true for all levels of y and $\dot{y}$, and if the system exhibits stable behavior, then Equation (16) can be approximately written

$$\tau_R \dot{y} + y \approx 0 \qquad (17)$$

where the equivalent time constant of the response is given by

$$\tau_R \approx \frac{y_{max}}{\dot{y}_{max}} \tag{18}$$

Thus, given a value of y_{max}, and the system requirements for the response time, one can choose a reasonable value of $\dot{y}_{max}$ for the quadratic weightings. For example, in attitude control tasks where a typical response time would be on the order of 2-3 seconds, the equivalent time constant (τ_R) should be on the order of 1 so that $\dot{y}_{max}$ is approximately equal to y_{max}. In trajectory control problems, the response time will be considerably longer, hence $\dot{y}_{max}$ is much less than y_{max}.

The other weighting coefficients in the cost functional, those for control rate, are generally chosen (for a well-designed, lightweight, force-type manipulator) to provide a neuromuscular time constant of 0.1 second. There are many situations where this may not be the correct value to use, however. For example, if the manipulator is a large displacement, high force gradient device such as elevator control on a large transport aircraft, then neuromuscular lags considerably larger than 0.1 second should be expected to be more representative, e.g., 0.2 to 0.5 seconds. In addition, there is an absolute limit on the velocity of hand movement that can be expected, with values of 2 - 5 inches per second being representative for a well-designed manipulator. Thus, the control rate weighting factor is chosen to provide the specified neuromuscular time constant; if this value corresponds to control rates larger than 2 - 5 inches per second, then this latter value should be considered.

3.6.3 CONTROLLER TIME DELAY

This parameter represents the pure transport time delay of the human operator, but also can be used to model the transport delays in the controlled element. The typical value for human operator reaction times is 0.2 second.

3.6.4 PROCESSOR DRIVING NOISE

This is the covariance of the white process noise driving the state equations. It is chosen to provide the appropriate RMS disturbance value.

3.6.5 ADDITIVE MOTOR NOISE

This is the covariance of the white noise component added to the human operator output (See Figure 1). It is typically chosen to provide a noise/signal ratio referenced to the control output of -25 dB (0.003π), but there are situations where this may lead to unrealistically small noise levels. In addition, poorly designed manipulators with much stiction and/or the effects of motion may increase this above the -25 dB level.

3.6.6 OBSERVATION THRESHOLDS

These parameters of the model generally are chosen to represent indifference thresholds and are strongly dependent on the format of the display. Typically, a reasonable value for these thresholds is the minimum resolution marking on the display, but in other instances the more appropriate value may be (say) 10 percent of the full-scale value. A pilot opinion is useful in this context also, since one can assess the indifference thresholds by asking experienced pilots what type of a static deviation they are willing to tolerate.

The threshold for the display element rate input can be chosen in a manner analogous to the weighting of the same quantity, i.e., for an equivalent time constant of response τ_R, we would expect that

$$\frac{\alpha_y}{\alpha_{\dot{y}}} \approx \tau_R \tag{19}$$

where α_y and $\alpha_{\dot{y}}$ are the threshold halfwidths on the displayed quantity y and its rate $\dot{y}$. That is, the ratio of the threshold of display position to display rate is the same as the ratio of maximum displayed quantity to its maximum rate.

These thresholds enter the calculation of the observation noise in the pilot model through the equation (See Equation (1))

$$V_{y_i} = \frac{\rho_i}{f_{c_i}} \left[\frac{\sigma_{y_i}}{N(\sigma_{y_i}, \alpha_i)} \right]^2 \tag{20}$$

where in the above expression, N is the describing function of the dead zone element shown in Figure 1, and α_i is the threshold value described above.

3.6.7 OBSERVATION NOISE RATIOS

The observation noise ratios are the parameters ρ_i in Equation (20) above, and for visual displays it has been determined that a value of 0.01π (-20 dB) generally provides a good fit with experimental data. However, for motion cue inputs (and perhaps VMC cue inputs) other values of noise/signal ratios may be appropriate. This ratio will be one of the parameters which will be varied in the examination of motion cue information.

3.6.8 ATTENTION ALLOCATION

The attention allocations are the fractions of attention devoted to each display element subject to the constraint of Equation (4). The fraction of control attention devoted to the i^{th} display enters into the computation of the noise covariances as indicated in Equation (20). It is through this effect that we expect to see differences between scanning behavior in motion and no-motion conditions. The vestibular inputs will be assigned $f_{c_i} = 1.0$, and the fraction of attention for the visual displays will be chosen to further minimize the performance index as indicated in Section 3.3.

In its most general form the model is truly a multi-input, multi-axis representation. However, when dynamical decoupling exists between axes, the attention allocation can be optimized on each axis separately for a few values of f_c. Then a final optimization can be easily performed to determine the overall allocation of attention among axes. This procedure provides considerable saving in computational effort compared to an attention allocation among all displays simultaneously.

3.6.9 SUMMARY

Table 1 summarizes the correspondence of the real world components and the model components as they exist at this point of the discussion. Note that the VMC/IMC cue may be represented by functional weightings, observation noise ratios, or thresholds. This ambiguity will be clarified in later sections of the report when we determine the relative sensitivity of model predictions to these parameters for VMC/IMC cues.

Table 1. Correspondence of Real World and Model Components.

Real World Component	Model Component
Airframe Dynamics Augmentation System Mission Phase Vestibular Afferent Dynamics Simulator Dynamics	Controlled-element Dynamics $\dot{x} = Ax + Bu$
Displays (Visual and Vestibular)	Measurement Vector $y = Cx + Du$
Mission Requirements VMC/IMC Cues Neuromuscular/Manipulator Dynamics	Cost Functional Weightings $J = E\left\{\int \left[y^T Q_y y + \dot{u}^T Q_r \dot{u}\right] dt\right\}$
Vestibular Cues VMC/IMC Cues	Observation Noise/Signal Ratio Display Thresholds
Disturbance Environment (Turbulence, Shear, Guidance Errors)	Shaping Filters in State Equation $\dot{x} = Ax + Bu + Ew$ and Noise Power $W = \mathrm{cov}(w)$
Workload Expectations	f_c
Attention Allocation	$\min_{f_{c_i}} J, \ \Sigma f_{c_i} = f_c, \ f_{c_i} \geq 0$

SECTION IV

MODEL DEVELOPMENT

This section of the report examines some of the experimental data reported in the literature to determine appropriate values of model parameters for incorporating motion cues and Visual Meteorological Condition (VMC) cues. The noise/signal ratio for the vestibular measurements is determined from roll tracking data recorded in Reference 17. These parameters are confirmed by applying the model to a VTOL hovering task described in Reference 23, which has data for fixed-base, angular motion only, and angular and linear motion cues. The effect of VMC cues on the pilot model is determined from a comparison of the pilot describing function data reported in Reference 58. The predictions of the model with combined motion and VMC cues is examined.

4.1 MODEL PARAMETERS FOR MOTION CUES

This subsection describes the inclusion of vestibular measurements in the optimal control model of the pilot to account for the effect of motion cues. The data base compiled by Shirley (Reference 17) was used for this purpose.

4.1.1 DESCRIPTION OF THE EXPERIMENT

A block diagram of the system used by Shirley is displayed in Figure 4, which shows the various parameters of the simulation. The two input paths to the human are the visual system, in which the error is converted by a scale factor, K_{dis}, to distance on a display, and the motion system, in which the error is converted to a roll angle through the scale factor K_{mot}. The operator's output (in cm) is converted to a voltage by a gain, K_{stick}. This voltage drives the plant which is then compared with the input signal (a sum of 10 sine waves).

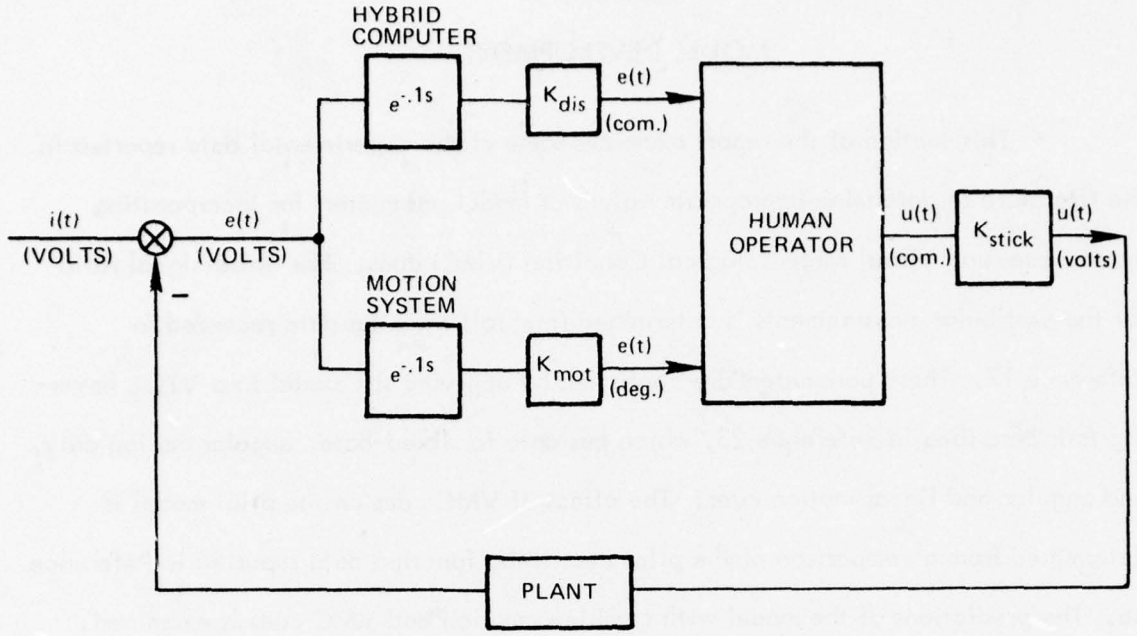

ROLL ANGLE PROPORTIONAL TO SYSTEM ERROR

K_{mot} (deg/volt) CHOSEN FOR EACH SET OF DYNAMICS

K_{dis}/K_{mot} = CONSTANT THROUGHOUT ENTIRE EXPERIMENT

Figure 4. Block Diagram of Shirley's Roll Tracking Experiment.

The motion system gain was chosen individually for each set of dynamics and resulted in reported excursions of approximately $\pm 5^{\circ}$ for easy-to-control dynamics, and $\pm 15^{\circ}$ for difficult-to-control dynamics. The ratio of display gain to motion gain is kept constant throughout the experiment. The exact value of the motion gain for each set of dynamics is not available from the data. However, an estimate of this gain may be obtained from the RMS tracking error. Table 2 presents estimates of the motion system gain for both easy and hard dynamics under the assumption that the motion limit (5° or 15°) is the 2σ value. Since the estimated motion system gain does not vary significantly, we have assumed a value of 1.6 deg/volt throughout. Note that if there

Table 2. Calculation of Motion System Gain.

Dynamics	Assumed 2σ Limit (deg)	$\overline{e^2}/\overline{i^2} = \text{rISE}$ (from Ref. 17)	Estimate of Motion Gain $K_{mot} = \frac{2\sigma \text{ Limit}}{2\sqrt{\text{rISE}\ 11.7}}$ deg/volt
$\frac{1}{s}$	5°	.23	1.52
$\frac{1}{s(s-1)}$	15°	1.66	1.70
$\frac{1}{s^2}$	15°	1.65	1.70
$\frac{1}{s(s+5)}$	5°	.38	1.18
$\frac{1}{s^2 - 2.5}$	15°	2.65	1.34

$$\overline{i^2} = \frac{\text{ISI volts}^2 \text{ sec}}{89.6 \text{ sec}} = 11.7 \text{ volts}^2 \text{ for ISI} = 1050$$

rISE = relative Integral Squared Error

were no vestibular or visual thresholds, the values of the motion and the display gains would not be a factor in the optimal control model of the human operator.

The dynamics of the motion system used in Shirley's experiment are approximated by a 0.1 second pure time delay up to a bandwidth of 10 radians per second. Following Dillow et al. (Reference 36), this time delay will be lumped with that of the human operator, a reasonable assumption when one views the location of the time delay in the block diagram. Thus the time delay parameter of the human operator is set at 0.3 second instead of the nominal 0.2 second.

The input signal for Shirley's experiments was a sum of ten sine waves with a 10 to 1 shelf at 2.5 radians per second for most of the runs. Dillow et al. have proposed approximating this by a rational spectrum derived from a four-pole filter driven by white noise with covariance W. Dillow et al. have derived a procedure for choosing an optimum break frequency for a four-pole filter approximation; for these conditions it turns out to be 2 rad/sec.

To find the value of W corresponding to the known value of mean square output (in volt^2), we note that the spectrum of the (approximate) input signal is given by

$$\Phi_{ii}(s) = \frac{W}{(s + \omega_0)^4(\omega_0 - s)^4} \tag{21}$$

where ω_0 is the break frequency of the filter. The mean square value of the filter output is given by

$$\overline{i^2} = \frac{1}{2\pi j} \int_{-j\infty}^{j\infty} \Phi_{ii}(s)\, ds = \text{residue of } \Phi_{ii}(s) \text{ at } s = -\omega_0 \tag{22}$$

To find the residue of this fourth order pole, we use the relation

$$\text{Res} = \frac{1}{3!}\frac{d^3}{ds^3}\left[(s+\omega_0)^4 \Phi_{ii}(s)\right]\Bigg|_{s=-\omega_0} \tag{23}$$

which provides

$$\overline{i^2} = \frac{20W}{(\omega_0 - s)^7}\Bigg|_{s=-\omega_0}$$

Solving this expression for W in terms of the mean square output provides

$$W = \frac{64}{10}\omega_0^7 \overline{i^2} = 9601 \text{ volts}^2 \text{ sec}^8 \text{ for ISI} = 1050 \tag{24}$$

Many of the controlled elements considered by Shirley were second order systems (and a pure delay of 0.1 second). Thus we will use the following state equations and measurement equations for the roll control of an arbitrary second-order system of the form

$$Y_c(s) = \frac{\gamma}{s^2 + \beta s + \alpha} \tag{25}$$

The system differential equations for this general second-order plant are given below:

Shaping Filter ($\omega_0 = 2.0$)

$$\begin{aligned}
\dot{x}_1 &= x_2 \qquad\qquad x_1(t) = \text{input } i(t) \\
\dot{x}_2 &= x_3 \\
\dot{x}_3 &= x_4 \\
\dot{x}_4 &= -16x_1 - 32x_2 - 24x_3 - 8x_4 + w(t)
\end{aligned} \tag{26}$$

Controlled Element

$$\dot{x}_5 = x_6$$

$$\dot{x}_6 = -\alpha x_5 - \beta x_6 + \gamma u \tag{27}$$

Semicircular Canal

$$\dot{x}_7 = x_8$$

$$\dot{x}_8 = -0.001852\, x_7 - 0.08888\, x_8 + K_{mot}\, \ddot{e}$$

$$= K_{mot}\, x_3 + \alpha K_{mot}\, x_5 + \beta K_{mot}\, x_6$$

$$- 0.001852\, x_7 - 0.08888\, x_8 - K_{mot}\, \gamma u \tag{28}$$

where $e = x_1 - x_5$

Otolith

The specific force f in g's is

$$f(\text{in g's}) = \left[\phi - \frac{\ell}{g}\ddot{\phi}\right]\frac{\pi}{180} \qquad \phi \text{ (in deg)}$$

$$= \left[e - \frac{\ell}{g}\ddot{e}\right]\underbrace{\frac{\pi}{180}K_{mot}}_{K'_{mot}}$$

where ℓ is the displacement of the otolith above the roll axis. The state equation becomes

$$\dot{x}_9 = -0.2\, x_9 + 0.2\, f(\text{in g's})$$

$$= 0.2\, K'_{mot}\left[x_1 - \frac{\ell}{g}x_3 - \left(1 + \alpha\frac{\ell}{g}\right)x_5\right.$$

$$\left. - \beta\frac{\ell}{g}x_6 + \gamma\frac{\ell}{g}u\right] - 0.2\, x_9 \tag{29}$$

With motion-only control, the following measurement equations apply.

Semicircular Canal (deg/sec^2)

$$y_{scc} = -1.289 \cdot 10^{-5} x_7 + 0.34785 x_8 + 0.00696 \ddot{e} K_{mot}$$

$$= 0.006960 K_{mot} x_3 + 0.006960 K_{mot} \alpha x_5$$

$$+ 0.00696 K_{mot} \beta x_6 - 1.289 \cdot 10^{-5} x_7 + 0.34785 x_8$$

$$- 0.006960 K_{mot} \gamma u \qquad (30)$$

Otolith (g's)

$$y_{oto} = -1.024 x_9 + 2.024 f \text{ (in g's)}$$

$$= + 2.024 K'_{mot} x_1 - 2.024 K'_{mot} \frac{\ell}{g} x_3$$

$$- 2.024 K'_{mot} \left(1 + \alpha \frac{\ell}{g}\right) x_5$$

$$- 2.024 K'_{mot} \frac{\ell}{g} \beta x_6 - 1.024 x_9 + 2.024 K'_{mot} \frac{\ell}{g} \gamma u \qquad (31)$$

Five second-order plants were chosen from Shirley's data to provide a representative cross section of controlled elements. These are shown in Table 3 with the relative Integral Squared Error (rISE) and standard deviation of the tracking error (σ_e). Note that the single integrator plant has been approximated by a second-order plant with high bandwidth filter to avoid the analytical (but not numerical) problems of defining the acceleration input to the vestibular system. The system matrices for the differential equations describing the controlled element and measurements are shown in Tables 4a through 4e for these five plants. Note that in all cases the E matrix (noise distribution matrix) is E' = (0,0,0,1,0,0,0,0,0).

Table 3. Roll Control Tasks from Shirley.

Plant	Vision rISE/ σ_e (volts)	Motion rISE/ σ_e (volts)	Vision/ Motion rISE/ σ_e (volts)	Shirley's Designation
$\frac{1}{s(s+4)}$	.34 1.99	.33 1.96	.24 1.67	Data 33
$\frac{1}{s} \cong \frac{1}{s(.02s+1)}$	.21 1.56	.15 1.32	.13 1.36	Data 7-8
$\frac{1}{s^2}$	1.09 3.56	.57 2.58	.44 2.27	Data 19
$\frac{15}{s^2+3s+15}$	.39 2.13	.32 1.94	.30 1.87	Data 47
$\frac{10}{s^2+10}$	.81 3.08	.66 2.78	.53 2.49	Data 40

The numerical values of the model parameters which are common to all five controlled elements are: the weighting coefficients on displayed quantities (set to the inverse square of the threshold values); the disturbance covariance (9601); the controller delay (0.3 second, which includes the controlled element delay); the motion noise/signal ratio (-25 dB); and the vestibular threshold values (0.19 deg/sec^2, 0.005 g's). No quadratic weightings were placed on state deviations or control displacement deviations, and the control-rate weightings were adjusted to provide a neuromuscular time constant of 0.1 second (see Table 5).

Table 4a. System Matrices for Shirley's Plant 1/s (s + 4).

$$A = \left[\begin{array}{cccc:cc:ccc} 0 & 1 & 0 & 0 & 0 & 0 & 0 & 0 & 0 \\ 0 & 0 & 1 & 0 & 0 & 0 & 0 & 0 & 0 \\ 0 & 0 & 0 & 1 & 0 & 0 & 0 & 0 & 0 \\ -16 & -32 & -24 & -8 & 0 & 0 & 0 & 0 & 0 \\ \hdashline 0 & 0 & 0 & 0 & 0 & 1 & 0 & 0 & 0 \\ 0 & 0 & 0 & 0 & 0 & -4 & 0 & 0 & 0 \\ \hdashline 0 & 0 & 0 & 0 & 0 & 0 & 0 & 1 & 0 \\ 0 & 0 & 1.6 & 0 & 0 & 6.4 & -0.001852 & -0.02083 & 0 \\ \hdashline 0.00525 & 0 & -0.0003472 & 0 & -0.005585 & -0.001388 & 0 & 0 & -0.2 \end{array}\right]$$

$$B' = \left[\begin{array}{cccc:cc:ccc} 0 & 0 & 0 & 0 & 0 & 1 & 0 & -1.6 & 0.0003472 \end{array}\right]$$

$$E' = \left[\begin{array}{cccc:cc:ccc} 0 & 0 & 0 & 1 & 0 & 0 & 0 & 0 & 0 \end{array}\right]$$

$$C = \left[\begin{array}{cccc:cc:ccc} 0 & 0 & 0.01114 & 0 & 0 & 0.04454 & -0.00001289 & 0.3479 & 0 \\ 0.05652 & 0 & -0.003514 & 0 & -0.05652 & -0.01405 & 0 & 0 & -1.024 \end{array}\right]$$

$$D = \left[\begin{array}{c} -0.01114 \\ 0.003514 \end{array}\right]$$

Table 4b. System Matrices for Shirley's Plant 1/s (.02s + 1).

$$A = \left[\begin{array}{cccc:cc:ccc} 0 & 1 & 0 & 0 & 0 & 0 & 0 & 0 & 0 \\ 0 & 0 & 1 & 0 & 0 & 0 & 0 & 0 & 0 \\ 0 & 0 & 0 & 1 & 0 & 0 & 0 & 0 & 0 \\ -16 & -32 & -24 & -8 & 0 & 0 & 0 & 0 & 0 \\ \hdashline 0 & 0 & 0 & 0 & 0 & 1 & 0 & 0 & 0 \\ 0 & 0 & 0 & 0 & 0 & -50 & 0 & 0 & 0 \\ \hdashline 0 & 0 & 0 & 0 & 0 & 0 & 0 & 1 & 0 \\ 0 & 0 & 1.6 & 0 & 0 & 80 & -0.001852 & -0.02083 & 0 \\ \hdashline 0.00585 & 0 & -0.0003472 & 0 & -0.005585 & -0.01736 & 0 & 0 & -0.2 \end{array}\right]$$

$$B' = \left[\begin{array}{cccc:cc:ccc} 0 & 0 & 0 & 0 & 0 & 50 & 0 & -80 & 0.01736 \end{array}\right]$$

$$E' = \left[\begin{array}{cccc:cc:ccc} 0 & 0 & 0 & 1 & 0 & 0 & 0 & 0 & 0 \end{array}\right]$$

$$C = \left[\begin{array}{cccc:cc:ccc} 0 & 0 & 0.01114 & 0 & 0 & 0.557 & -0.00001289 & 0.3479 & 0 \\ 0.05652 & 0 & -0.003514 & 0 & -0.05652 & -0.1757 & 0 & 0 & -1.024 \end{array}\right]$$

$$D = \begin{bmatrix} -0.557 \\ 0.1757 \end{bmatrix}$$

Table 4c. System Matrices for Shirley's Plant $1/s^2$.

$$A = \left[\begin{array}{cccc:cc:ccc} 0 & 1 & 0 & 0 & 0 & 0 & 0 & 0 & 0 \\ 0 & 0 & 1 & 0 & 0 & 0 & 0 & 0 & 0 \\ 0 & 0 & 0 & 1 & 0 & 0 & 0 & 0 & 0 \\ -16 & -32 & -24 & -8 & 0 & 0 & 0 & 0 & 0 \\ \hdashline 0 & 0 & 0 & 0 & 0 & 1 & 0 & 0 & 0 \\ 0 & 0 & 0 & 0 & 0 & 0 & 0 & 0 & 0 \\ \hdashline 0 & 0 & 0 & 0 & 0 & 0 & 0 & 1 & 0 \\ 0 & 0 & 1.6 & 0 & 0 & 0 & -0.001852 & -0.02083 & 0 \\ \hdashline 0.00585 & 0 & -0.0003472 & 0 & -0.005585 & 0 & 0 & 0 & -0.2 \end{array}\right]$$

$$B' = \left[\begin{array}{cccc:cc:ccc} 0 & 0 & 0 & 0 & 0 & 1 & 0 & -1.6 & 0.0003472 \end{array}\right]$$

$$E' = \left[\begin{array}{cccc:cc:ccc} 0 & 0 & 0 & 1 & 0 & 0 & 0 & 0 & 0 \end{array}\right]$$

$$C = \left[\begin{array}{cccc:cc:ccc} 0 & 0 & 0.01114 & 0 & 0 & 0 & -0.00001289 & 0.3479 & 0 \\ 0 & 0 & -0.003514 & 0 & -0.05652 & 0 & 0 & 0 & -1.024 \end{array}\right]$$

$$D = \left[\begin{array}{c} -0.0111 \\ 0.003514 \end{array}\right]$$

Table 4d. System Matrices for Shirley's Plant $15/(s^2 + 3s + 15)$.

$$A = \left[\begin{array}{cccc:cc:cc:c} 0 & 1 & 0 & 0 & 0 & 0 & 0 & 0 & 0 \\ 0 & 0 & 1 & 0 & 0 & 0 & 0 & 0 & 0 \\ 0 & 0 & 0 & 1 & 0 & 0 & 0 & 0 & 0 \\ -16 & -32 & -24 & -8 & 0 & 0 & 0 & 0 & 0 \\ \hdashline 0 & 0 & 0 & 0 & 0 & 1 & 0 & 0 & 0 \\ 0 & 0 & 0 & 0 & -15 & -3 & 0 & 0 & 0 \\ \hdashline 0 & 0 & 0 & 0 & 0 & 0 & 0 & 1 & 0 \\ 0 & 0 & 1.6 & 0 & 24 & 4.8 & -0.001852 & -0.02083 & 0 \\ \hdashline 0.00585 & 0 & -0.0003472 & 0 & -0.01079 & -0.001041 & 0 & 0 & -0.2 \end{array}\right]$$

$$B' = \left[\begin{array}{cccc:cc:cc:c} 0 & 0 & 0 & 0 & 0 & 15 & 0 & 24 & 0.005208 \end{array}\right]$$

$$E' = \left[\begin{array}{cccc:cc:cc:c} 0 & 0 & 0 & 1 & 0 & 0 & 0 & 0 & 0 \end{array}\right]$$

$$C = \left[\begin{array}{cccc:cc:cc:c} 0 & 0 & 0.01114 & 0 & 0.1670 & 0.03341 & -0.00001289 & 0.3479 & 0 \\ 0.05652 & 0 & -0.003514 & 0 & -0.1092 & -0.01053 & 0 & 0 & -1.024 \end{array}\right]$$

$$D = \left[\begin{array}{c} -0.1670 \\ 0.05271 \end{array}\right]$$

Table 4e. System Matrices for Shirley's Plant $10/(s^2 + 10)$.

$$A = \left[\begin{array}{cccc:cc:ccc} 0 & 1 & 0 & 0 & 0 & 0 & 0 & 0 & 0 \\ 0 & 0 & 1 & 0 & 0 & 0 & 0 & 0 & 0 \\ 0 & 0 & 0 & 1 & 0 & 0 & 0 & 0 & 0 \\ -16 & -32 & -24 & -8 & 0 & 0 & 0 & 0 & 0 \\ \hdashline 0 & 0 & 0 & 0 & 0 & 1 & 0 & 0 & 0 \\ 0 & 0 & 0 & 0 & -10 & 0 & 0 & 0 & 0 \\ \hdashline 0 & 0 & 0 & 0 & 0 & 0 & 0 & 1 & 0 \\ 0 & 0 & 1.6 & 0 & 16 & 0 & -0.001852 & -0.02083 & 0 \\ \hdashline 0.00585 & 0 & -0.0003472 & 0 & -0.009057 & 0 & 0 & 0 & -0.2 \end{array}\right]$$

$$B' = \left[\begin{array}{cccc:cc:ccc} 0 & 0 & 0 & 0 & 0 & 10 & 0 & -16 & 0.003472 \end{array}\right]$$

$$E' = \left[\begin{array}{cccc:cc:ccc} 0 & 0 & 0 & 1 & 0 & 0 & 0 & 0 & 0 \end{array}\right]$$

$$C = \left[\begin{array}{cccc:cc:ccc} 0 & 0 & 0.01114 & 0 & 0.1114 & 0 & -0.00001289 & 0.3479 & 0 \\ 0.05652 & 0 & -0.003514 & 0 & -0.09166 & 0 & 0 & 0 & -1.024 \end{array}\right]$$

$$D = \left[\begin{array}{c} -0.1114 \\ 0.03514 \end{array}\right]$$

Table 5. Control-Rate Weighting Coefficients for Shirley's Cases. (T_N = 0.1 sec)

Controlled Element	Q_r (sec^2/in^2)	$\dot{u}_{max}$ (in/sec)
$\frac{1}{s(s+4)}$	0.012	9.13
$\frac{1}{s(0.02s+1)}$	2.20	0.67
$\frac{1}{s^2}$	0.035	5.35
$\frac{15}{s^2+3s+15}$	2.476	0.64
$\frac{10}{s^2+10}$	2.468	0.64

The only remaining unspecified parameter in the model is the vestibular noise/signal ratio, which is the one under investigation. The RMS error predictions of the model are compared with the experimentally observed RMS tracking errors in Figure 5. It can be seen from the figure that three of the five controlled elements chosen for analysis give a consistent noise/signal ratio of approximately -18 dB for agreement between the model and the experimental data. The higher predictions of the 1/s plant, and the lower predictions of the $10/(s^2 + 10)$ plant could arise from the effect of different levels of motor noise induced by motion effects. Since the 1/s plant is generally a very easy control task that would result in smooth motion, a lower value of signal to noise ratio would be expected as compared to the highly oscillatory and

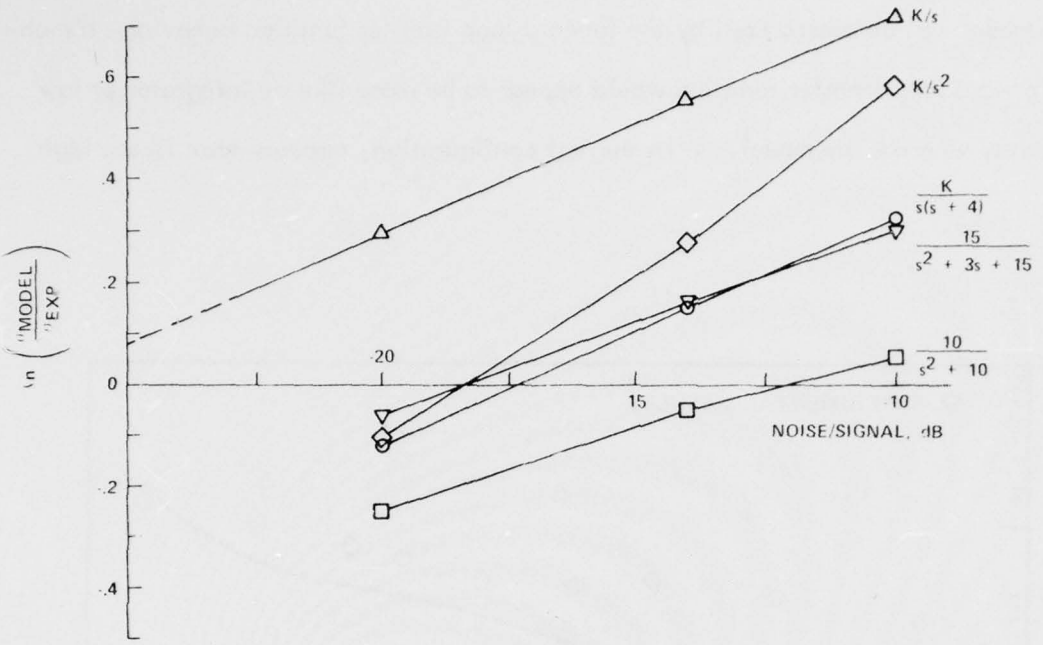

Figure 5. RMS Tracking Error: Comparison of Model Predictions With Shirley's Experimental Data.

more abrupt motions resulting in the control of $10/(s^2 + 10)$. This explanation would be appropriate for the oscillatory plant, but is not entirely satisfactory for the integrator, since the -25 dB value is appropriate for fixed-base tracking conditions.

To further explore the predictions of the model, Figures 6a through 6e depict the describing functions predicted by the model and the corresponding experimental data recorded by Shirley. For all of the plants except 1/s, there is good to excellent agreement between the experimental results and the analytical predictions in the mid to high frequency range. All describing functions show a characteristic decrease in amplitude and increase in phase at frequencies below approximately 0.3 rad/sec, which is consistent with a low frequency differentiator. On the other hand, the describing function for 1/s has the same basic form, but is obviously operating at too low a gain, which also explains the model's prediction of a larger RMS tracking error

than actually observed. The low frequency discrepancies between the experimental data and the model can be summarized by the forward loop transfer function behavior: the observed forward loop transfer function would appear to be more like an integrator at low frequencies, whereas the model, in its current configuration, appears more like a high

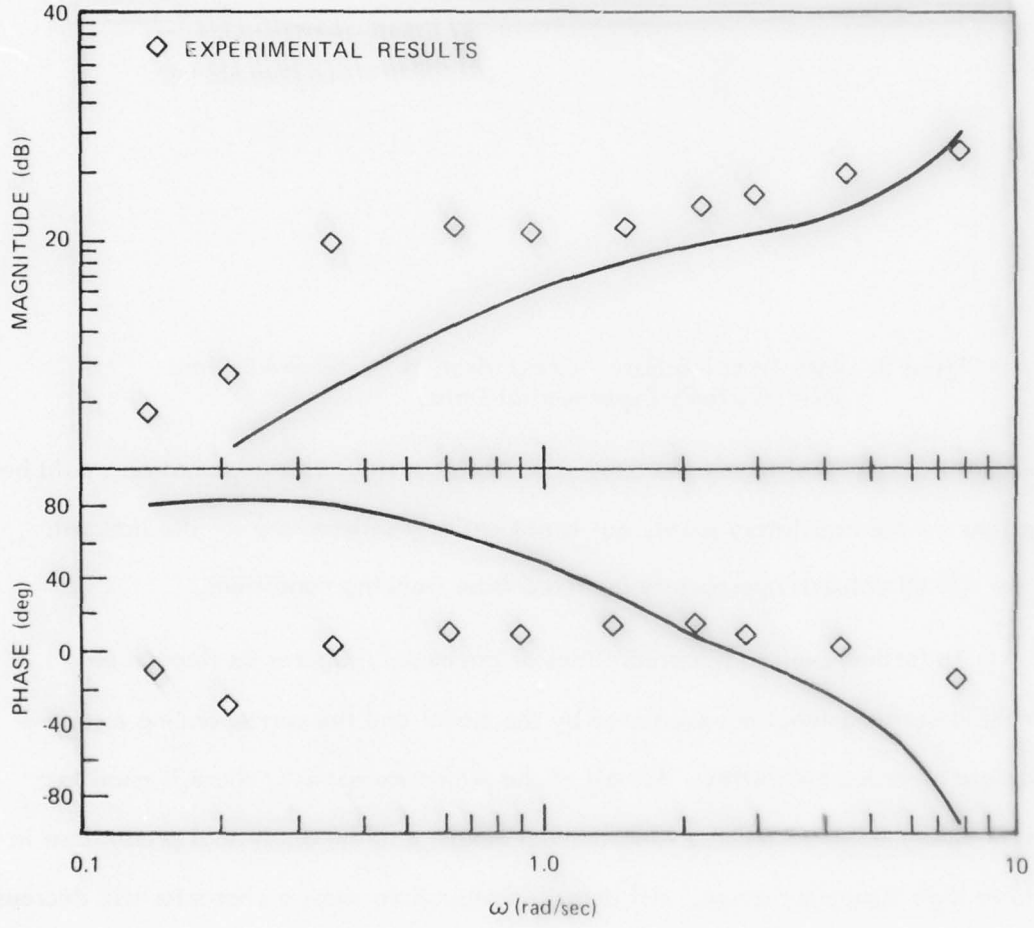

Figure 6a. Comparison of Model Describing Functions With Shirley's Experimental Data. ($Y_c = 1/s\ (s + 4)$)

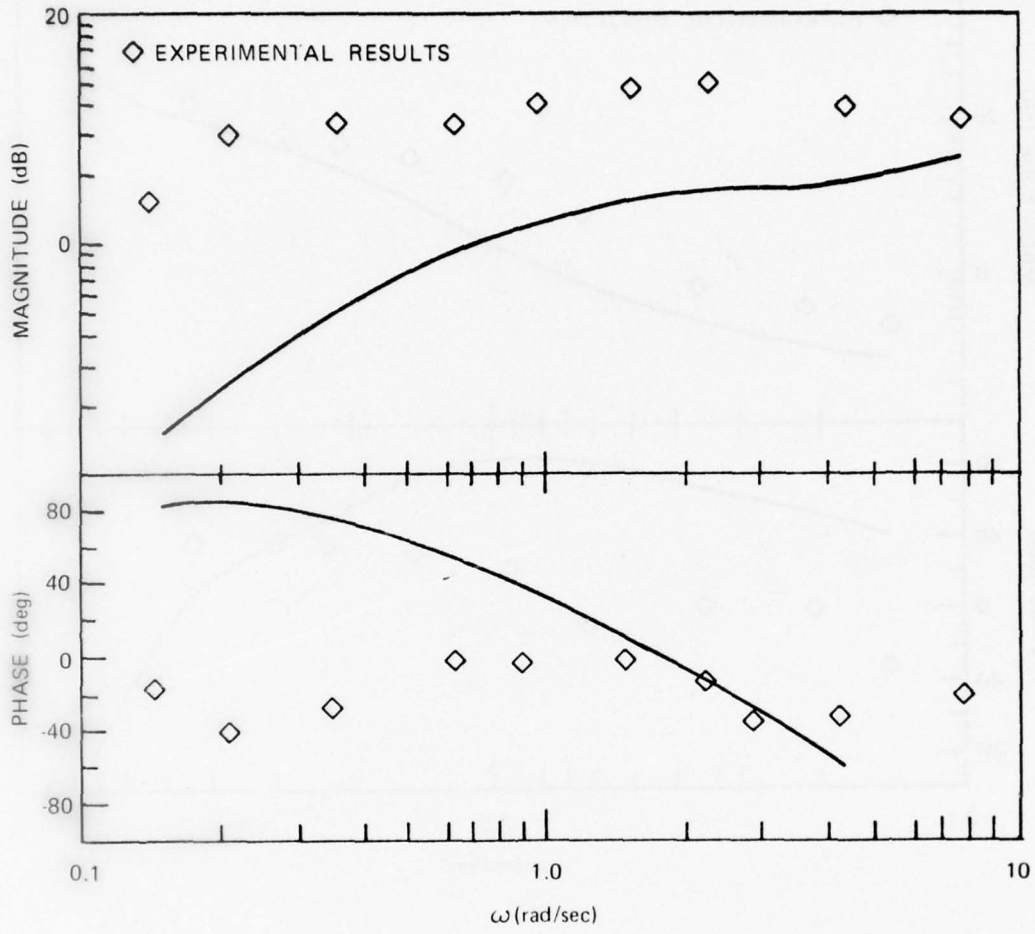

Figure 6b. Comparison of Model Describing Functions With Shirley's Experimental Data. ($Y_c = 1/s\ (.02s + 1)$)

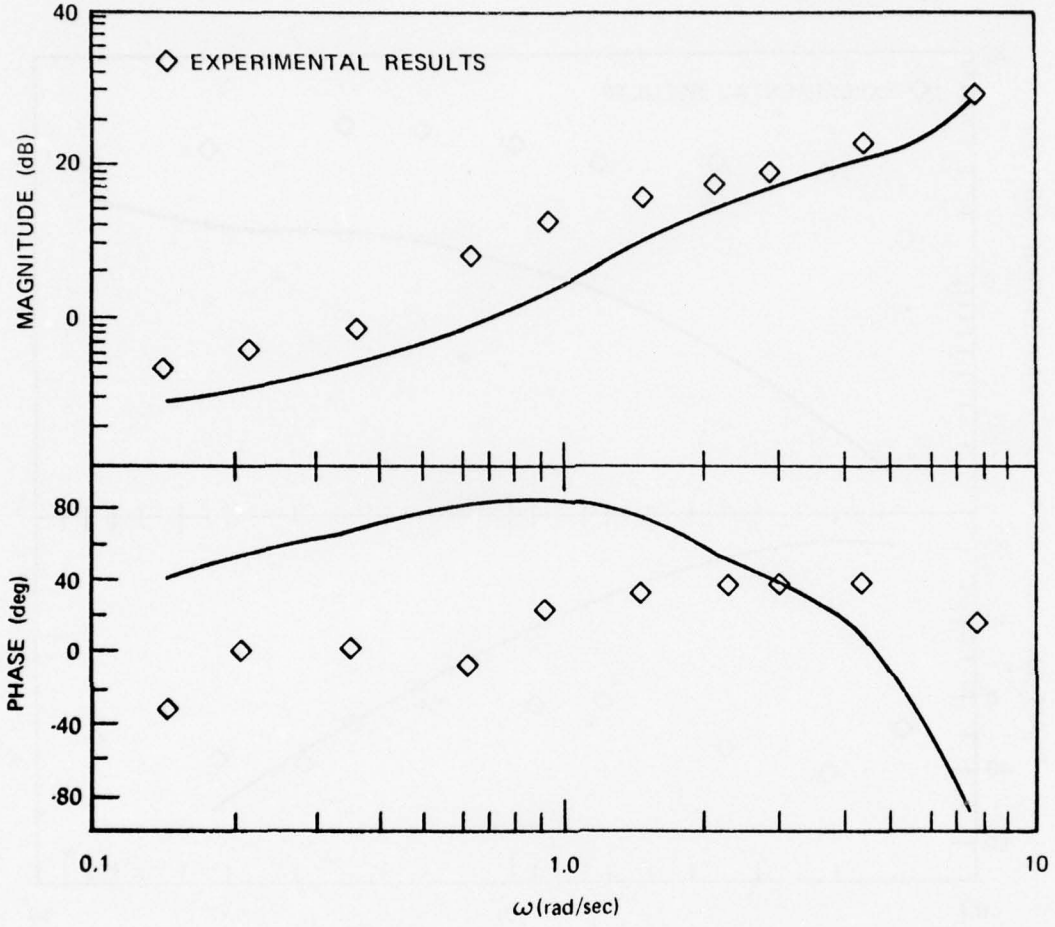

Figure 6c. Comparison of Model Describing Functions With Shirley's Experimental Data. ($Y_c = 1/s^2$)

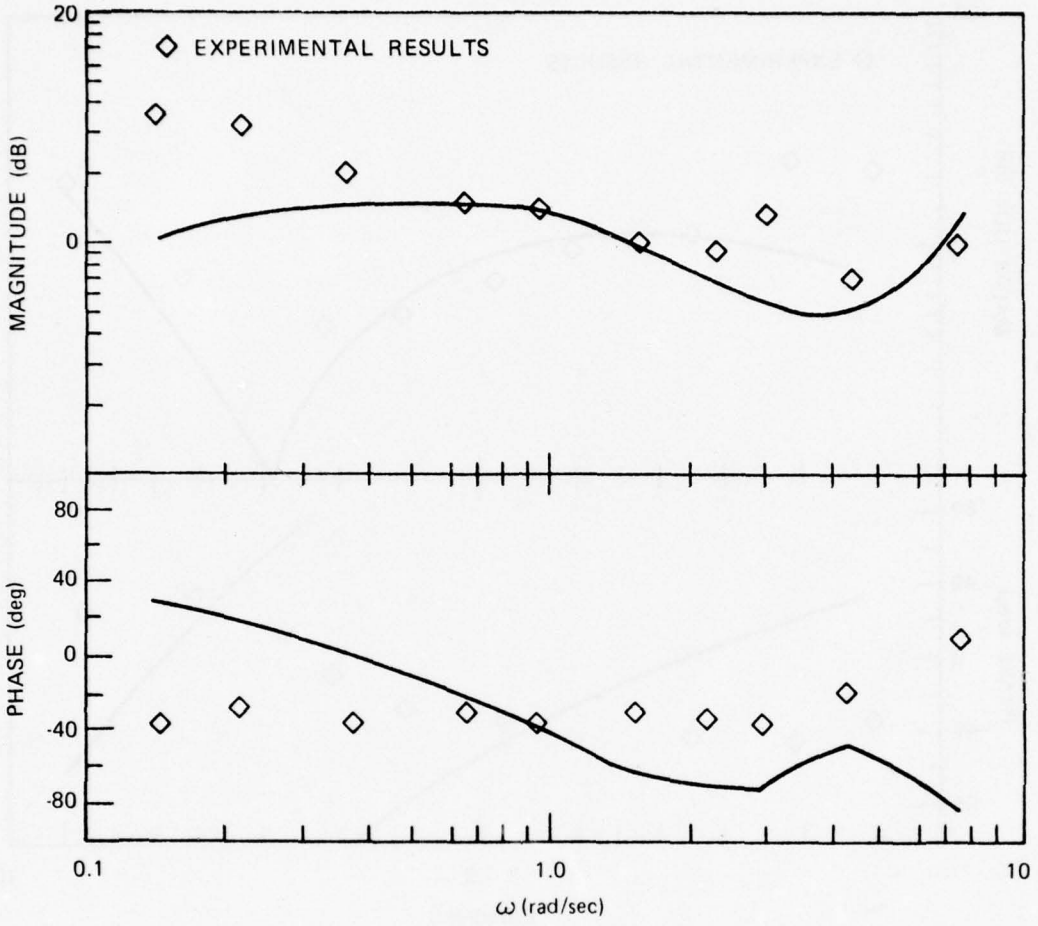

Figure 6d. Comparison of Model Describing Functions With Shirley's Experimental Data. ($Y_c = 15/(s^2 + 3s + 15)$)

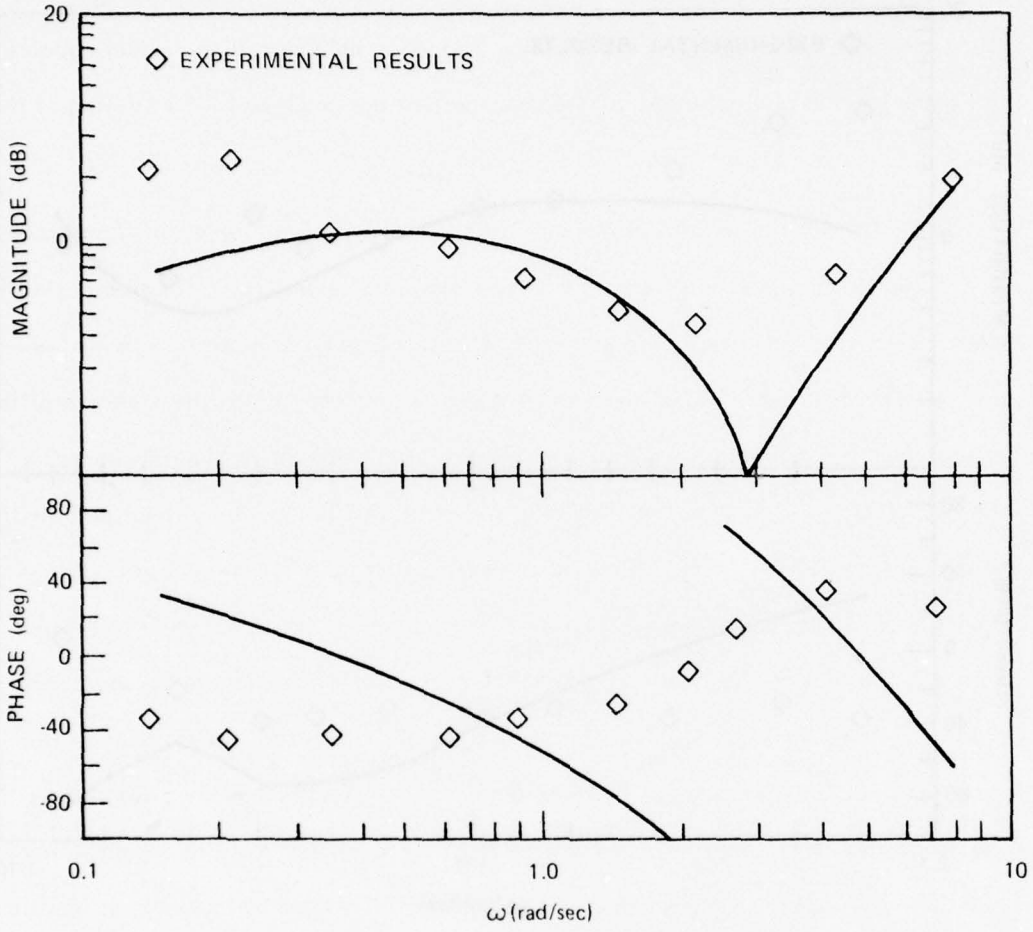

Figure 6e. Comparison of Model Describing Functions With Shirley's Experimental Data. ($Y_c = 10/(s^2 + 10)$)

gain at low frequencies. This can be shown to be the optimal control strategy for a first order correlated input. Thus, the low frequency behavior of the model appears to be an inherent characteristic of the optimization approach and the modeling of the motor noise at the output of the model.

To explore the appropriateness of the cost function, the optimal control model was exercised with different relative weights on semicircular canal and otolith measurements. Our hypothesis was that an increased weight on the otolith measurement would raise the pilot gain at low frequencies because the low frequency otolith measurement is essentially one of angle with respect to the vertical. However, increasing the weighting on the otolith measurement in the cost functional had negligible effect on the determination of the feedback gains, hence, the control strategy was essentially the same as when the otolith and semicircular canal were weighted equally. Increasing the relative importance of the semicircular canal measurement provided only a more pronounced deviation from the experimental data at the lower frequencies. Consequently, with the optimal control structure of the pilot model, the low frequency open-loop transfer function is likely to appear more as a gain rather than integrator, and this may differ from experimentally observed describing functions in some instances.

While it must be recognized that there is a deviation in the describing function predictions at low frequency, the measurement of describing functions is not reliable at these frequencies, and nearly the same control performance may be obtained in this portion of the spectrum if the human operator's gain is high enough. Thus, it was decided to continue to use the noise/signal ratio of -18 dB to represent the vestibular system remnant. This is a good prediction of RMS performance for three plants, and, as will be seem subsequently, it gives good predictions of performance in other situations as well.

4.2 APPLICATION OF THE MOTION CUE MODEL TO VTOL HOVERING

This section describes the application of the optimal control model of the pilot to the VTOL hovering task described in Ringland, Stapleford, and Magdaleno (Reference 23). The model has been applied to the following motion conditions:

- Fixed-Base (FB)
- Moving-Base, Angular Motion Only (MBA)
- Moving-Base, Linear and Angular Cues (MBL)

Three tracking tasks were conducted simultaneously; these were:

- Longitudinal
- Lateral
- Vertical

For the longitudinal and lateral tracking tasks, experimental data are available for both "good" and "bad" dynamics, corresponding to the degree of aerodynamic damping; a total of 14 tracking tasks were possible in these conditions. In addition, these data provided an opportunity to compare visual scanning behavior with and without motion cues to the attention allocation among instruments as predicted by the model.

4.2.1 DESCRIPTION OF THE EXPERIMENT

This section describes the experiment used in the VTOL hovering task as described in Reference 23. The equations of motion of the vehicle are given by

- Longitudinal

$$\left.\begin{aligned} s(s - X_u)x + g\theta &= -X_u u_g \\ -M_u sx + s(s - M_q)\theta &= M_{\delta_e}\delta_e - M_u u_g \end{aligned}\right\} \qquad (32)$$

- Lateral

$$\left.\begin{aligned} s(s - Y_v)y - g\varphi &= -Y_v v_g \\ -L_v sy + s(s - L_p)\varphi &= L_{\delta_a}\delta_a - L_v v_g \end{aligned}\right\} \quad (33)$$

- Vertical

$$s(s - Z_w - Z'_w)z = Z_{\delta_c}\delta_c \quad (34)$$

The heading of the simulator was held constant through all experimental runs. The disturbance input to these equations were generated from first-order shaping filters with a time constant of 1 second (these were also included in the state equations). The state equations were further augmented by the dynamics of the simulator drive system, which were significant in the longitudinal direction. As shown in Reference 23, the motion system can be approximated by a first-order lag with a time constant of 0.1 second. The aerodynamic parameters used for examining the various motion conditions are shown in Table 6. The control sensitivities used in the experimental investigation are given in Table 7; we chose those values of gain corresponding to "good" configurations for each of three tracking tasks. The configurations resulting from the possible combinations of the dynamics are shown in Table 8. The majority of experimental results were given for configurations number 1, 3, 4, and 6 which correspond to the four possibilities of "good" and "bad" dynamics in each of the longitudinal and lateral axes. These are the systems examined with the model. The displays used by the pilot are shown schematically in Figure 7.

Table 6. Vehicle Aerodynamic Parameters (Reference 23).

a) Longitudinal Dynamics

Fixed Parameters:

$gM_u = 0.2\ sec^{-3}$, $X_u = -0.1\ sec^{-1}$

Variable Parameters:

$M_q (sec^{-1})$	Descriptor
-4.0	"Good"
1.0	"Mediocre"
0	"Bad"

b) Lateral Dynamics

Fixed Parameters:

$gL_v = -0.2\ sec^{-3}$, $Y_v = -0.1\ sec^{-1}$

Variable Parameters:

$L_p (sec^{-1})$	Descriptor
-4.0	"Good"
-0.5	"Bad"

c) Vertical Dynamics

Variable Parameters:

$Z_w (sec^{-1})$	$Z'_w (sec^{-1})$	Descriptor
-1.00	-3.00	"Good"
-1.00	-0	"Mediocre"
-0.25	0	"Bad"

Table 7. Control Sensitivities (Reference 23).

a) Longitudinal Task, M_{δ_e} $\frac{rad/sec^2}{inch}$

Configuration Descriptor	Optimum Gain	Subject		
		RG	EF	GB
"Good"	0.066	0.006	0.070	0.043
"Mediocre"	0.047	0.037	0.037	0.037
"Bad"	0.042	0.031	0.031	0.031

b) Lateral Task, L_{δ_a} $\frac{rad/sec^2}{inch}$

Configuration Descriptor	Optimum Gain	Subject		
		RG	EF	GB
"Good"	0.074	0.089	0.095	0.053
"Bad"	0.040	0.039	0.095	0.053

c) Vertical Task, Z_{δ_c} $\frac{ft/sec^2}{inch}$

Configuration Descriptor	Optimum Gain	Subject		
		RG	EF	GB
"Good"	-4.3	-4.91	-4.91	-4.91
"Mediocre"	-2.9	-3.10	-3.10	-3.10
"Bad"	-2.2	-0.77	-0.77	-0.77

Table 8. Vehicle Configurations (Reference 23).

Configuration No.	Longitudinal	Lateral	Vertical	ℓ_x
1	"Good"	"Good"	"Good"	0 ft
2	"Mediocre"	"Good"	"Good"	0 ft
3	"Bad"	"Good"	"Good"	0 ft
4	"Good"	"Bad"	"Good"	0 ft
5	"Mediocre"	"Bad"	"Good"	0 ft
6	"Bad"	"Bad"	"Good"	0 ft
7	"Good"	"Good"	"Mediocre"	0 ft
8	"Good"	"Good"	"Bad"	0 ft
9	"Good"	"Good"	"Good"	20 ft
10	"Mediocre"	"Good"	"Good"	20 ft
11	"Bad"	"Good"	"Good"	20 ft

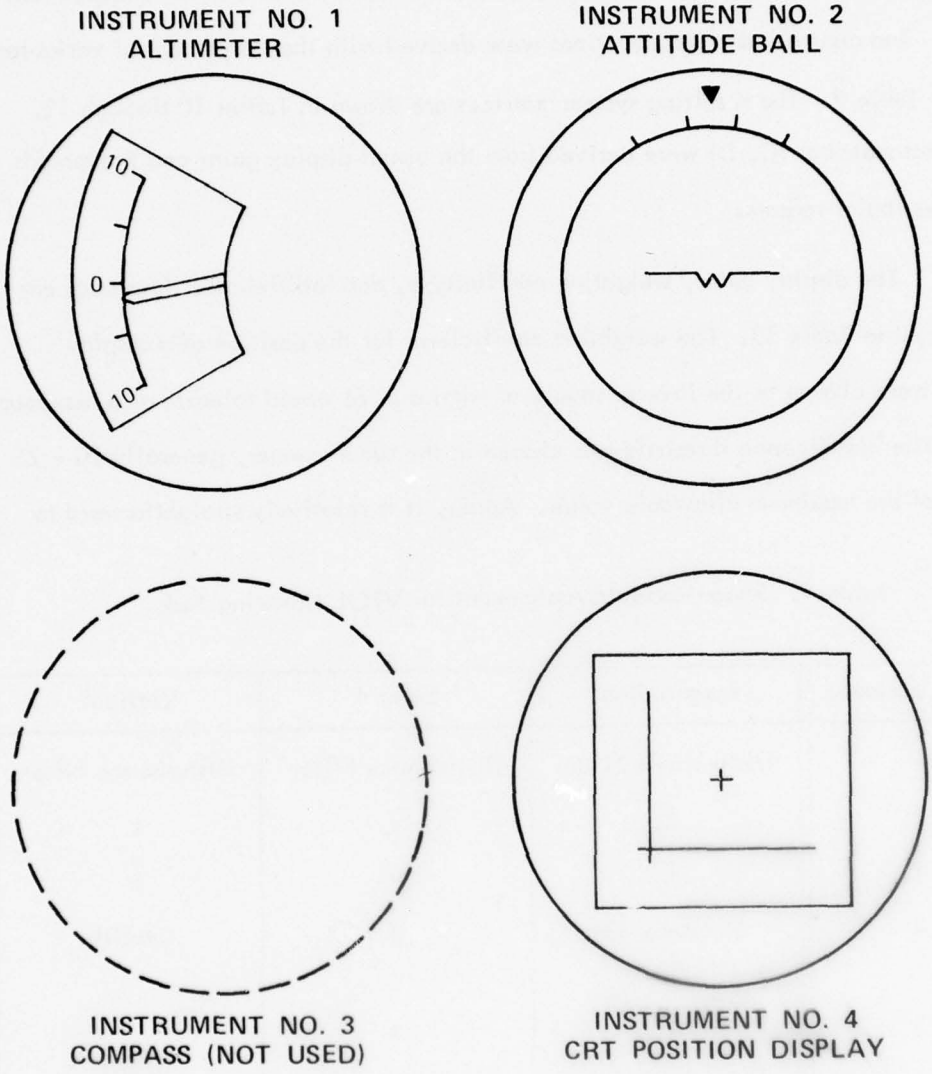

Figure 7. Display Panel Arrangement (Reference 23).

4.2.2 MODEL PARAMETERS

The controlled element dynamics for the control task are decoupled — thus the complete task may be considered as the simultaneous control of three independent systems. The controlled-state equations were derived with the assignment of variables shown in Table 9. The resulting system matrices are shown in Tables 10 through 12. The output matrices (C, D) were derived from the visual display gains and the models of the vestibular sensors.

The display gains, weighting coefficients, and indifference thresholds are summarized in Table 13. The weighting coefficients for the position of a display element were chosen as the inverse square of what a pilot would tolerate as a maximum value. The indifference threshold was chosen in the same manner, generally 20 - 25 percent of the maximum allowable value. Again, it is relatively straightforward to

Table 9. State-Variable Assignment for VTOL Hovering Task.

State Variable	Longitudinal	Lateral	Vertical
1	Disturbance Filter	Disturbance Filter	Disturbance Filter
2	x	y	z
3	$\dot{x}$	$\dot{y}$	$\dot{z}$
4	Simulator Lag* $(\ddot{x})$	ϕ	Otolith
5	θ	$\dot{\phi}$	
6	q	SCC_1	
7	SCC_1	SCC_2	
8	SCC_2	Otolith	
9	Otolith		

* Included only for MBL.

Table 10a. RS&M System Matrices - Longitudinal, Good, FB.

$$A = \begin{bmatrix} -1 & 0 & 0 & 0 & 0 & 0 & 0 & 0 \\ 0 & 0 & 1 & 0 & 0 & 0 & 0 & 0 \\ 0.1 & 0 & -0.1 & -32.17 & 0 & 0 & 0 & 0 \\ 0 & 0 & 0 & 0 & 1 & 0 & 0 & 0 \\ -0.006217 & 0 & 0.006217 & 0 & -4 & 0 & 0 & 0 \\ 0 & 0 & 0 & 0 & 0 & 0 & 1 & 0 \\ -0.3562 & 0 & 0.3562 & 0 & -229.2 & -0.001852 & -0.08888 & 0 \\ 0 & 0 & 0 & -0.2 & 0 & 0 & 0 & -0.2 \end{bmatrix}$$

$$B' = \begin{bmatrix} 0 & 0 & 0 & 0 & 0.066 & 0 & 3.782 & 0 \end{bmatrix}$$

$$E' = \begin{bmatrix} 1 & 0 & 0 & 0 & 0 & 0 & 0 & 0 \end{bmatrix}$$

$$C = \begin{bmatrix} 0 & 0.1099 & 0 & 0 & 0 & 0 & 0 & 0 \\ 0 & 0 & 0.1099 & 0 & 0 & 0 & 0 & 0 \\ 0 & 0 & 0 & 286.5 & 0 & 0 & 0 & 0 \\ 0 & 0 & 0 & 0 & 286.5 & 0 & 0 & 0 \end{bmatrix}$$

$$D' = \begin{bmatrix} 0 & 0 & 0 \end{bmatrix}$$

Table 10b. RS&M System Matrices - Longitudinal, Good, MBA.

$$A = \begin{bmatrix} -1 & 0 & 0 & 0 & 0 & 0 & 0 & 0 \\ 0 & 0 & 1 & 0 & 0 & 0 & 0 & 0 \\ 0.1 & 0 & -0.1 & -32.17 & 0 & 0 & 0 & 0 \\ 0 & 0 & 0 & 0 & 1 & 0 & 0 & 0 \\ -0.006217 & 0 & 0.006217 & 0 & -4 & 0 & 0 & 0 \\ 0 & 0 & 0 & 0 & 0 & 0 & 1 & 0 \\ -0.3562 & 0 & 0.3562 & 0 & -229.2 & -0.001852 & -0.08888 & 0 \\ 0 & 0 & 0 & -0.2 & 0 & 0 & 0 & -0.2 \end{bmatrix}$$

$$B' = \begin{bmatrix} 0 & 0 & 0 & 0 & 0.066 & 0 & 3.782 & 0 \end{bmatrix}$$

$$E' = \begin{bmatrix} 1 & 0 & 0 & 0 & 0 & 0 & 0 & 0 \end{bmatrix}$$

$$C = \begin{bmatrix} 0 & 0.1099 & 0 & 0 & 0 & 0 & 0 & 0 \\ 0 & 0 & 0.1099 & 0 & 0 & 0 & 0 & 0 \\ 0 & 0 & 0 & 286.5 & 0 & 0 & 0 & 0 \\ 0 & 0 & 0 & 0 & 286.5 & 0 & 0 & 0 \\ -0.002479 & 0 & 0.002479 & 0 & -1.595 & -0.00001289 & 0.3475 & 0 \\ 0 & 0 & 0 & -2.024 & 0 & 0 & 0 & -1.024 \end{bmatrix}$$

$$D' = \begin{bmatrix} 0 & 0 & 0 & 0 & 0.02632 & 0 \end{bmatrix}$$

Table 10c. RS&M System Matrices - Longitudinal, Good, MBL.

$$A = \begin{bmatrix} -1 & 0 & 0 & 0 & 0 & 0 & 0 & 0 & 0 \\ 0 & 0 & 1 & 0 & 0 & 0 & 0 & 0 & 0 \\ 0 & 0 & 0 & 1 & 0 & 0 & 0 & 0 & 0 \\ 1 & 0 & -1 & -10 & -321.7 & 0 & 0 & 0 & 0 \\ 0 & 0 & 0 & 0 & 0 & 1 & 0 & 0 & 0 \\ -0.006217 & 0 & 0.006217 & 0 & 0 & -4 & 0 & 0 & 0 \\ 0 & 0 & 0 & 0 & 0 & 0 & 0 & 1 & 0 \\ -0.3562 & 0 & 0.3562 & 0 & 0 & -229.2 & -0.001852 & -0.08888 & 0 \\ 0 & 0 & 0 & -0.006217 & -0.2 & 0 & 0 & 0 & -0.2 \end{bmatrix}$$

$$B' = \begin{bmatrix} 0 & 0 & 0 & 0 & 0 & 0.066 & 0 & 3.782 & 0 \end{bmatrix}$$

$$E' = \begin{bmatrix} 1 & 0 & 0 & 0 & 0 & 0 & 0 & 0 & 0 \end{bmatrix}$$

$$C = \begin{bmatrix} 0 & 0.1099 & 0 & 0 & 0 & 0 & 0 & 0 & 0 \\ 0 & 0 & 0.1099 & 0 & 0 & 0 & 0 & 0 & 0 \\ 0 & 0 & 0 & 0 & 286.5 & 0 & 0 & 0 & 0 \\ 0 & 0 & 0 & 0 & 0 & 286.5 & 0 & 0 & 0 \\ -0.002479 & 0 & 0.002479 & 0 & 0 & -1.595 & -0.00001289 & 0.3475 & 0 \\ 0 & 0 & 0 & -0.006292 & -2.024 & 0 & 0 & 0 & -1.024 \end{bmatrix}$$

$$D' = \begin{bmatrix} 0 & 0 & 0 & 0 & 0.02632 & 0 \end{bmatrix}$$

Table 10d. RS&M System Matrices - Longitudinal, Bad, FB.

$$A = \begin{bmatrix} -1 & 0 & 0 & 0 & 0 & 0 & 0 & 0 \\ 0 & 0 & 1 & 0 & 0 & 0 & 0 & 0 \\ 0.1 & 0 & -0.1 & -32.17 & 0 & 0 & 0 & 0 \\ 0 & 0 & 0 & 0 & 1 & 0 & 0 & 0 \\ -0.006217 & 0 & 0.006217 & 0 & 0 & 0 & 0 & 0 \\ 0 & 0 & 0 & 0 & 0 & 0 & 1 & 0 \\ -0.3562 & 0 & 0.3562 & 0 & 0 & -0.001852 & -0.08888 & 0 \\ 0 & 0 & 0 & -0.2 & 0 & 0 & 0 & -0.2 \end{bmatrix}$$

$$B' = \begin{bmatrix} 0 & 0 & 0 & 0 & 0.066 & 0 & 3.782 & 0 \end{bmatrix}$$

$$E' = \begin{bmatrix} 1 & 0 & 0 & 0 & 0 & 0 & 0 & 0 \end{bmatrix}$$

$$C = \begin{bmatrix} 0 & 0.1099 & 0 & 0 & 0 & 0 & 0 & 0 \\ 0 & 0 & 0.1099 & 0 & 0 & 0 & 0 & 0 \\ 0 & 0 & 0 & 286.5 & 0 & 0 & 0 & 0 \\ 0 & 0 & 0 & 0 & 286.5 & 0 & 0 & 0 \end{bmatrix}$$

$$D' = \begin{bmatrix} 0 & 0 & 0 & 0 \end{bmatrix}$$

Table 10e. RS&M System Matrices - Longitudinal, Bad, MBA.

$$A = \begin{bmatrix} -1 & 0 & 0 & 0 & 0 & 0 & 0 & 0 \\ 0 & 0 & 1 & 0 & 0 & 0 & 0 & 0 \\ 0.1 & 0 & -0.1 & -32.17 & 0 & 0 & 0 & 0 \\ 0 & 0 & 0 & 0 & 1 & 0 & 0 & 0 \\ -0.006217 & 0 & 0.006217 & 0 & 0 & 0 & 0 & 0 \\ 0 & 0 & 0 & 0 & 0 & 0 & 1 & 0 \\ -0.3562 & 0 & 0.3562 & 0 & 0 & -0.001852 & -0.08888 & 0 \\ 0 & 0 & 0 & -0.2 & 0 & 0 & 0 & -0.2 \end{bmatrix}$$

$$B' = \begin{bmatrix} 0 & 0 & 0 & 0 & 0.066 & 0 & 3.782 & 0 \end{bmatrix}$$

$$E' = \begin{bmatrix} 1 & 0 & 0 & 0 & 0 & 0 & 0 & 0 \end{bmatrix}$$

$$C = \begin{bmatrix} 0 & 0.1099 & 0 & 0 & 0 & 0 & 0 & 0 \\ 0 & 0 & 0.1099 & 0 & 0 & 0 & 0 & 0 \\ 0 & 0 & 0 & 286.5 & 0 & 0 & 0 & 0 \\ 0 & 0 & 0 & 0 & 286.5 & 0 & 0 & 0 \\ -0.002479 & 0 & 0.002479 & 0 & 0 & -0.00001289 & 0.3475 & 0 \\ 0 & 0 & 0 & -2.024 & 0 & 0 & 0 & -1.024 \end{bmatrix}$$

$$D' = \begin{bmatrix} 0 & 0 & 0 & 0 & 0.02632 & 0 \end{bmatrix}$$

Table 10f. RS&M System Matrices - Longitudinal, Bad, MBL.

$$A = \begin{bmatrix} -1 & 0 & 0 & 0 & 0 & 0 & 0 & 0 & 0 \\ 0 & 0 & 1 & 0 & 0 & 0 & 0 & 0 & 0 \\ 0 & 0 & 0 & 1 & 0 & 0 & 0 & 0 & 0 \\ 1 & 0 & -1 & -10 & -321.7 & 0 & 0 & 0 & 0 \\ 0 & 0 & 0 & 0 & 0 & 1 & 0 & 0 & 0 \\ -0.006217 & 0 & 0.006217 & 0 & 0 & 0 & 0 & 0 & 0 \\ 0 & 0 & 0 & 0 & 0 & 0 & 0 & 1 & 0 \\ -0.3562 & 0 & 0.3562 & 0 & 0 & 0 & -0.001852 & -0.08888 & 0 \\ 0 & 0 & 0 & -0.006217 & -0.2 & 0 & 0 & 0 & -0.2 \end{bmatrix}$$

$$B' = \begin{bmatrix} 0 & 0 & 0 & 0 & 0 & 0.066 & 0 & 3.782 & 0 \end{bmatrix}$$

$$E' = \begin{bmatrix} 1 & 0 & 0 & 0 & 0 & 0 & 0 & 0 & 0 \end{bmatrix}$$

$$C = \begin{bmatrix} 0 & 0.1099 & 0 & 0 & 0 & 0 & 0 & 0 & 0 \\ 0 & 0 & 0.1099 & 0 & 0 & 0 & 0 & 0 & 0 \\ 0 & 0 & 0 & 0 & 286.5 & 0 & 0 & 0 & 0 \\ 0 & 0 & 0 & 0 & 0 & 286.5 & 0 & 0 & 0 \\ -0.002479 & 0 & 0.002479 & 0 & 0 & 0 & -0.00001289 & 0.3475 & 0 \\ 0 & 0 & 0 & -0.06292 & -2.024 & 0 & 0 & 0 & -1.024 \end{bmatrix}$$

$$D' = \begin{bmatrix} 0 & 0 & 0 & 0 & 0.02632 & 0 \end{bmatrix}$$

Table 11a. RS&M System Matrices - Lateral, Good, FB.

$$A = \begin{bmatrix} -1 & 0 & 0 & 0 & 0 & 0 & 0 & 0 \\ 0 & 0 & 1 & 0 & 0 & 0 & 0 & 0 \\ 0.1 & 0 & -1 & 32.17 & 0 & 0 & 0 & 0 \\ 0 & 0 & 0 & 0 & 1 & 0 & 0 & 0 \\ 0.006217 & 0 & -0.006217 & 0 & -4 & 0 & 0 & 0 \\ 0 & 0 & 0 & 0 & 0 & 0 & 1 & 0 \\ 0.3562 & 0 & -0.3562 & 0 & -229.2 & -0.001852 & -0.08888 & 0 \\ -0.0006217 & 0 & 0 & 0 & 0 & 0 & 0 & -0.2 \end{bmatrix}$$

$$B' = \begin{bmatrix} 0 & 0 & 0 & 0 & 0.0742 & 0 & 4.24 & 0 \end{bmatrix}$$

$$E' = \begin{bmatrix} 1 & 0 & 0 & 0 & 0 & 0 & 0 & 0 \end{bmatrix}$$

$$C = \begin{bmatrix} 0 & 0.1099 & & 0 & 0 & 0 & 0 & 0 \\ 0 & 0 & 0.1099 & 0 & 0 & 0 & 0 & 0 \\ 0 & 0 & 0 & 286.5 & 0 & 0 & 0 & 0 \\ 0 & 0 & 0 & 0 & 286.5 & 0 & 0 & 0 \end{bmatrix}$$

$$D' = \begin{bmatrix} 0 & 0 & 0 & 0 \end{bmatrix}$$

Table 11b. RS&M System Matrices - Lateral, Good, MBA.

$$A = \begin{bmatrix} -1 & 0 & 0 & 0 & 0 & 0 & 0 & 0 \\ 0 & 0 & 1 & 0 & 0 & 0 & 0 & 0 \\ 0.1 & 0 & -1 & 32.17 & 0 & 0 & 0 & 0 \\ 0 & 0 & 0 & 0 & 1 & 0 & 0 & 0 \\ 0.006217 & 0 & -0.006217 & 0 & -4 & 0 & 0 & 0 \\ 0 & 0 & 0 & 0 & 0 & 0 & 1 & 0 \\ 0.3562 & 0 & -0.3562 & 0 & -229.2 & -0.001852 & -0.08888 & 0 \\ 0 & 0 & 0 & 0.2 & 0 & 0 & 0 & -0.2 \end{bmatrix}$$

$$B' = \begin{bmatrix} 0 & 0 & 0 & 0 & 0.0742 & 0 & 4.24 & 0 \end{bmatrix}$$

$$E' = \begin{bmatrix} 1 & 0 & 0 & 0 & 0 & 0 & 0 & 0 \end{bmatrix}$$

$$C = \begin{bmatrix} 0 & 0.1099 & 0 & 0 & 0 & 0 & 0 & 0 \\ 0 & 0 & 0.1099 & 0 & 0 & 0 & 0 & 0 \\ 0 & 0 & 0 & 286.5 & 0 & 0 & 0 & 0 \\ 0 & 0 & 0 & 0 & 286.5 & 0 & 0 & 0 \\ 0.00247 & 0 & -0.002479 & 0 & -1.595 & -0.00001289 & 0.3475 & 0 \\ 0 & 0 & 0 & 2.024 & 0 & 0 & 0 & -1.024 \end{bmatrix}$$

$$D' = \begin{bmatrix} 0 & 0 & 0 & 0 & 0.0295 & 0 \end{bmatrix}$$

Table 11c. RS&M System Matrices - Lateral, Good, MBL.

$$A = \begin{bmatrix} -1 & 0 & 0 & 0 & 0 & 0 & 0 & 0 \\ 0 & 0 & 1 & 0 & 0 & 0 & 0 & 0 \\ 0.1 & 0 & -1 & 32.17 & 0 & 0 & 0 & 0 \\ 0 & 0 & 0 & 0 & 1 & 0 & 0 & 0 \\ 0.006217 & 0 & -0.006217 & 0 & -4 & 0 & 0 & 0 \\ 0 & 0 & 0 & 0 & 0 & 0 & 1 & 0 \\ 0.3562 & 0 & -0.3562 & 0 & -229.2 & -0.001852 & -0.08888 & 0 \\ -0.0006217 & 0 & 0 & 0 & 0 & 0 & 0 & -0.2 \end{bmatrix}$$

$$B' = \begin{bmatrix} 0 & 0 & 0 & 0 & 0.0742 & 0 & 4.24 & 0 \end{bmatrix}$$

$$E = \begin{bmatrix} 1 & 0 & 0 & 0 & 0 & 0 & 0 & 0 \end{bmatrix}$$

$$C = \begin{bmatrix} 0 & 0.1099 & 0 & 0 & 0 & 0 & 0 & 0 \\ 0 & 0 & 0.1099 & 0 & 0 & 0 & 0 & 0 \\ 0 & 0 & 0 & 286.5 & 0 & 0 & 0 & 0 \\ 0 & 0 & 0 & 0 & 286.5 & 0 & 0 & 0 \\ 0.00247 & 0 & -0.002479 & 0 & -1.595 & -0.00001289 & 0.3475 & 0 \\ -0.006292 & 0 & 0.006292 & 0 & 0 & 0 & 0 & -1.024 \end{bmatrix}$$

$$D' = \begin{bmatrix} 0 & 0 & 0 & 0 & 0.0295 & 0 \end{bmatrix}$$

Table 11d. RS&M System Matrices - Lateral, Bad, FB.

$$A = \begin{bmatrix} -1 & 0 & 0 & 0 & 0 & 0 & 0 & 0 \\ 0 & 0 & 1 & 0 & 0 & 0 & 0 & 0 \\ 0.1 & 0 & -1 & 32.17 & 0 & 0 & 0 & 0 \\ 0 & 0 & 0 & 0 & 1 & 0 & 0 & 0 \\ 0.006217 & 0 & -0.006217 & 0 & -0.5 & 0 & 0 & 0 \\ 0 & 0 & 0 & 0 & 0 & 0 & 1 & 0 \\ 0.3562 & 0 & -0.3562 & 0 & -28.65 & -0.001852 & -0.08888 & 0 \\ -0.0006217 & 0 & 0 & 0 & 0 & 0 & 0 & -0.2 \end{bmatrix}$$

$$B' = \begin{bmatrix} 0 & 0 & 0 & 0 & 0.0742 & 0 & 4.24 & 0 \end{bmatrix}$$

$$E' = \begin{bmatrix} 1 & 0 & 0 & 0 & 0 & 0 & 0 & 0 \end{bmatrix}$$

$$C = \begin{bmatrix} 0 & 0.1099 & 0 & 0 & 0 & 0 & 0 & 0 \\ 0 & 0 & 0.1099 & 0 & 0 & 0 & 0 & 0 \\ 0 & 0 & 0 & 286.5 & 0 & 0 & 0 & 0 \\ 0 & 0 & 0 & 0 & 286.5 & 0 & 0 & 0 \end{bmatrix}$$

$$D' = \begin{bmatrix} 0 & 0 & 0 & 0 \end{bmatrix}$$

Table 11e. RS&M System Matrices - Lateral, Bad, MBA.

$$A = \begin{bmatrix} -1 & 0 & 0 & 0 & 0 & 0 & 0 & 0 \\ 0 & 0 & 1 & 0 & 0 & 0 & 0 & 0 \\ 0.1 & 0 & -1 & 32.17 & 0 & 0 & 0 & 0 \\ 0 & 0 & 0 & 0 & 1 & 0 & 0 & 0 \\ 0.006217 & 0 & -0.006217 & 0 & -0.5 & 0 & 0 & 0 \\ 0 & 0 & 0 & 0 & 0 & 0 & 1 & 0 \\ 0.3562 & 0 & -0.3562 & 0 & 28.65 & -0.001852 & -0.08888 & 0 \\ 0 & 0 & 0 & 0.2 & 0 & 0 & 0 & -0.2 \end{bmatrix}$$

$$B' = \begin{bmatrix} 0 & 0 & 0 & 0 & 0.0742 & 0 & 4.24 & 0 \end{bmatrix}$$

$$E' = \begin{bmatrix} 1 & 0 & 0 & 0 & 0 & 0 & 0 & 0 \end{bmatrix}$$

$$C = \begin{bmatrix} 0 & 0.1099 & & 0 & 0 & 0 & 0 & 0 \\ 0 & 0 & 0.1099 & 0 & 0 & 0 & 0 & 0 \\ 0 & 0 & 0 & 286.5 & 0 & 0 & 0 & 0 \\ 0 & 0 & 0 & 0 & 286.5 & 0 & 0 & 0 \\ 0.00247 & 0 & -0.002479 & 0 & -0.1994 & -0.00001289 & 0.3475 & 0 \\ 0 & 0 & 0 & 2.024 & 0 & 0 & 0 & -1.024 \end{bmatrix}$$

$$D' = \begin{bmatrix} 0 & 0 & 0 & 0 & 0.0295 & 0 \end{bmatrix}$$

Table 11f. RS&M System Matrices - Lateral, Bad, MBL.

$$A = \begin{bmatrix} -1 & 0 & 0 & 0 & 0 & 0 & 0 & 0 \\ 0 & 0 & 1 & 0 & 0 & 0 & 0 & 0 \\ 0.1 & 0 & -1 & 32.17 & 0 & 0 & 0 & 0 \\ 0 & 0 & 0 & 0 & 1 & 0 & 0 & 0 \\ 0.006217 & 0 & -0.006217 & 0 & -0.5 & 0 & 0 & 0 \\ 0 & 0 & 0 & 0 & 0 & 0 & 1 & 0 \\ 0.3562 & 0 & -0.3562 & 0 & 28.65 & -0.001852 & -0.08888 & 0 \\ -0.0006217 & 0 & 0 & 0 & 0 & 0 & 0 & -0.2 \end{bmatrix}$$

$$B' = \begin{bmatrix} 0 & 0 & 0 & 0 & 0.0742 & 0 & 4.24 & 0 \end{bmatrix}$$

$$E' = \begin{bmatrix} 1 & 0 & 0 & 0 & 0 & 0 & 0 & 0 \end{bmatrix}$$

$$C = \begin{bmatrix} 0 & 0.1099 & 0 & 0 & 0 & 0 & 0 & 0 \\ 0 & 0 & 0.1099 & 0 & 0 & 0 & 0 & 0 \\ 0 & 0 & 0 & 286.5 & 0 & 0 & 0 & 0 \\ 0 & 0 & 0 & 0 & 286.5 & 0 & 0 & 0 \\ 0.00247 & 0 & -0.002479 & 0 & -0.1994 & -0.00001289 & 0.3475 & 0 \\ -0.006292 & 0 & 0.006292 & 0 & 0 & 0 & 0 & -1.024 \end{bmatrix}$$

$$D' = \begin{bmatrix} 0 & 0 & 0 & 0 & 0.0295 & 0 \end{bmatrix}$$

Table 12a. RS&M System Matrices - Vertical, Good, MB.

$$A = \begin{bmatrix} -1 & 0 & 0 & 0 \\ 0 & 0 & 1 & 0 \\ 1 & 0 & -4 & 0 \\ -0.0062 & 0 & 0.0249 & -0.2 \end{bmatrix}$$

$$B' = \begin{bmatrix} 0 & 0 & -4.3 & 0.0267 \end{bmatrix}$$

$$E' = \begin{bmatrix} 1 & 0 & 0 & 0 \end{bmatrix}$$

$$C = \begin{bmatrix} 0 & 1 & 0 & 0 \\ 0 & 0 & 1 & 0 \\ 0.0629 & 0 & 0.2516 & -1.024 \end{bmatrix}$$

$$D = \begin{bmatrix} 0 \\ 0 \\ 0.2706 \end{bmatrix}$$

Table12b. RS&M System Matrices - Vertical, Good, FB.

$$A = \begin{bmatrix} -1 & 0 & 0 \\ 0 & 0 & 1 \\ 1 & 0 & -4 \end{bmatrix}$$

$$B' = \begin{bmatrix} 0 & 0 & -4.3 \end{bmatrix}$$

$$E' = \begin{bmatrix} 1 & 0 & 0 \end{bmatrix}$$

$$C = \begin{bmatrix} 0 & 1 & 0 \\ 0 & 0 & 1 \end{bmatrix}$$

$$D = \begin{bmatrix} 0 \\ 0 \end{bmatrix}$$

Table 13. Display Gains, Weighting Coefficients and Indifference Thresholds.

Display Variables	Display Gain	Weighting Coefficient	Indifference Threshold
x,y	1 in/9.1 ft	$1/(1\text{ in})^2$	.2 in
u,v	(1 in/sec)/(9.1 fps)	$(5\text{ sec}/1\text{ in})^2$	.2 in/5 sec
θ, ϕ	$5(180/\pi)$ deg/rad	$1/(10\text{ deg})^2$	2 deg
$\dot{\theta}, \dot{\phi}$	$5(180/\pi)\frac{\text{deg/sec}}{\text{rad/sec}}$	$(1\text{ sec}/10\text{ deg})^2$	2 deg/1 sec
z	1.0	$1/(10\text{ ft})^2$	2 ft
w	1.0	$(5\text{ sec}/10\text{ ft})^2$	2 ft/5 sec
Semicircular Canal	1.0	0	$.57\text{ deg/sec}^2$
Otolith	1.0	0	.015 g

obtain weighting coefficients and indifference thresholds on position of a display element (such as attitude), but it is more difficult to assign the same quantities for the rates. In Table 13 the technique suggested in Section 3 has been used to find the ratio $y_{max}/\dot{y}_{max}$, i.e., the equivalent time constant of the desired response. For the translational variables an equivalent time constant of 5 seconds was chosen, whereas the same ratio was taken as 1 second for the attitude control task.

Incorporating both visual and motion cues into the Kalman filter portion of the model is straightforward, but the question of weighting vestibular "outputs" must be addressed. In the motion-only conditions run by Shirley, this was not a problem because there are no visual terms to compete with the vestibular terms in a cost functional.

AD-A047 071 AEROSPACE SYSTEMS INC BURLINGTON MASS F/G 5/8
PILOT MODELING FOR MANNED SIMULATION. VOLUME I.(U)
DEC 76 R E CURRY, W C HOFFMAN, L R YOUNG F33615-75-C-3069
UNCLASSIFIED ASI-TR-76-29-VOL-1 AFFDL-TR-76-124-VOL-1 NL

2 OF 2
ADA047071

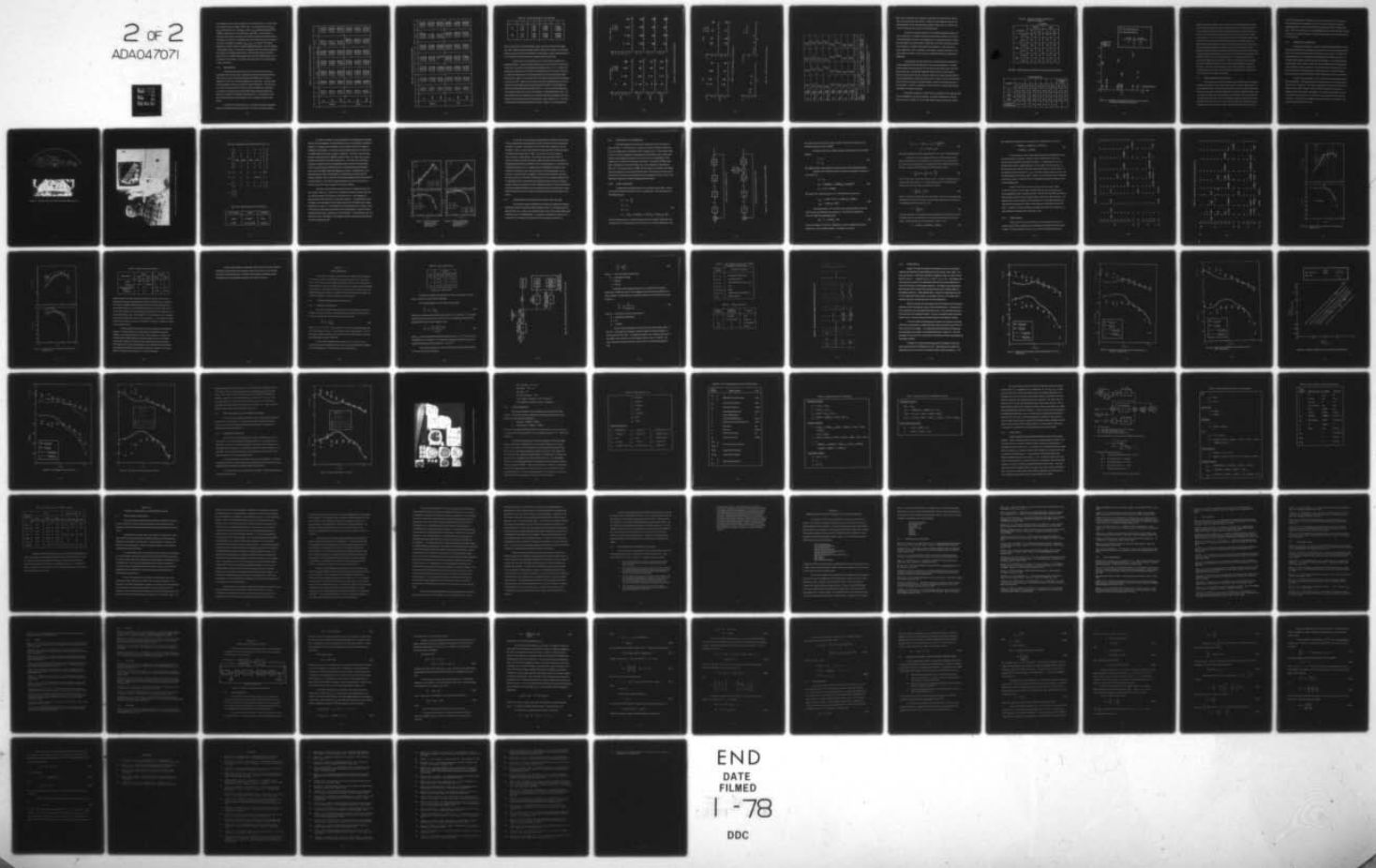

END
DATE FILMED
1-78
DDC

One attempt was made at choosing weights for the vestibular outputs, in a manner similar to choosing weights for display element rates. If a representative ratio of $\dot{\phi}_{max}/\ddot{\phi}_{max}$ could be found, then, since $\dot{\phi}_{max}$ is known, $\ddot{\phi}_{max}$ could be calculated and the vestibular weights chosen as the inverse square of this value. This would allow a "bootstrap" determination of angle rate and vestibular weights from the maximum allowable angle. From Dillow et al. (Reference 36) it was found that the ratio of weights on roll rate and acceleration correspond to $\dot{\phi}_{max}/\ddot{\phi}_{max} = 0.1$ second. This relative weighting was tried but found to be totally unacceptable because of too much weighting on the vestibular outputs. We have taken the opposite tack at this juncture and placed zero weight on the vestibular measurements, so that the model treats the vestibular signal strictly as an additional measurement used in the control feedback loop, but not as variables to be minimized. The validity of this approach will be re-examined later in other control tasks.

4.2.3 MODEL RESULTS

The RMS tracking performance for each of the three tracking tasks was determined under the various motion conditions and vehicle dynamics outlined above. These results are shown in Tables 14a through 14c for different levels of control workload, f_c, the fraction of attention applied to the control task. The data in these tables are plotted as a function of workload in Figures 8 through 10. The characteristics to note in these plots are that motion cues reduce the RMS error as expected in this situation of veridical motion, and the "bad" dynamics generally exhibit more sensitivity to changes in workload than "good" dynamics. It is well known that the slope of these performance versus workload curves is an important element in pilot opinion.

At each level of control attention, f_c, the allocation between the position display and attitude display has been optimized. The ratio of the control attention

Table 14a. Longitudinal Performance versus Workload.

		f_c	σ_x (ft)	σ_u (ft/sec)	σ_θ (deg/sec)	σ_q (deg/sec)	f_x/f_θ	J
GOOD	FB	0.25	2.362	0.4758	0.3217	0.2323	14.38	0.1914
		0.50	1.997	0.4224	0.2959	0.222	29.303	0.1513
		0.75	1.832	0.3966	0.2825	0.2160	46.62	0.1340
		1.0	1.736	0.3810	0.2741	0.2122	29.30	0.1242
	MBL	0.25	2.416	0.4868	0.3274	0.2365	14.38	0.1998
		0.50	2.045	0.4325	0.3014	0.2261	26.75	0.1481
		0.75	1.878	0.4064	0.2879	0.2202	34.75	0.1403
		1.0	1.776	0.390	0.2792	0.2162	40.67	0.1297
	MBA	0.25	2.293	0.4603	0.3122	0.2275	14.38	0.1805
		0.50	1.964	0.4149	0.2192	0.2193	29.27	0.1465
		0.75	1.810	0.3916	0.2794	0.2141	41.90	0.1310
		1.0	1.717	0.3768	0.2715	0.2105	34.71	0.1217
BAD	FB	0.25	5.333	1.050	0.9878	0.9619	0.08696	1.319
		0.50	3.727	0.7833	0.7414	0.7643	0.1062	0.7565
		0.75	3.154	0.6731	0.6359	0.6743	0.1299	0.4717
		1.0	2.816	0.6118	0.5787	0.6245	0.1364	0.4795
	MBL	0.25	5.295	1.070	1.006	0.9809	0.0869	1.354
		0.50	3.895	0.7928	0.7414	0.7655	0.1063	0.7754
		0.75	3.208	0.6824	0.6417	0.6812	0.1234	0.5870
		1.0	2.859	0.6192	0.5833	0.6303	0.1312	0.4911
	MBA	0.25	3.874	0.8042	0.7769	0.8182	0.8317	0.8317
		0.50	3.272	0.6920	0.6623	0.7105	0.1643	0.6196
		0.75	2.909	0.6265	0.5976	0.6497	0.1563	0.5114
		1.0	2.683	0.5827	0.5538	0.6079	0.1442	0.4453

Table 14b. Lateral Performance versus Workload.

		f_c	σ_y	σ_v	σ_φ	σ_p	f_y/f_θ	J
GOOD	FB	0.25	2.774	0.5867	0.4137	0.3153	16.2414	0.2918
		0.50	2.337	0.5175	0.3771	0.2984	25.3158	0.2295
		0.75	2.141	0.4845	0.3584	0.2891	33.483	0.2029
		1.0	2.025	0.4643	0.3466	0.2829	29.303	0.1875
	MBL	0.25	2.757	0.5801	0.4081	0.3106	11.50	0.2859
		0.50	2.313	0.5112	0.3723	0.2944	26.75	0.2243
		0.75	2.123	0.4796	0.3547	0.2858	25.813	0.1991
		1.0	2.006	0.4596	0.3432	0.2799	30.25	0.1840
	MBA	0.25	2.632	0.5547	[illegible]3929	0.3050	12.333	0.2642
		0.50	2.272	0.5032	[illegible]676	0.2935	29.27	0.2183
		0.75	2.106	0.4766	[illegible]30	0.2862	27.53	0.1971
		1.0	2.0	0.4587	[illegible]28	0.2809	28.412	0.1835
BAD	FB	0.25	4.957	1.015	0.8875	0.8457	0.1876	1.092
		0.50	3.732	0.7914	0.7030	0.7162	0.1891	0.6988
		0.75	3.199	0.6958	0.6234	0.6543	0.1862	0.5546
		1.0	2.885	0.640	0.5764	0.6165	0.1905	0.4772
	MBL	0.25	4.856	0.9946	0.8640	0.8188	0.2346	1.041
		0.50	3.653	0.7833	0.6979	0.7082	0.2190	0.6816
		0.75	3.171	0.6902	0.6176	0.6469	0.1922	0.5444
		1.0	2.865	0.6361	0.5724	0.6113	0.2225	0.4705
	MBA	0.25	3.799	0.8069	0.7305	0.7603	0.4184	0.7483
		0.50	3.273	0.7115	0.6446	0.6853	0.2759	0.5902
		0.75	2.951	0.6534	0.5924	0.6394	0.2435	0.5033
		1.0	2.733	0.6137	0.5571	0.6073	0.2315	0.4480

Table 14c. Vertical Performance versus Workload.

	f_c	σ_z	σ_w	J
FB	0.1	1.699	0.3862	0.0676
	0.2	1.518	0.3810	0.06102
	0.3	1.429	0.3771	0.05784
MB	0.1	1.702	0.3615	0.06414
	0.2	1.521	0.3555	0.05749
	0.3	1.429	0.3514	0.05423

spent on the position and attitude displays f_x/f_θ is also shown in Tables 14a through 14c, which indicate that bad dynamics generally require more attention to the attitude display to derive the necessary information for stabilization, whereas with good dynamics, the attention can be devoted to the ultimate position control task.

A prediction of overall performance for the three motion conditions was obtained as follows. Because the pilots said they spent very little time on the altitude control task, we used the vertical performance predictions for $f_c = 0.1$. To obtain the performance predictions for the lateral and longitudinal axes, the fraction of attention on lateral and longitudinal axes was found by hand, which minimizes the total RMS hovering error, sugject to the constraint that the attention on both lateral and longitudinal axes sum to 0.9. Results of our previous studies have indicated, however, that the minimum in overall RMS position is generally quite flat relative to the allocation of attention between longitudinal and lateral tasks; i.e., one can trade off longitudinal versus lateral position error with very little change in overall RMS position error. The only requirement for this insensitivity is that enough attention be applied to any "bad" dynamics to be beyond the knee of the performance versus workload curve. The results of the total task performance predictions are shown in Figure 11, which compares the

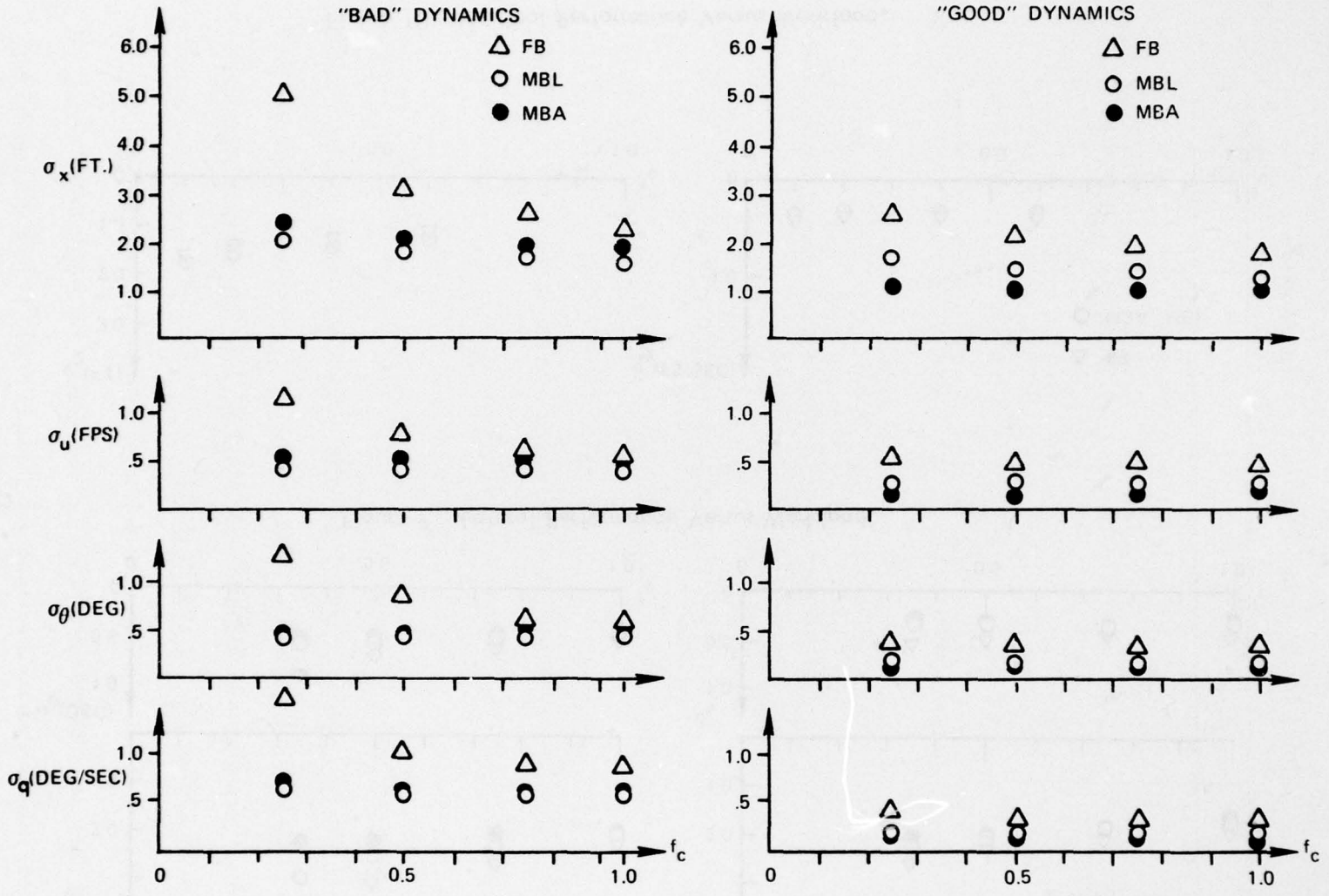

Figure 8. Longitudinal Performance Versus Workload.

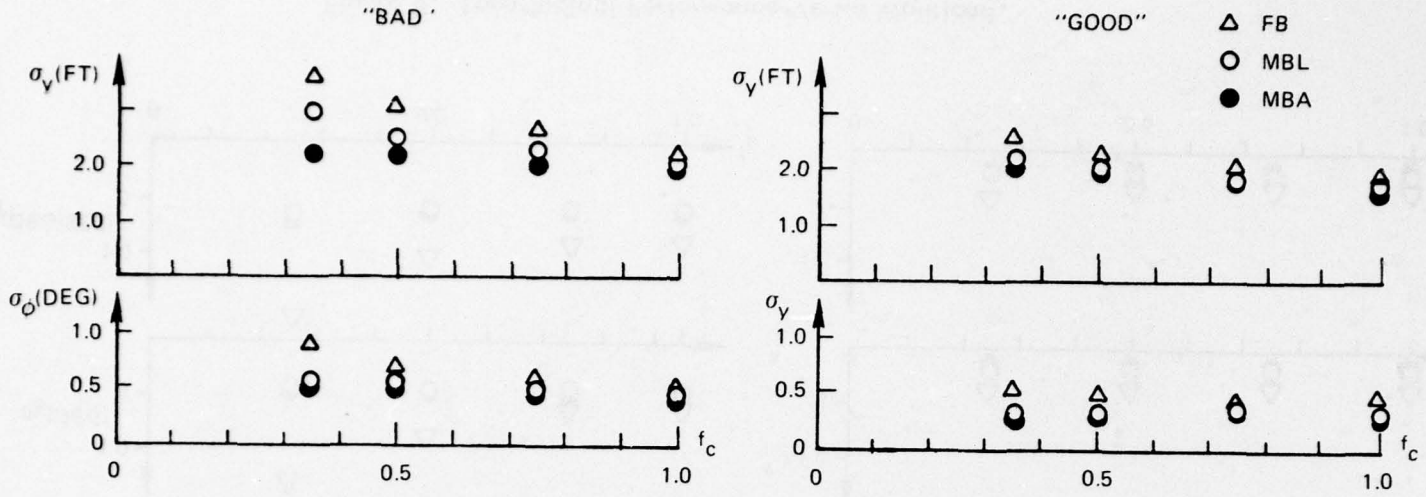

Figure 9. Lateral Performance Versus Workload.

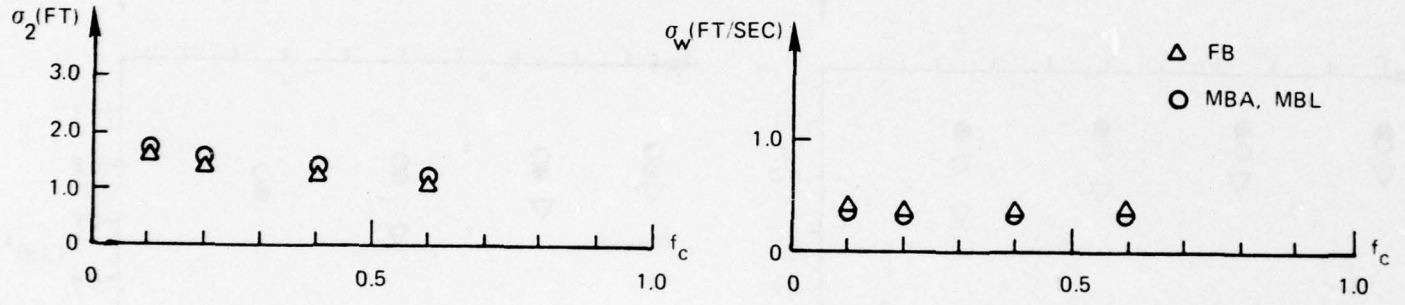

Figure 10. Vertical Performance Versus Workload.

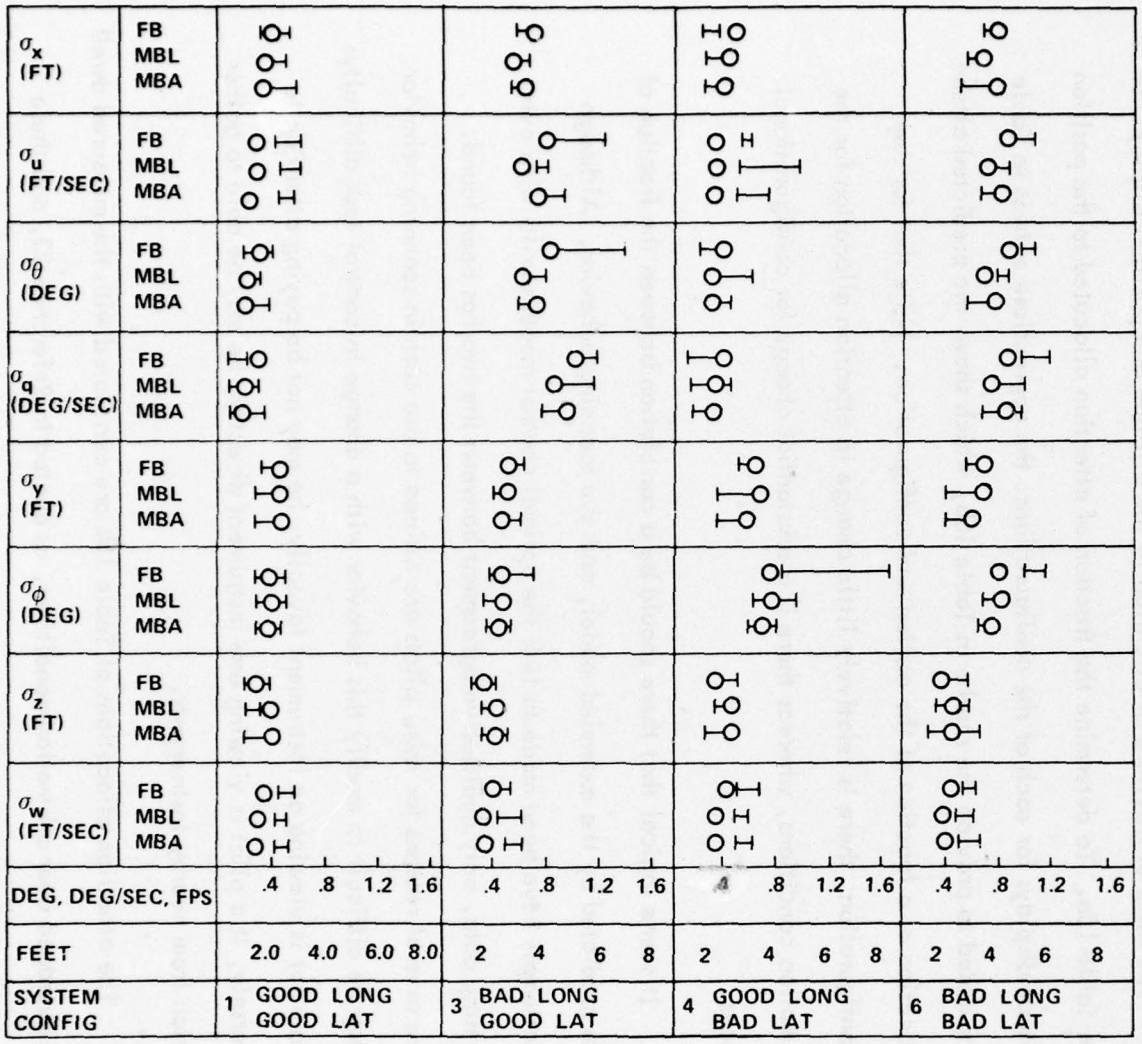

Figure 11. Preliminary Predictions of Total Task Performance (Circles) Compared to Range of Means of Three Subjects.

RMS values of important state variables as predicted by the model with the range of mean values observed for three subjects. There is excellent agreement between the model predictions and the observed range of subject means, both on a relative basis (with and without motion cues) and on an absolute basis.

The ratio of fractions of attention to the attitude and position displays are shown in Table 15a. To determine the fraction of attention allocated to the position and attitude displays for each of the configurations, the appropriate entries to Table 15a were added to provide the results in Table 15b, which shows the predicted attention allocation as a function of the motion and configuration. Note that for any given configuration, there is relatively little change in attention allocation for the various motion conditions, whereas there is a substantial change for configurational differences.

It seems logical that there should be a correlation between the fraction of attention predicted by the extended model, and eye scanning behavior. Although several attempts have been made to link the optimal control model results with overt eye scanning data, only qualitative agreement between the two has been found. There are several reasons for this: pilots are trained to use certain scanning behavior, and it may be difficult to modify this behavior with a change in control task difficulty; even if a pilot is viewing an instrument foveally, he may not be paying attention to it; conversely, if a pilot is viewing one instrument directly, he may be able to gather information from nearby instruments.

The attention allocations of Table 15b are correlated with the measured dwell fraction averaged over all motion conditions, as quoted in Reference 23, and these results are shown in Figure 12. For the dwell fraction observed on both the attitude

Table 15a. Fraction of Attention Allocation by Motion and Dynamics.

MOTION		DYNAMICS: GOOD f_{att}	GOOD f_{pos}	BAD f_{att}	BAD f_{pos}
FB	LON	.02	.43	.39	.06
	LAT	.02	.43	.39	.06
MBL	LON	.02	.43	.39	.06
	LAT	.02	.43	.39	.06
MBA	LON	.01	.44	.36	.09
	LAT	.01	.44	.36	.09

Table 15b. Predicted Attention Allocation by Motion and Configuration.

MOTION	CONFIGURATION 1 f_{att}	1 f_{pos}	3 f_{att}	3 f_{pos}	4 f_{att}	4 f_{pos}	6 f_{att}	6 f_{pos}	Average for Motion f_{att}	Average for Motion f_{pos}
FB	.04	.86	.41	.49	.41	.49	.78	.12	.41	.49
MBL	.04	.86	.41	.49	.41	.49	.78	.12	.41	.49
MBA	.02	.88	.40	.50	.37	.53	.72	.12	.38	.52
Average for Configuration	.03	.87	.41	.49	.40	.50	.76	.14		

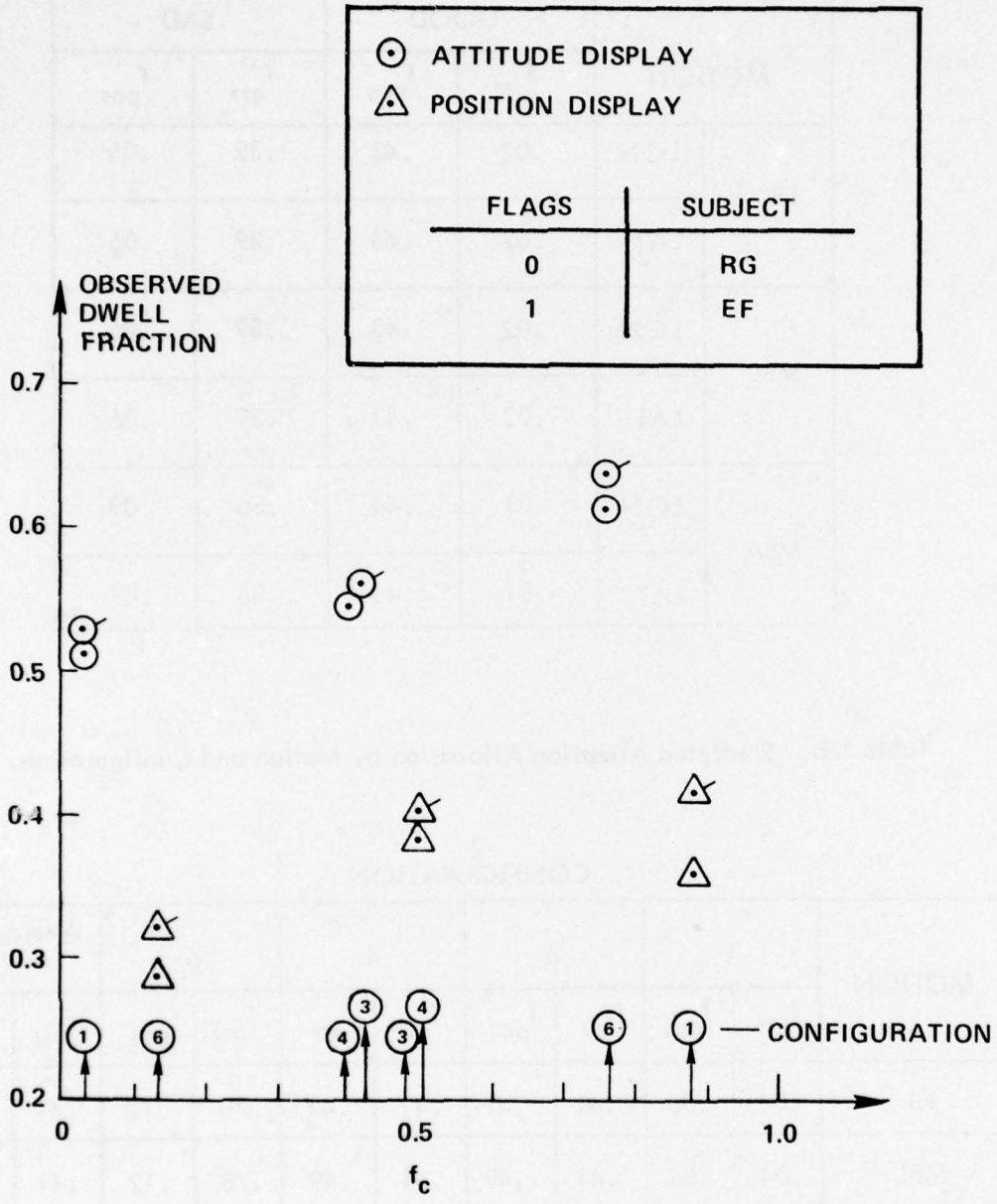

Figure 12. Correlation of Observed Dwell Fractions with Fractions of Attention-Configuration Differences.

display and the position display, there is a fairly linear relationship between the dwell fraction and the fraction of attention derived from the model. The eye scanning statistics are relatively insensitive to these configurational changes; for example, the dwell fraction on the attitude display varies between 0.5 and 0.6 over the range of configurations examined. Thus the fraction of attention derived from the model certainly varies in the same manner as the observed dwell fraction (and the relationship appears to be fairly linear), although there is a difference between the attitude and position displays. A closer correspondence between the fraction of attention and dwell fraction might be obtained by artificially imposing constraints that the fraction of attention on the attitude instrument should always be greater than (say) 0.5 to account for pilot scanning habits. The attention allocation, as used in the present model, is a normative description (i.e., how the pilot should allocate his attention). Thus, the examination of more eye movement data may indicate that pilot attention will have to be bounded to reflect pilot limitations. This result would be consistent with the other constraints currently in use with the optimal control model: the pilot minimizes the quadratic cost functional subject to constraints on his inherent capabilities.

4.3 MODEL PARAMETERS FOR VMC CUES

The characteristics of the human operator when utilizing VMC cues have been qualitatively described by use of larger attitude angles to maintain a tighter control on position (Reference 23). Unfortunately, this reference contains no substantial data which could be used to explore the various manifestations of VMC cues within the model. However, Reference 25 provides a fairly complete set of VMC/IMC experimental differences in which the effects of VMC cues can be summarized as allowing the pilot to operate at a higher gain than under IMC cues. As mentioned in Section 3.5, this behavior can be introduced into the model by three methods: decreasing the noise/signal ratio on atti-

tude rate (corresponding to increased acuity of roll rate); decreasing the threshold on roll rate (again due to increased acuity of roll rate); and decreasing the quadratic weighting penalty for roll rate (thus allowing the system to operate at a higher loop gain). The first two methods are more physiologically based, whereas the last technique (similarly for increased roll angles in the VTOL hovering task) are based on differences in pilot behavior.

4.3.1 EXPERIMENTAL DESCRIPTION

To explore the differences in angular rate threshold (and effectively, noise/signal ratio) and the effect of attitude rate on the model, we chose a fixed-base tracking task for which pilot describing function data have been obtained by Newell and Smith (Reference 25). In both cases the controlled-element dynamics are $K/s(s - 1)$, with the primary difference being in the form of the display: a conventional attitude indicator (IMC cues) as shown in Figure 13; and a wide field contract analog display (VMC condition) as shown in Figure 14. The command input for each case was a sum of sine waves with a rectangular spectrum (shelf frequency at 2.5 radians/second). The system matrices for both the IMC and VMC tracking tasks are shown in Table 16a.

The IMC tracking condition is the conventional use of the optimal model of the human operator. The model parameters to predict the results of this IMC tracking task are shown in Table 16b. The maximum allowable roll deviation was based on the display by the attitude indicator, and the indifference threshold was chosen at 2 degrees because of the layout of the display. The weights and thresholds for the roll rate were chosen on the basis of a 1 second time constant response for this attitude control task. The control rate weighting was chosen to obtain a neuromuscular time constant of approximately 0.1 second.

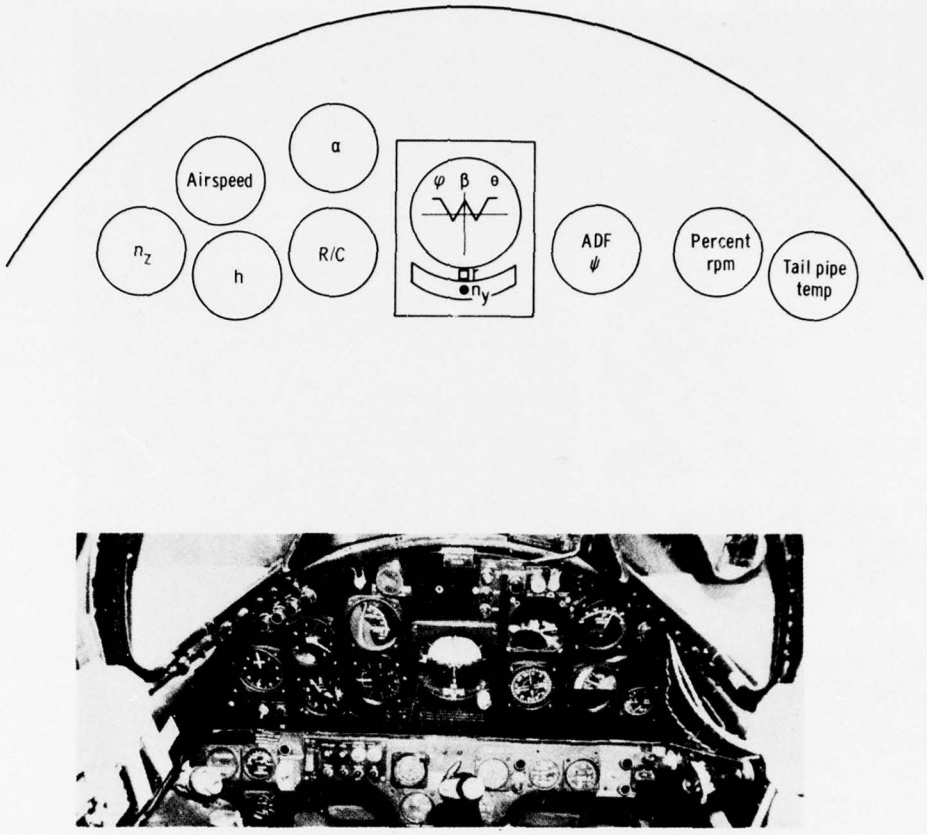

Figure 13. Instrument Display for IMC Experiments (Reference 25).

Figure 14. Contact-Analog Display for VMC Experiments (Reference 25).

Table 16a. System Matrices for Newell-Smith K/s(s - 1).

$$A = \begin{bmatrix} 0 & 1 & 0 & 0 & 0 & 0 \\ 0 & 0 & 1 & 0 & 0 & 0 \\ 0 & 0 & 0 & 1 & 0 & 0 \\ -5.063 & -8.819 & -7.682 & -3.92 & 0 & 0 \\ 0 & 0 & 0 & 0 & 0 & 1 \\ 0 & 0 & 0 & 0 & 0 & 1 \end{bmatrix}$$

$$B' = \begin{bmatrix} 0 & 0 & 0 & 0 & 0 & 120 \end{bmatrix}$$

$$E' = \begin{bmatrix} 0 & 0 & 0 & 5.063 & 0 & 0 \end{bmatrix}$$

$$C = \begin{bmatrix} 1 & 0 & 0 & 0 & -1 & 0 \\ 0 & 1 & 0 & 0 & 0 & -1 \end{bmatrix}$$

$$D = \begin{bmatrix} 0 \\ 0 \end{bmatrix}$$

Table 16b. Model Parameters for IMC Tracking.

Input Variable	Weight	Threshold
ϕ (deg)	$1/(5 \text{ deg})^2$	2 deg
$\dot{\phi}$ (deg)	$(1 \text{ sec}/5 \text{ deg})^2$	2 deg/sec

To evaluate the effect on the model predictions of changing roll rate thresholds and roll rate weightings, the describing functions were calculated for thresholds of 2 deg/sec, 0.7 deg/sec and 0.2 deg/sec, and for maximum roll rates of 5 deg/sec, 10 deg/sec and 50 deg/sec. In each one of these conditions there is an overlap with the nominal IMC tracking case, as shown in Table 16b. The effect on the describing function of changing roll rate threshold is shown in Figure 15, along with the experimentally measured data for the IMC tracking task. It is obvious that, under these conditions, changing the roll rate threshold has almost no effect on the describing function, primarily because the RMS roll rate is substantially above the threshold value even at the highest threshold (2 degrees per second). Essentially then, all of these describing functions are predictions of the describing function for the IMC tracking conditions, and it is seen that there is good agreement between the experiment and the predictions. Note that the experimental data as well as the model show a fall-off in gain at the lower frequencies under these conditions.

The effect on the predicted describing function for changing maximum roll rate is shown in Figure 16. Here we see a substantial alteration of the describing function with the change of this parameters, indicating that it is a more appropriate representation of VMC tracking cues under these conditions. The experimental data in this figure are the describing functions determined from the wide-field contact analog display shown in Figure 14. The comparison of the experimental data in Figures 15 and 16 indicate that when operating with the contact analog display, the pilot can obtain substantially higher gains, especially at lower frequencies. In this particular case, the maximum roll rate of 50 deg/sec in the quadratic penalty provides an excellent description of the experimental data.

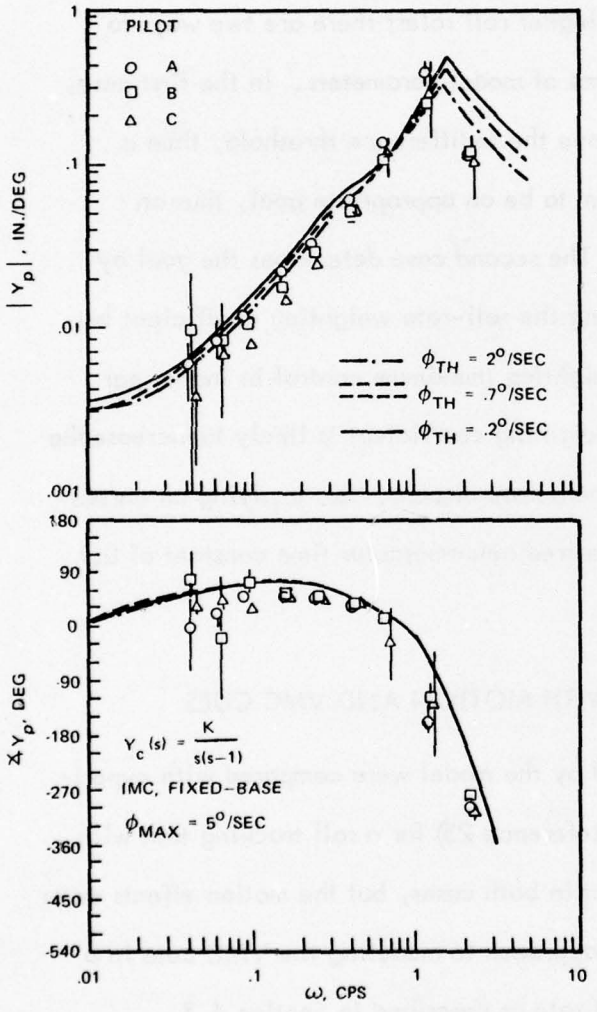

Figure 15. Effect of Attitude Rate Threshold on Pilot Describing Function (Reference 25).

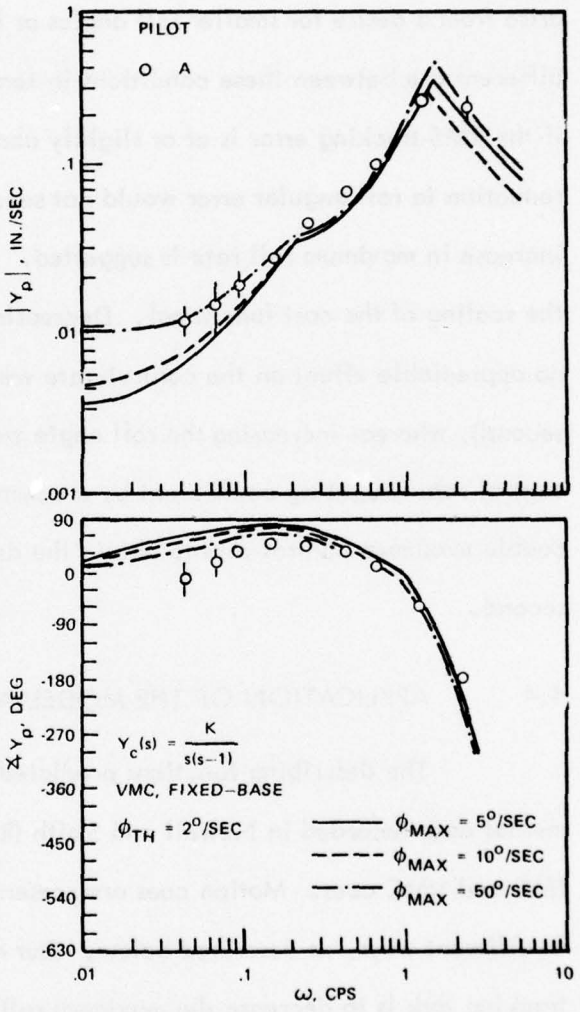

Figure 16. Effect of Attitude Rate Cost Weighting on Pilot Describing Function (Reference 25).

For the roll control tracking task described here, the effect of a wide view contact analog display (an approximation to VMC conditions) seems to be well represented by an increase in the maximum roll rate, rather than a decrease in roll rate thresholds. This is true under these conditions because the RMS roll rates are substantially above that threshold even in IMC, and reduction of the rate thresholds does not improve tracking ability. The increase in pilot gain under VMC may arise from a desire for smaller roll angles or higher roll rates; there are two ways to differentiate between these conditions in terms of model parameters. In the first case, if the RMS tracking error is at or slightly above the indifference threshold, then a reduction in roll angular error would not seem to be an appropriate goal, thus an increase in maximum roll rate is suggested. The second case determines the goal by the scaling of the cost functional. Decreasing the roll-rate weighting coefficient has no appreciable effect on the control-rate weighting (maximum control in inches per second), whereas increasing the roll angle weighting coefficient is likely to increase the control rate weighting coefficient by a commensurate amount, thus implying an unreasonable maximum control rate to obtain the desired neuromuscular time constant of 0.1 second.

4.4 APPLICATION OF THE MODEL WITH MOTION AND VMC CUES

The describing functions predicted by the model were compared with experimental data recorded in Newell and Smith (Reference 25) for a roll tracking task with IMC and VMC cues. Motion cues are present in both cases, but the motion effects enter in different ways, as described below. Our approach to modeling the VMC cues in a tracking task is to decrease the maximum roll rate as described in Section 4.3.

4.4.1 DESCRIPTION OF THE EXPERIMENT

The block diagrams of the two system configurations used in the study are shown in Figure 17. Configuration C corresponds to Newell and Smith's configuration A-2* and configuration D corresponds to their configuration A-2. The mnemonic labels C and D are used to correspond to Command input and Disturbance input, respectively. Because of the preshaping of the (sum of sine waves) input in configuration D, both configurations are identical in fixed-base experiments. During the T-33 flight experiments, configuration C was used with IMC cues, and configuration D was used with VMC cues. With configuration C in flight, the roll angle error indicated on the display does not correspond to the actual aircraft bank angle. The motion cues transmit the aircraft motion but not the input command portion of the displayed roll error, similar to the experiments conducted by Junker and Replogle (Reference 39).

4.4.2 MODEL PARAMETERS

To approximate the shelf spectrum of the sum-of-sine-waves input, we have used a fourth-order Butterworth filter which is maximally flat. The state equations for the shaping filter are

$$\begin{aligned}
\dot{x}_1 &= x_2 = \frac{di}{dt} \\
\dot{x}_2 &= x_3 \\
\dot{x}_3 &= x_4 \\
\dot{x}_4 &= -\omega_o^4 x_1 - 2.613\omega_o^3 x_2 - 3.414\omega_o^2 x_3 - 2.613\omega_o x_4 + \omega_o^4 w
\end{aligned} \tag{35}$$

The only information given in Newell and Smith is that the maximum amplitude of the command was 8^o. If we assume this to be the 3σ limit on a Gaussian distribution, then

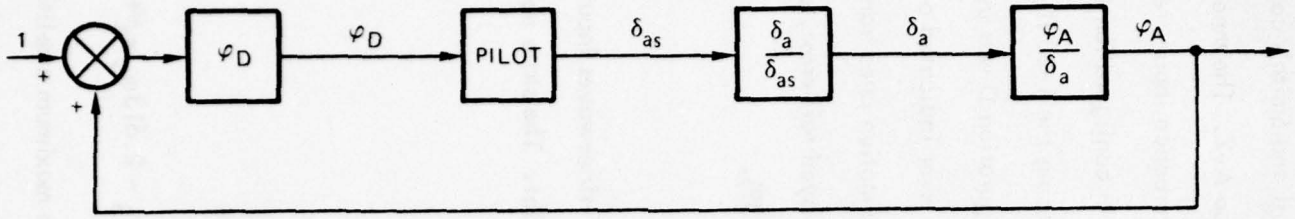

CONFIGURATION C (COMMAND INPUT)

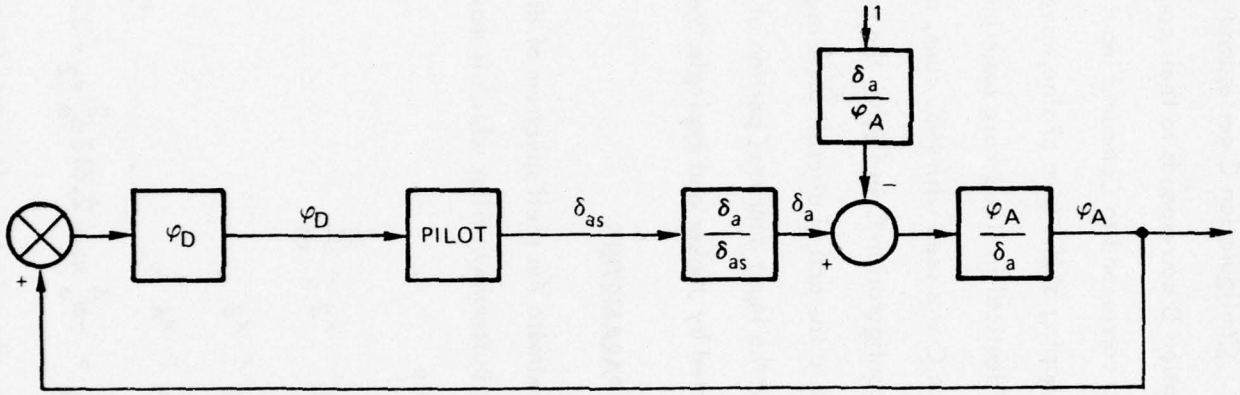

CONFIGURATION D (DISTURBANCE INPUT)

Figure 17. Block Diagram of Control Tasks (NASA TN D-5007).

the variance of the white driving noise in Equation (35) should be chosen such that the RMS command level (x_1) is 2.667°.

The fifth and sixth state variables represent the equations for the controlled elements

$$\begin{aligned} \dot{\phi} &= \dot{x}_5 \\ \ddot{\phi} &= \dot{x}_6 \end{aligned} \tag{36}$$

The righthand sides of these equations will be derived for both configurations below.

Equations for the vestibular system are the same as described in Section 3.4 and are given by

$$\begin{aligned} \dot{x}_7 &= x_8 \\ \dot{x}_8 &= -0.001852\, x_7 - 0.08888\, x_8 + \dot{\omega}\ (\text{deg/sec}^2) \\ \dot{x}_9 &= 0.2\, x_9 + 0.2f(\text{g's}) \end{aligned} \tag{37}$$

The output of the vestibular systems, i.e., the measurements are given by

$$\begin{aligned} y_{scc} &= -1.289 \cdot 10^{-5}\, x_7 + 0.34785\, x_8 + 0.00696\, \dot{\omega} \\ y_{oto} &= -1.024\, x_9 + 2.024\, f \end{aligned} \tag{38}$$

For configuration C, the only input to the controlled element is from the pilot's control stick deflection (here denoted u). The differential equation for roll rate in flight becomes (Reference 25)

$$\ddot{\phi}_A = \dot{\omega} = -2.857\, \dot{\phi}_A + 45u \tag{39}$$

The rate of change of roll rate for configuration D is more complex because of the shaped input to the controlled element. This equation is given by

$$\ddot{\phi}_A = \dot{x}_6 = -2.857\, x_6 + .5\left[u - \frac{\ddot{u} + 2.857\,\dot{i}}{45}\right] \qquad (40)$$

$$= x_2 - x_3 - 2.857\, x_6 + 45u$$

where the second portion of the bracketed expression is the output of the shaping filter.

The specific force is an important element in the otolith equations and is derived from three sources: gravitational forces, aerodynamic forces, and constraint forces from linear acceleration due to roll accelerations with a displacement from the roll axis. In general the lateral component of specific force (in g's) is

$$f = \frac{2\pi}{360}\left(\sin \phi_A - \frac{V^2}{gR}\cos \phi_A - \frac{\ell\,\ddot{\phi}_A}{g}\right. \qquad (41)$$

where V is the linear velocity and R is the turn radius. If there is no translation of the center of gravity during roll ($R = \infty$, lateral component of lift is cancelled by side force) then for small roll angles the specific force (in g's) is

$$f = \frac{2\pi}{360}\left(\phi_A - \frac{\ell}{g}\ddot{\phi}_A\right) \qquad (42)$$

where ℓ is the distance from the roll axis to the otoliths. If the turn is aerodynamically coordinated, then the lateral component of gravitational specific force is counteracted by centripetal acceleration in the turn, thus

$$f = -\frac{2\pi}{360}\frac{\ell}{g}\ddot{\phi}_A \qquad (43)$$

The former condition will be assumed in further development of the equations, with the realization that the second condition can be derived by eliminating the ϕ_A (x_5) term below. Thus the specific force for configuration C is (for $\ell = 4$ ft):

$$f = 0.01745\, x_5 + 0.00620\, x_6 - 0.09765u \qquad (44)$$

The corresponding expression for the specific force in configuration D is given by

$$f = 0.00620\, x_2 + 0.002170\, x_3 + 0.01745\, x_5 + 0.00620\, x_6 - 0.09765u \tag{45}$$

It is now possible to see the major differences between configurations C and D during moving base conditions. Equations (39) and (40) describe the input to the semicircular canals during the motion condition. In configuration D, since the attitude of the aircraft is displayed directly, the roll angle is the tracking error, so that the semicircular canals are receiving the second derivative of the error signal. In configuration C the error signal is $(i - \phi_A)$, so that the vestibular system is not receiving the second derivative of the error signal. However, the motion felt is due to the pilot's control inputs, hence, it might be of value in separating command from response in the visually displayed error.

Tables 17 and 18 show the system matrices used in the study. Table 19 shows the assumed values of weights and thresholds derived from the description of the experimental setup in Newell and Smith. Note that the only difference between IMC and VMC conditions is the decreased weight on roll rate in VMC conditions. The thresholds seem to be reasonable in VMC conditions with a well defined horizon as a reference for the grease pencil stripes on the windscreen as described by Newell and Smith. In reality, we do not know how well defined the horizon was in these tests, so these indifference thresholds may be optimistic values.

4.4.3 MODEL RESULTS

Figures 18 and 19 show the predictions of the extended pilot model with motion cues and VMC cues along with the experimental describing functions measured in flight. For these describing functions, the control-rate weighting was based on

Table 17. System Matrices for Newell-Smith Configuration C.

$$A = \begin{bmatrix} 0 & 1 & 0 & 0 & 0 & 0 & 0 & 0 & 0 \\ 0 & 0 & 1 & 0 & 0 & 0 & 0 & 0 & 0 \\ 0 & 0 & 0 & 1 & 0 & 0 & 0 & 0 & 0 \\ -5.063 & -8.819 & -7.682 & -3.92 & 0 & 0 & 0 & 0 & 0 \\ 0 & 0 & 0 & 0 & 0 & 1 & 0 & 0 & 0 \\ 0 & 0 & 0 & 0 & 0 & -2.857 & 0 & 0 & 0 \\ 0 & 0 & 0 & 0 & 0 & 0 & 0 & 1 & 0 \\ 0 & 0 & 0 & 0 & 0 & -2.857 & 0.001852 & -0.08888 & 0 \\ 0 & 0 & 0 & 0 & 0.00349 & 0.00124 & 0 & 0 & -0.2 \end{bmatrix}$$

$$B' = [\ 0 \quad 0 \quad 0 \quad 0 \quad 0 \quad 45 \quad 0 \quad 45 \quad -0.01953\ ]$$

$$E' = [\ 0 \quad 0 \quad 0 \quad 5.063 \quad 0 \quad 0 \quad 0 \quad 0 \quad 0\ ]$$

$$C = \begin{bmatrix} 1 & 0 & 0 & 0 & 1 & 0 & 0 & 0 & 0 \\ 0 & 1 & 0 & 0 & 0 & 1 & 0 & 0 & 0 \\ 0 & 0 & 0 & 0 & 0 & -0.01988 & -0.00001289 & 0.3479 & 0 \\ 0 & 0 & 0 & 0 & 0.03532 & 0.01255 & 0 & 0 & -1.024 \end{bmatrix}$$

$$D = [\ 0 \quad 0 \quad 0.3132 \quad -0.1976\ ]$$

Table 18. System Matrices for Newell-Smith Configuration D.

$$A = \begin{bmatrix} 0 & 1 & 0 & 0 & 0 & 0 & 0 & 0 & 0 \\ 0 & 0 & 1 & 0 & 0 & 0 & 0 & 0 & 0 \\ 0 & 0 & 0 & 1 & 0 & 0 & 0 & 0 & 0 \\ -5.063 & -8.819 & -7.682 & -3.92 & 0 & 0 & 0 & 0 & 0 \\ 0 & 0 & 0 & 0 & 0 & 1 & 0 & 0 & 0 \\ 0 & 2.857 & 1 & 0 & 0 & -2.857 & 0 & 0 & 0 \\ 0 & 0 & 0 & 0 & 0 & 0 & 0 & 1 & 0 \\ 0 & 2.857 & 1 & 0 & 0 & -2.857 & 0.001852 & -0.08888 & 0 \\ 0 & -0.00124 & -0.0000434 & 0 & 0.00349 & 0.00124 & 0 & 0 & -0.2 \end{bmatrix}$$

$$B' = \begin{bmatrix} 0 & 0 & 0 & 0 & 0 & 45 & 0 & 45 & -0.01953 \end{bmatrix}$$

$$E' = \begin{bmatrix} 0 & 0 & 0 & 5.063 & 0 & 0 & 0 & 0 & 0 \end{bmatrix}$$

$$C = \begin{bmatrix} 0 & 0 & 0 & 0 & 1 & 0 & 0 & 0 & 0 \\ 0 & 0 & 0 & 0 & 0 & 1 & 0 & 0 & 0 \\ 0 & 0.01988 & 0.00696 & 0 & 0 & -0.01988 & -0.00001289 & 0.3479 & 0 \\ 0 & -0.01255 & -0.004392 & 0 & 0.03532 & 0.01255 & 0 & 0 & -1.024 \end{bmatrix}$$

$$D = \begin{bmatrix} 0 & 0 & 0.3132 & -0.1976 \end{bmatrix}$$

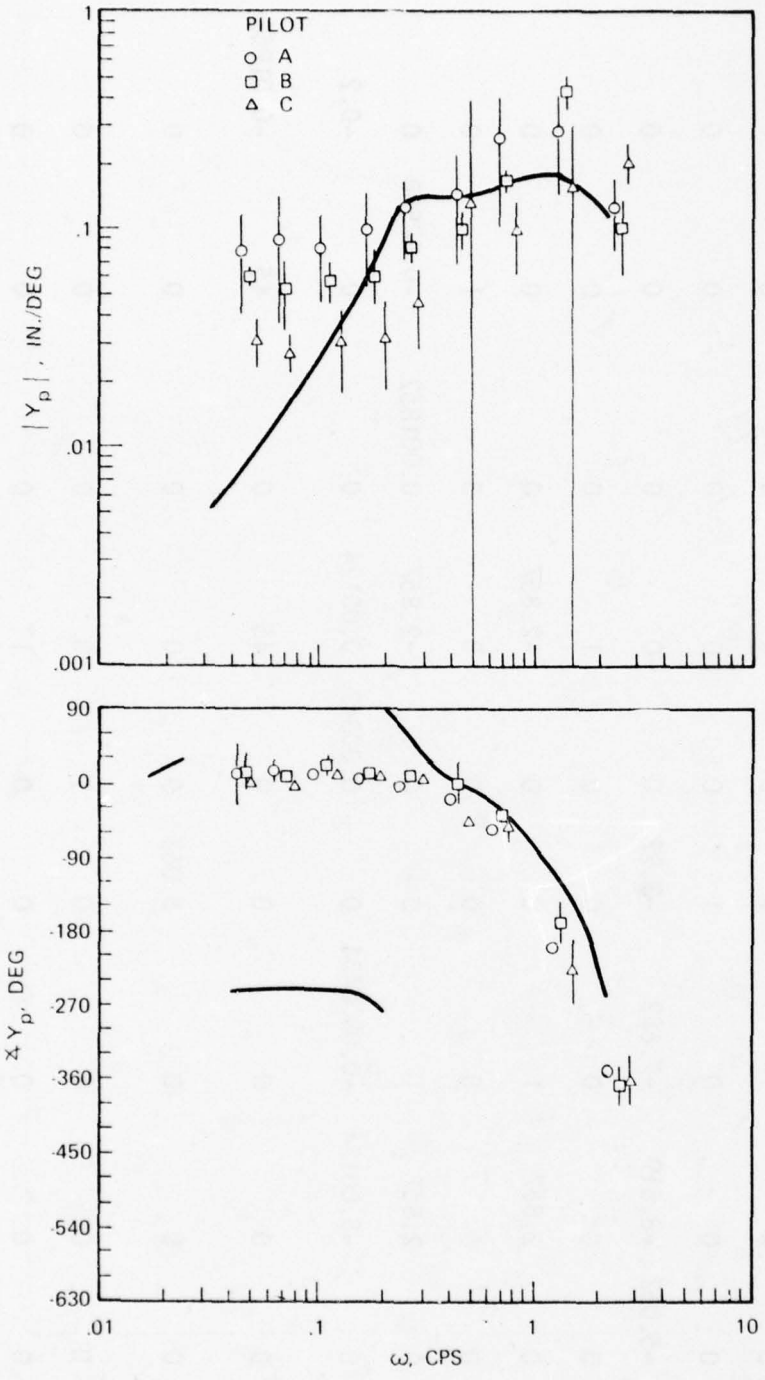

Figure 18. Describing Function Comparison with Motion Cues (Reference 25).

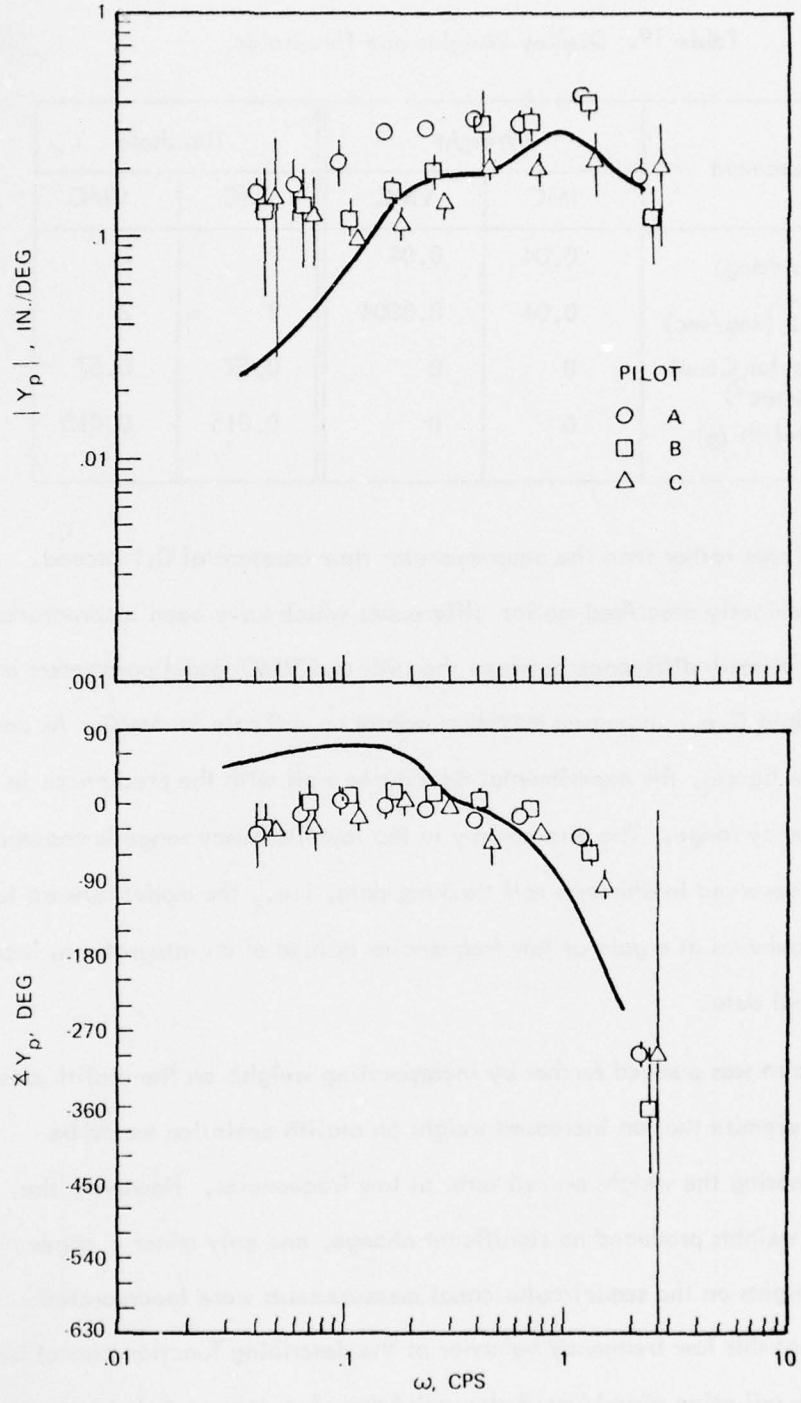

Figure 19. Describing Function Comparison With VMC Cues (Reference 25).

Table 19. Display Weights and Thresholds.

Measurement	Weight		Threshold	
	IMC	VMC	IMC	VMC
ϕ (deg)	0.04	0.04	2	2
$\dot{\phi}$ (deg/sec)	0.04	0.0004	2	2
Semicircular Canal (deg/sec^2)	0	0	0.57	0.57
Otolith (g)	0	0	0.015	0.015

maximum physical rate rather than the neuromuscular time constant of 0.1 second. Other than the previously described motion differences which have been incorporated in the model, the primary difference between the IMC and VMC model parameters is the decreased weight (i.e., increased maximum value) on roll rate for VMC. As can be seen from these figures, the experimental data agree well with the predictions in the mid to high frequency range. The discrepancy in the low frequency range is analogous to the deviations observed in Shirley's roll tracking data, i.e., the model forward loop transfer function behaves as a gain at low frequencies instead of an integrator as implied by the experimental data.

This point was pursued further by incorporating weights on the otolith measurement, on the premise that an increased weight on otolith deviation would be analogous to increasing the weight on roll error at low frequencies. However, the increased otolith weights produced no significant change, and only minor changes occurred when weights on the semicircular canal measurements were incorporated. Thus it appears that this low frequency behavior of the describing function cannot be resolved by simply adjusting visual/vestibular weighting, but appears to be a characteristic of the optimal control model as it is currently formulated.

In spite of this problem, the agreement between the model and the analytical predictions is quite good over the frequency range of most interest, and as has been seen for the VTOL hovering task, the model is quite capable of predicting the RMS performance and scanning behavior associated with motion cue effects.

SECTION V

MODEL APPLICATION

In this section, the model, with the parameters determined from the development phase, is applied to two problems for which experimental data exist with motion cues. The first experiment was conducted by Stapleford, Peters and Alex (Reference 15) and consisted of a 2 degree-of-freedom roll control task in the NASA 6 degree-of-freedom VTOL simulator. The second set of experiments consisted of data recorded during a simulated CTOL approach to landing, in which both VMC and IMC cues were available, but in which the predominant cues were obtained from the instruments.

5.1 2 DEGREE-OF-FREEDOM ROLL CONTROL TASK

5.1.1 EXPERIMENT DESCRIPTION

The experimental description in Reference 15 is quite complete, and will be described here only as it pertains to that portion of the experiment on which the model was used. Controlled element dynamics were always of the form

$$\frac{\phi_m}{c} = Y_c = \frac{K_c}{s(s+a)} \tag{46}$$

where $a = 0$, 1, or 10 sec^{-1}. The controller was a low inertia, spring restrained, side stick with ±15 degrees of travel. It had a breakout torque of approximately 1.5 in-lbs and a gradient of approximately 0.32 in-lb/deg. The pilot-selected gains (K_c) for each of the four subjects are shown in Table 20.

The overall block diagram of the simulation is shown in Figure 20. The disturbance input (d) was composed of 10 sine waves having a rectangular shelf spectrum, with a break frequency at 1.44 rad/sec and an rms input of 0.4 deg.

Table 20. Pilot-selected Gains.

a (sec^{-1})	Subject			
	GB	GC	RG	MJ
0	6.5	5	5	7.5
1	2.5	4	5	10
10	65	15	25	75

Gain, K_c, in units of sec^{-2}

The display consisted of the roll angle error shown to the pilot on a 5-inch attitude indicator, and was inertially stabilized.

The roll angle washout circuit has the transfer function

$$\frac{\phi_i}{\phi} = Y_\phi = \frac{s}{s + P_\phi} \tag{47}$$

where p_ϕ is an experimental parameter having values 0.5, 1, and 2 sec^{-1}. To simulate the low side force characteristics of a VTOL in hover, the following transfer function between lateral position and roll angle was used

$$\frac{y_i}{\phi} = Y_y = \frac{(\ell_z - \ell_s)s^2 + bs + g}{(s + p_y)^2} \tag{48}$$

where ℓ_z is the simulated pilot displacement along the z axis, $\ell_s = 1.5$ ft is the actual displacement in the simulator, b is an experimental parameter (usually 0), and p_y is an experimental parameter having values 0.5, 1, or 2 sec^{-1}.

The simulator dynamics were tested and found to be closely approximated by a first-order lag in the roll dynamics:

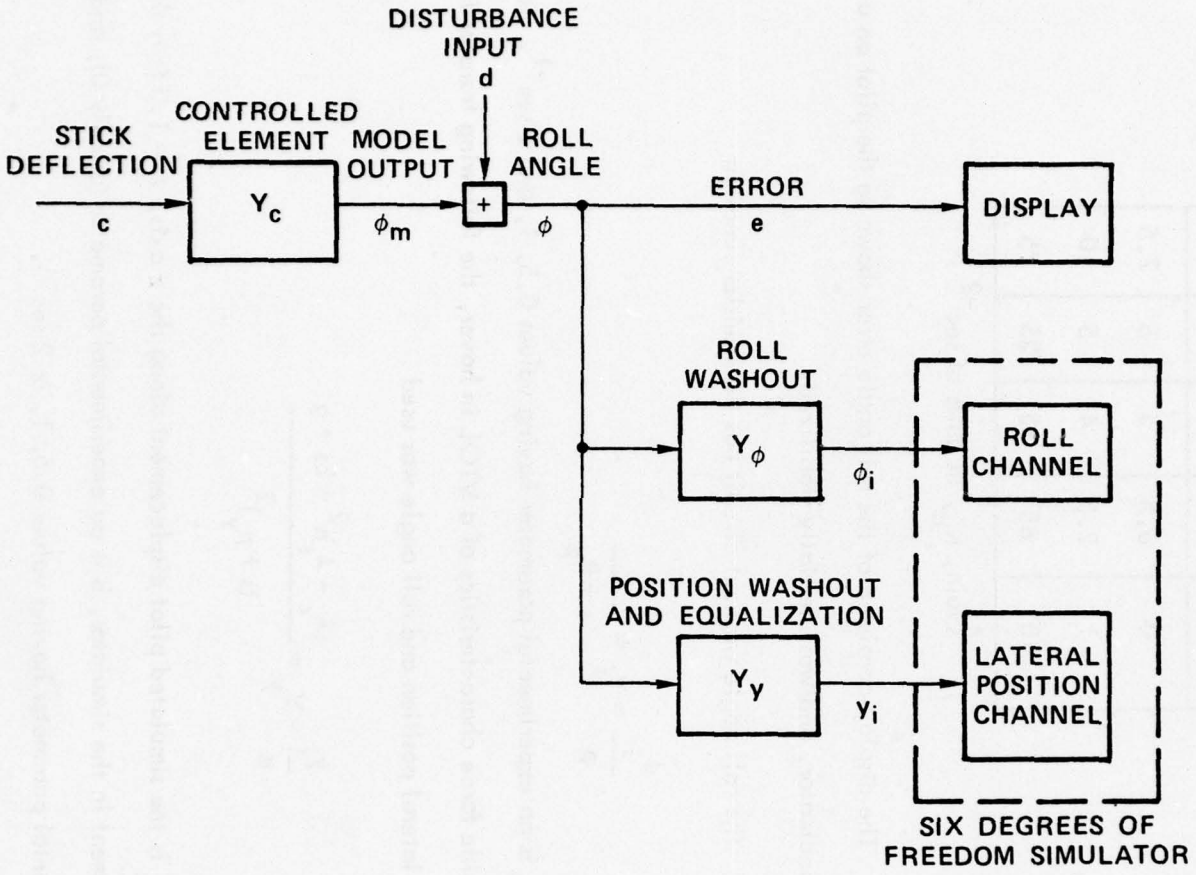

Figure 20. Simulation Schematic Diagram for 2-DOF Roll Control Task.

$$\frac{\phi_s}{\phi_i} \doteq \frac{e^{-\tau s}}{Ts + 1} \tag{49}$$

where ϕ_s = actual roll angle of simulator cab

ϕ_i = commanded roll angle

τ = 0.04 sec

T = 1/12 sec

The lateral position dynamics show run to run variability for frequencies greater than 3 radians per second (it was suggested that the acceleration elements were being reached). An approximation to the position dynamics of the simulator drive system is given by

$$\frac{y_s}{y_i} \doteq \frac{\omega_s^2}{s^2 + 2\zeta_s \omega_s s + \omega_s^2} \tag{50}$$

where y_s = actual lateral position of simulator cab

y_i = commanded lateral position

ζ_s = 0.7

ω_s = 5 rad/sec

The state variable assignment for the optimal control pilot model is shown in Table 21, where again the rectangular disturbance spectrum has been modeled by a fourth-order Butterworth filter. The displayed variables, their weighting coefficients in the quadratic cost functional, and the threshold values are shown in Table 22. The system matrices for the optimal control model are shown in Table 23 for the general case.

Table 21. State Variable Assignment for 2 Degree-of-Freedom Roll Control Task.

State Variable	Simulation Component
$x_1 - x_4$	disturbance shaping filter
x_5, x_6	controlled element
x_7, x_8	roll angle dynamics ϕ_i/ϕ, ϕ_s/ϕ_i
x_9, x_{10}	y_i/ϕ
x_{11}, y_{12}	y_s/y_i
y_{13}, x_{14}	semicircular canal dynamics
x_{15}	otolith dynamics

Table 22. Displayed Variables.

Display Variable	Weighting Coefficient	Threshold
ϕ	$1/(5 \text{ deg})^2$	2 deg
$\dot{\phi}$	$(1 \text{ sec}/5 \text{ deg})^2$	2 deg/sec
SCC	0	0.57 deg/sec^2
OTO	0	0.015 g

Table 23. System Matrices for 2 Degree-of-Freedom Roll Control Task.

$$A = \begin{bmatrix}
0 & 1 & 0 & 0 & 0 & 0 & 0 & 0 & 0 & 0 & 0 & 0 & 0 & 0 & 0 \\
0 & 0 & 1 & 0 & 0 & 0 & 0 & 0 & 0 & 0 & 0 & 0 & 0 & 0 & 0 \\
0 & 0 & 0 & 1 & 0 & 0 & 0 & 0 & 0 & 0 & 0 & 0 & 0 & 0 & 0 \\
-4.2986 & -7.8 & -7.0787 & -3.7624 & 0 & 0 & 0 & 0 & 0 & 0 & 0 & 0 & 0 & 0 & 0 \\
0 & 0 & 0 & 0 & 0 & 1 & 0 & 0 & 0 & 0 & 0 & 0 & 0 & 0 & 0 \\
0 & 0 & 0 & 0 & 0 & -a & 0 & 0 & 0 & 0 & 0 & 0 & 0 & 0 & 0 \\
0 & 0 & 0 & 0 & 0 & 0 & 0 & 1 & 0 & 0 & 0 & 0 & 0 & 0 & 0 \\
0 & 12 & 0 & 0 & 0 & 12 & $-12\,p_\phi$ & $-(12+p_\phi)$ & 0 & 0 & 0 & 0 & 0 & 0 & 0 \\
0 & 0 & 0 & 0 & 0 & 0 & 0 & 0 & 0 & 1 & 0 & 0 & 0 & 0 & 0 \\
0.5615 & 0.0175b & $0.0175(z_2 - z_3)$ & 0 & 0.5615 & $0.0175[b - a(z_2 - z_3)]$ & 0 & 0 & $-p_y^2$ & $-2p_y$ & 0 & 0 & 0 & 0 & 0 \\
0 & 0 & 0 & 0 & 0 & 0 & 0 & 0 & 0 & 0 & 0 & 1 & 0 & 0 & 0 \\
0 & 0 & 0 & 0 & 0 & 0 & 0 & 0 & 25 & 0 & -25 & -7 & 0 & 0 & 0 \\
0 & 0 & 0 & 0 & 0 & 0 & 0 & 0 & 0 & 0 & 0 & 0 & 0 & 1 & 0 \\
0 & 12 & 0 & 0 & 0 & 12 & $-12p_\phi$ & $-(12+p_\phi)$ & 0 & 0 & 0 & 0 & -0.001852 & -0.08888 & 0 \\
0 & 0.001952 & 0 & 0 & 0 & 0.001953 & $-0.003491 - 0.001453\,p_\phi$ & $-0.0001627 \cdot (12+p_\phi)$ & 0.1554 & 0 & -0.1554 & -0.0435 & 0 & 0 & -0.2
\end{bmatrix}$$

$$B = \begin{bmatrix} 0 \\ 0 \\ 0 \\ 0 \\ 0 \\ K \\ 0 \\ 0 \\ 0 \\ (z_2 - z_3)\,0.0175\,K \\ 0 \\ 0 \\ 0 \\ 0 \\ 0 \end{bmatrix} \qquad E = \begin{bmatrix} 0 \\ 0 \\ 0 \\ 4.2986 \\ 0 \\ 0 \\ 0 \\ 0 \\ 0 \\ 0 \\ 0 \\ 0 \\ 0 \\ 0 \\ 0 \end{bmatrix}$$

$$C = \begin{bmatrix}
-1 & 0 & 0 & 0 & -1 & 0 & 0 & 0 & 0 & 0 & 0 & 0 & 0 & 0 & 0 \\
0 & -1 & 0 & 0 & 0 & -1 & 0 & 0 & 0 & 0 & 0 & 0 & 0 & 0 & 0 \\
0 & 0.08352 & 0 & 0 & 0 & 0.08352 & $-0.08352\,p_\phi$ & $-0.00696(12+p_\phi)$ & 0 & 0 & 0 & 0 & -0.00001289 & 0.3475 & 0 \\
0 & 0.01976 & 0 & 0 & 0 & 0.01976 & -0.03533 & $-0.01976 - 0.001647\,p_\phi$ & 1.573 & 0 & -1.573 & -0.4404 & 0 & 0 & -1.024
\end{bmatrix}$$

$$D = \begin{bmatrix} 0 & 0 & 0 & 0 \end{bmatrix}$$

5.1.2 MODEL RESULTS

Figures 21 through 23 compare the describing functions for moving-base conditions and fixed-base conditions obtained with the optimal control model. Also shown are the experimental results obtained by Stapleford, Peters and Alex with subject RG in the nominal condition ($P_\phi = P_y = .5\ sec^{-1}$, $\ell_z = b = 0$). These figures indicate that both the model and the experimental data show only small differences between the fixed-base and moving-base conditions. The model and the experimental data both agree that the closed loop describing function gain is slightly higher for moving-base conditions. Above approximately 1 rad/sec the model agrees very well with the experimental data; however, as discussed in Section 5, the model predicts somewhat lower gain and less phase lag at the lower frequencies.

Figure 24 compares the mean-squared errors for fixed-base and moving-base conditions with the experimental results for three controlled plants. The errors have been normalized by the mean-squared disturbance input. The model predictions show the same trend as the experimental results. However, the model predicts consistently large errors with motion and somewhat smaller errors for the fixed-base condition.

To show the effects of changing the disturbance input spectrum, the Butterworth filter was replaced by a fourth-order Dillow filter for the plant $K_c/s(s+10)$ with the rms input level unchanged. The closed loop describing functions for fixed-base and moving-base are compared with the experimental data in Figure 25. Note that changing the input filter has as much effect as the difference between moving-base and fixed-base conditions.

The effects of varying the simulator dynamics and thereby the vestibular inputs were examined for controlled plant K_c/s^2. Figure 26 shows the closed loop describing function for variations in the lateral position washout parameter p_y. This

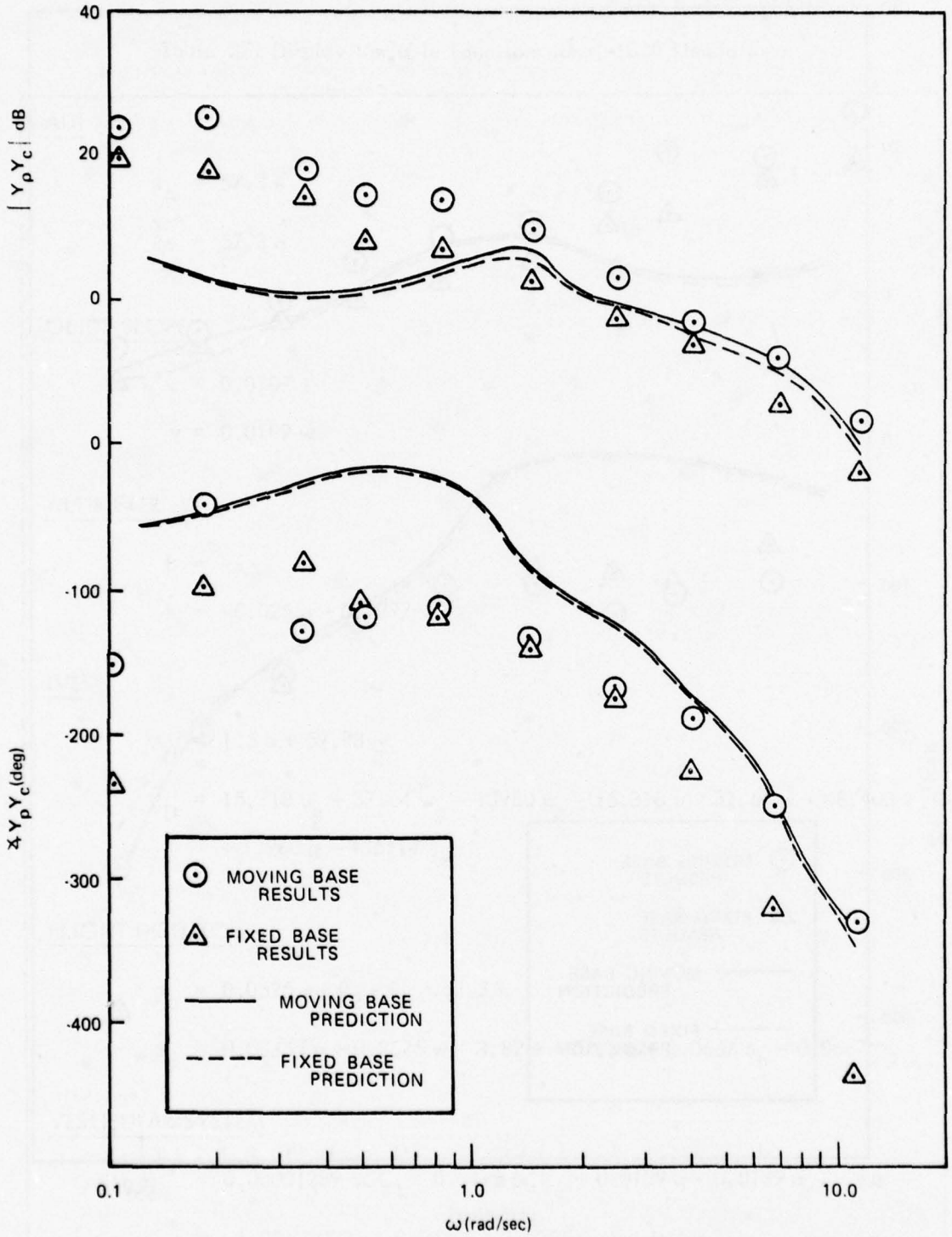

Figure 21. Comparison of Fixed-Base and Moving-Base Results for K/s(s+1) (Subject RG).

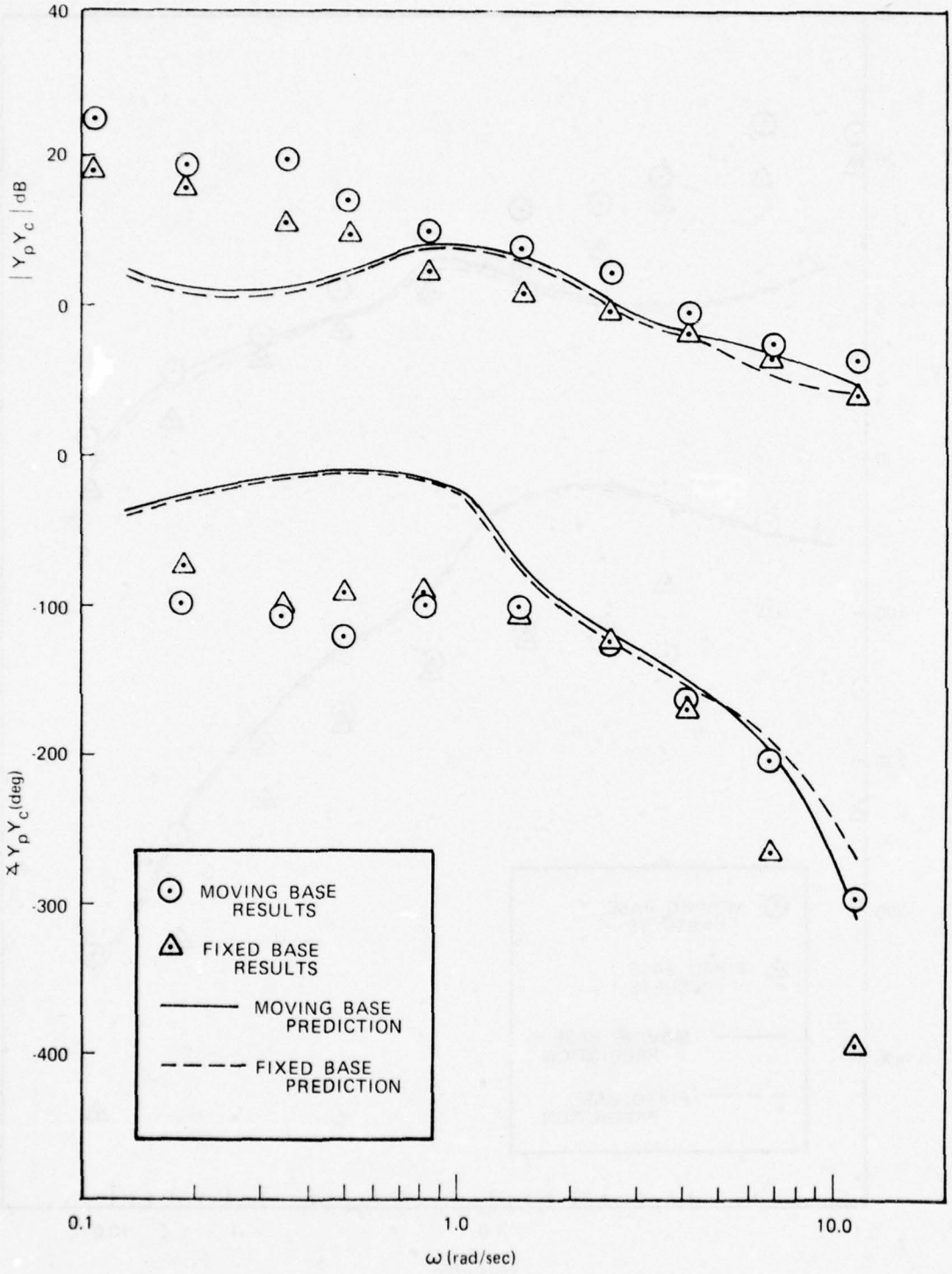

Figure 22. Comparison of Fixed-Base and Moving-Base Results for K/s(s+10). (Subject RG).

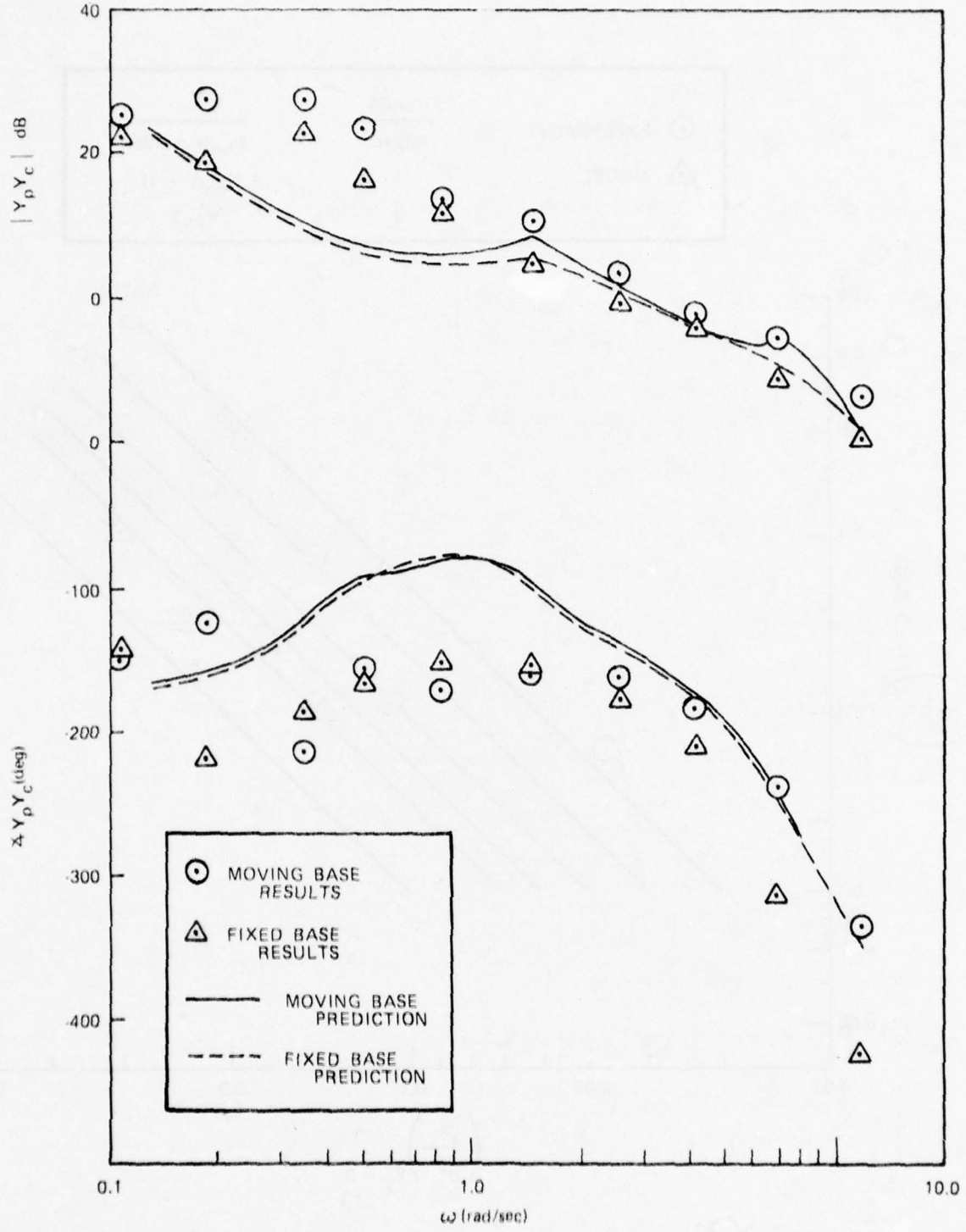

Figure 23. Comparison of Fixed-Base and Moving-Base Results for K/s^2. (Subject RG).

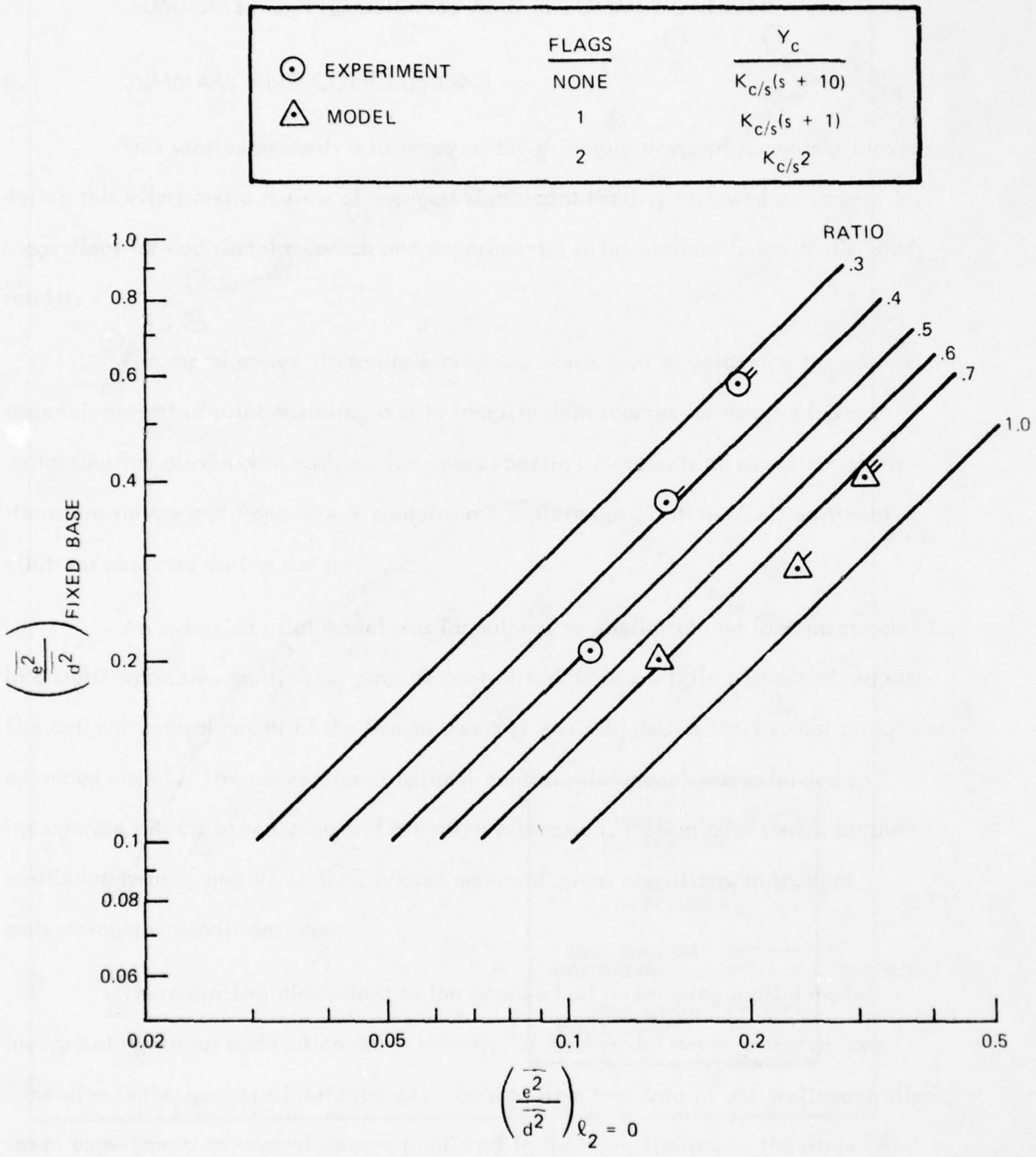

Figure 24. Comparison of RMS Errors for Fixed-Base and Moving Base.

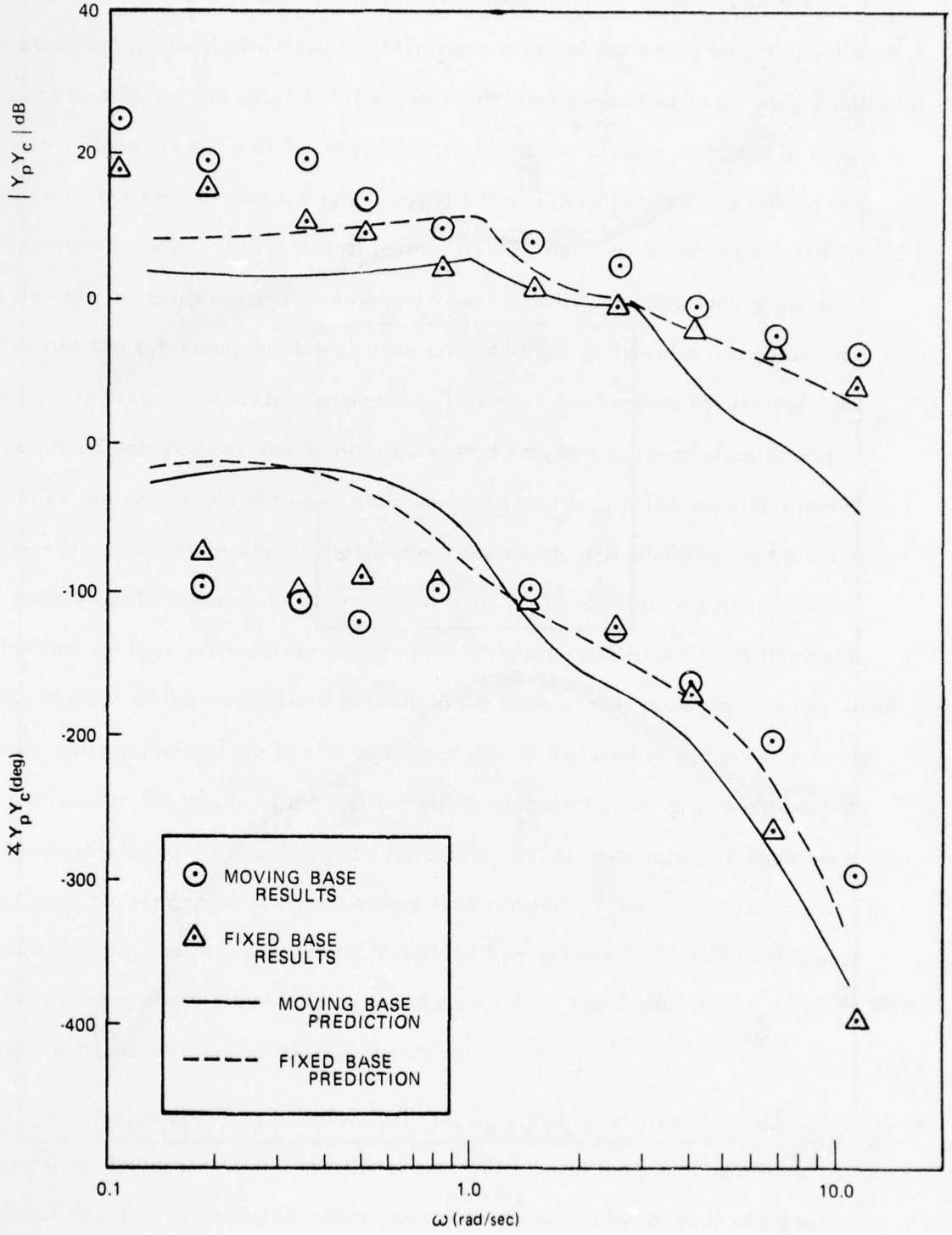

Figure 25. K/s(s+10) Results with Dillow Filter.

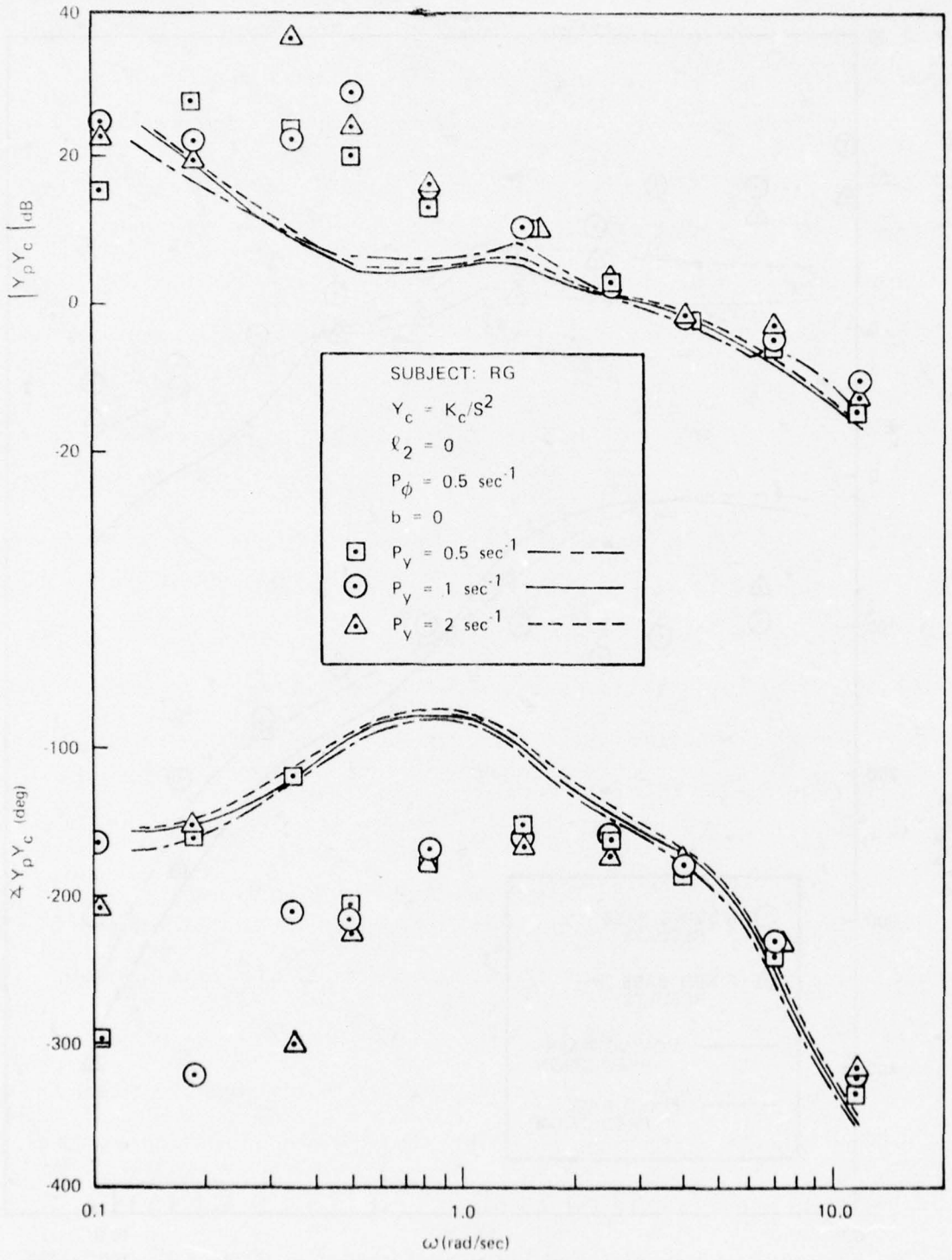

Figure 26. Effect of Lateral Position Washout Variations.

parameter changes just the linear acceleration cues for the pilot; varying p_y from 0.5 sec^{-1} to sec^{-1} showed no significant effects on the describing function nor the RMS results. This conclusion was confirmed by the experimental data in Reference 15. Similarly, varying the roll washout parameter, p_ϕ, from 0.5 sec^{-1} to 2 sec^{-1} had very little effect on the predicted results, as shown in Figure 27. This variation alters both the rotary motion cues and the linear acceleration cues. Again the model predictions agree with the observed experimental results.

5.2 PILOT PERFORMANCE IN LOW VISIBILITY APPROACH

In this section the extended pilot model is used to predict system performance during a low visibility approach. The experimental data was generated during two phases of a low visibility approach simulation reported in detail in Reference 58 (Phase 1) and Reference 59 (Phase 2).

5.2.1 EXPERIMENT DESCRIPTION

The aircraft for this simulation was the military C-135B transport which is quite similar to the commercial Boeing 707 (Reference 60). The configuration for the experiment was fixed at a weight of 160,000 lbs, flaps setting at 50°, and gear down. The experimental run began from a trimmed flight condition at 956 feet altitude on a 3° glide slope. The aerodynamic coefficients were updated as a function of the current flight condition, but did not change significantly.

A conventional flight control system was used in the simulation: the controls included wheel (aileron), column (elevator), and rudders (yaw) and four throttle settings. Figure 28 shows the instrument panel layout used in the simulation.

The cockpit motion system had 3 degrees of freedom -- pitch, roll, and heave within the following limits:

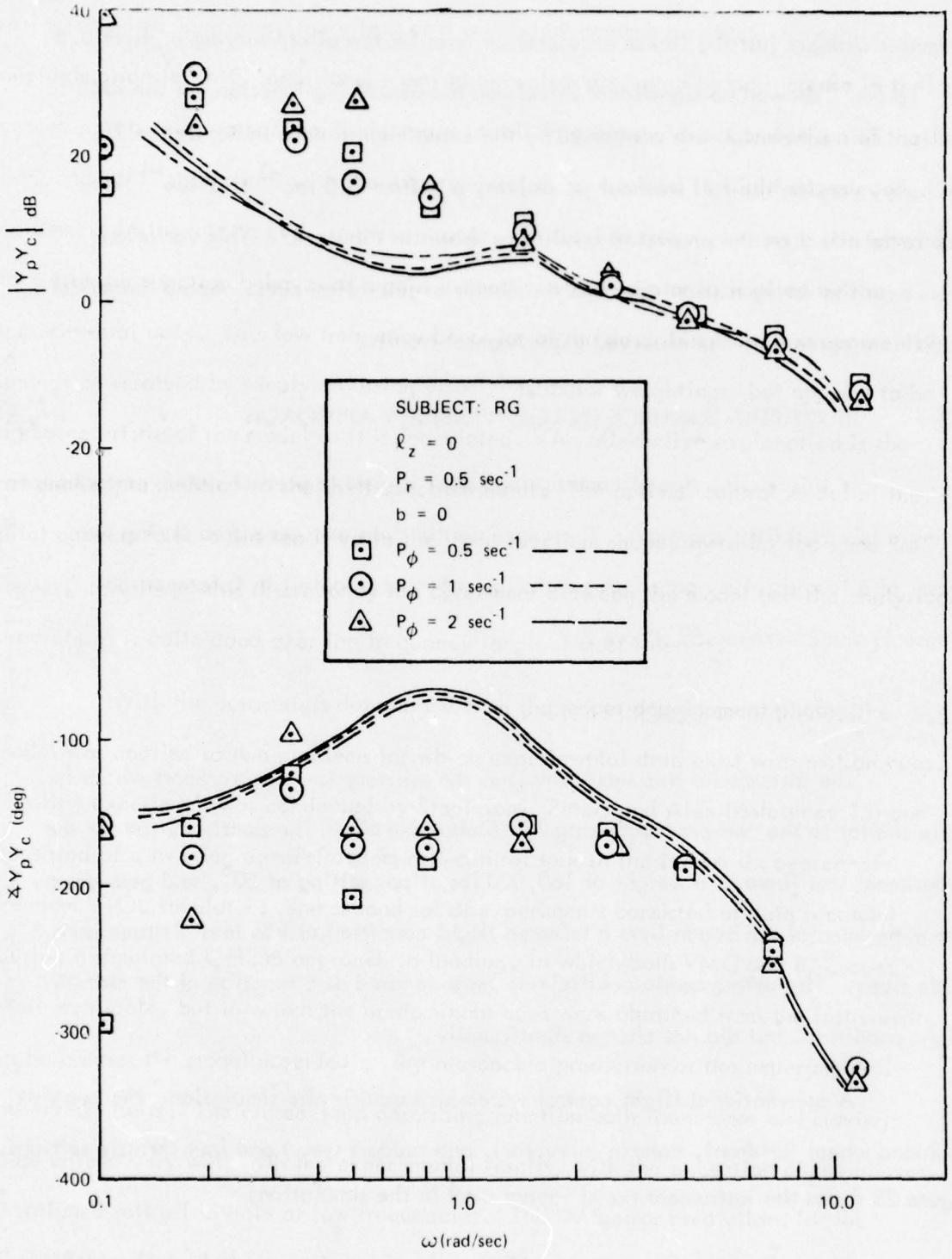

Figure 27. Effect of Roll Washout Variations.

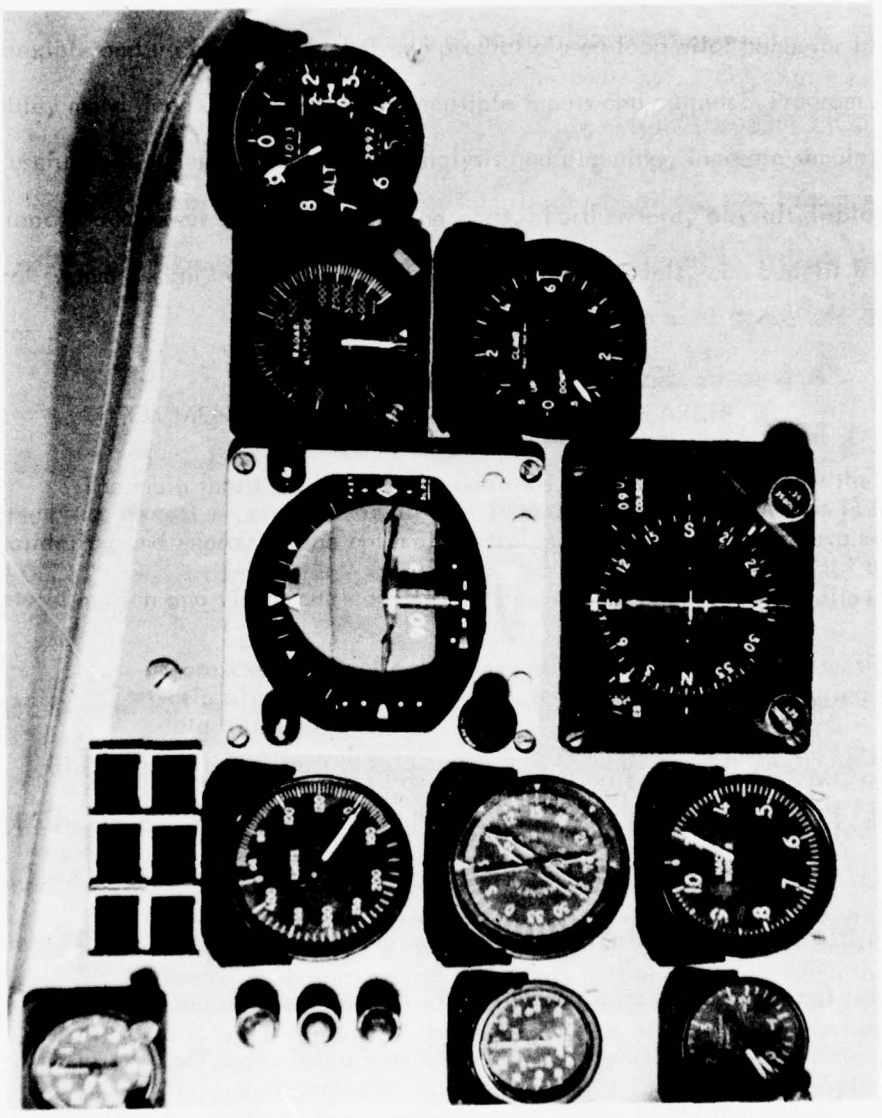

Figure 28. Instrument Panel Layout for Low-Visibility Approach Simulator.

vertical position: $\pm$13 inches

pitch angle: $+14^{\circ}$, -6°

roll angle: $\pm 9^{\circ}$

vertical acceleration: $\pm .8g$

initial angular acceleration in roll: 50 deg/sec^2

initial angular acceleration in pitch: 50 deg/sec^2

5.2.2 MODEL DESCRIPTION

The model was applied to the longitudinal control task of the C-135B approach. The statistical results in Reference 59 divide the approach into two segments based on the range from touchdown:

1. Approach: 10,000 ft - 5,000 ft
2. Final approach: 5,000 ft - 1,500 ft

Because the ASI optimal control pilot model is a stationary one, a frozen point analysis was performed for the midway point in the initial approach segment; i.e., 7,500 ft from touchdown.

The model disturbance input was chosen to represent the Mil Spec 8785B random wind described in Reference 61. The rms gust disturbances were 2.5 fps, 1.65 fps, and .33°/sec for the longitudinal, vertical and pitch inputs respectively (Reference 59). The dynamic equations of motion were written in the aircraft body axis reference frame, assuming stabilized flight on a 3° glide slope. At 7500 ft from touchdown, this corresponds to an altitude of 393 ft; however, since the stability derivatives do not change significantly, the tabulated values from Reference 58 were used for an altitude of 500 ft. These data are summarized in Table 24. The simulator dynamics were approximated by first-order lags of 0.3 sec in heave and 0.5 sec in pitch (Reference 60). The state variable assignments for the model are summarized in Table 25, and the linear equations of motion are shown in Table 26.

Table 24. C-135B Longitudinal Data.

V_T = 233 ft/sec

u_o = 233 ft/sec

w_o = 6.358 ft/sec

γ_o = -3 deg

θ_o = -1.439 deg

h_o = 393 ft

R_o = 7500 ft

STABILITY DERIVATIVES

X_u = -0.013632 sec^{-1}	Z_u = -0.2553 sec^{-1}	M_u = 0.000 3245 rad/sec/ft
X_w = 0.09922 sec^{-1}	Z_w = -0.6274 sec^{-1}	M_w = 0.004662 rad/sec/ft
$X_{\dot{w}}$ = 0.0	$Z_{\dot{w}}$ = 0.0	$M_{\dot{w}}$ = -0.001216 rad/ft
X_q = 0.0 ft/sec	Z_q = 0.0 ft/sec	M_q = -0.7167 sec^{-1}
X_{δ_e} = -0.4686 ft/sec^2/rad	Z_{δ_e} = -7.269 ft/sec^2/rad	M_{δ_e} = -0.9016 sec^{-2}

Table 25. State Variable Assignments for C-135B Simulation.

State Variable	Model Variable	Units
u_g, d	longitudinal gust disturbance	ft/sec
w_g	vertical gust disturbance	ft/sec
q_g	pitch gust disturbance	rad/sec
u	forward speed (body axis)	ft/sec
z	vertical displacement	ft
w	vertical speed (body axis)	ft/sec
w_s	simulator vertical speed (body axis)	ft/sec
θ	pitch angle	rad
q	pitch rate	rad/sec
θ_s	simulator pitch angle	rad
q_s	simulator pitch rate	rad/sec
SCC_1, SCC_2	semi-circular canal dynamics	
OTO_1	forward otolith dynamics	
OTO_2	normal otolith dynamics	
θ_h, θ_2	flight director dynamics	

Table 26. Equations of Motion for C-135B Model.

DISTURBANCE INPUTS

$$\dot{u}_g = -0.219\, u_g + 1.66\, w_1$$

$$\dot{d} = -0.592\, w_g + 1.27\, w_2$$

$$\dot{w}_g = 0.592\, d - 1.18\, w_g + 2.19\, w_2$$

$$\dot{q}_g = 0.00355\, d - 0.00708\, w_g - 1.40\, q_g + 0.0131\, w_2$$

AIRCRAFT DYNAMICS

$$\dot{u} = 0.03632\, u_g - 0.09922\, w_g - 0.03632\, u + 0.09922\, w - 32.1648\theta - 6.358\, q - 0.4686\, \delta_e$$

$$\dot{z} = 0.025\, u + 0.9997\, w$$

$$\dot{w} = 0.2553\, u_g + 0.6274\, w_g - 0.2553\, u - 0.6274\, w + 0.8068\, \theta + 233\, q - 7.269\, \delta_e$$

$$\dot{\theta} = q$$

$$\dot{q} = -0.0006349\, u_g + 0.0007198\, d + 0.00246\, w_g + 0.7167\, q_g + 0.0006349\, u - 0.003899\, w - 0.00098\, \theta - q + 0.00266\, w_2$$

SIMULATOR DYNAMICS

$$\dot{w}_s = 3.33\, w - 3.33\, w_s$$

$$\dot{\theta}_s = q_s$$

$$\dot{q}_s = 2q - 2q_s$$

Table 26. Equations of Motion for C-135B Model (Continued).

VESTIBULAR DYNAMICS

$$SCC_1 = SCC_2$$

$$SCC_2 = -0.001852\ SCC_1 - 0.08888\ SCC_2 + 2q - 2q_s$$

$$OTO_1 = -0.2\ OTO_1 + 0.1990\ \theta_s - 0.0932\ q + 0.0932\ q_s$$

$$OTO_2 = -0.2\ OTO_2 + 0.0207\ w - 0.0207\ w_s - 0.00502\ \theta_s - 0.7708\ q + 0.7708\ q_s$$

FLIGHT DIRECTOR DYNAMICS

$$\dot{\theta}_h = -0.005\ u - 0.1999\ w - 2\ \theta_h$$

$$\dot{\theta}_2 = 0.0667\ \theta_h - 0.0667\ \theta_2 + 3.82\ \theta$$

The primary displays used by the pilot for longitudinal control are assumed to be the ADI ($\theta, \dot{\theta}$), ILS glideslope ($r, \dot{r}$), altimeter ($h, \dot{h}$), VSI ($V_D, \dot{V}_D$). In addition, the Collins FD-109 Pitch Axis Flight Director was available (Figure 29). The vestibular inputs consisted of semicircular sensations of pitch acceleration and otolith detection of specific force along the forward and normal axes. The pilot's head was assumed to be 7.5 ft above and 62 ft ahead of the aircraft center of gravity. The displayed variable equations are summarized in Table 27; their corresponding cost weightings and thresholds are presented in Table 28. Only one control input was assumed for the longitudinal control task, since it is evident from the experimental data shown in References 58 and 59 that, as would be expected, the throttles are used only in the very last stages of the approach. Because the longitudinal control is through the rather large moment of inertia and stiff elevator column, we set the weight on control rate to correspond to a maximum value of approximately three inches per second.

5.2.3 MODEL RESULTS

Table 29 compares the predicted RMS longitudinal errors with the average (10,000' - 5,000') stationary statistics for selected variables reported in Reference 59. The model results are presented for three situations, each using a total fraction of longitudinal control attention of 0.5. In the first case, the attention allocation among the five instruments was optimized, and the pilot's strategy was to spend as much time as possible on the flight director. In the second case, the control attention was equally distributed among the instruments ($f_{c_i} = 0.1$). Finally the maximum pitch rate used in the cost function was increased by an order of magnitude to represent the VMC situation. However, the results are nearly identical for all three cases. Note that the RMS pitch errors and RMS altitude errors agree very closely with the experimental data. However, the experimental results exhibit considerably more control activity, and consequently larger pitch rate errors than predicted by the model.

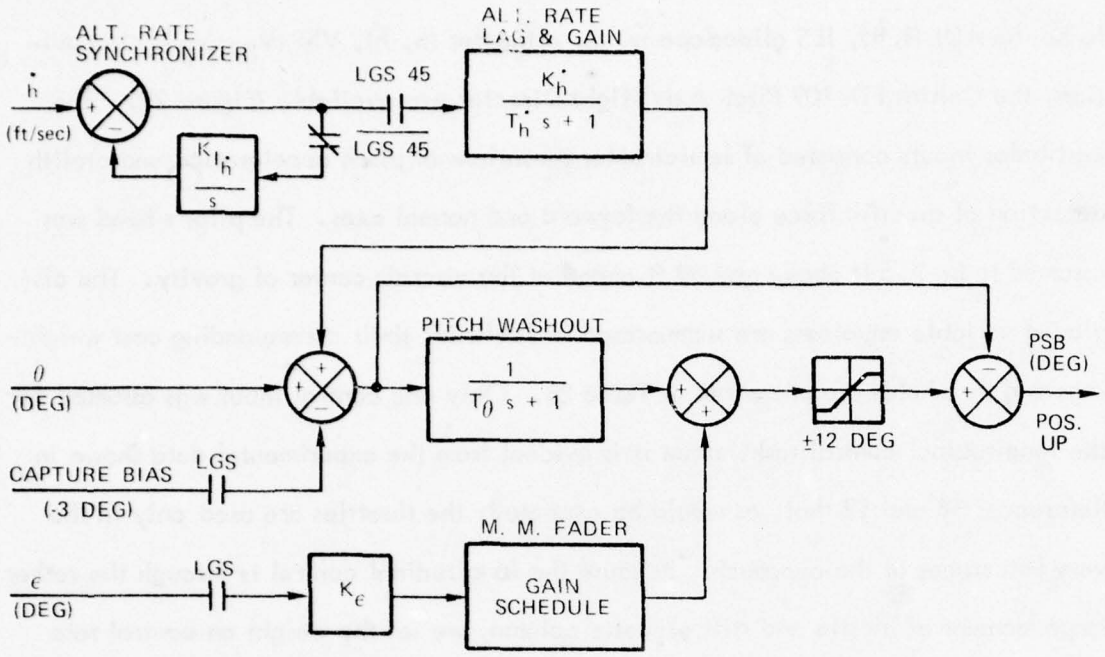

1. Switching Logic:
   (a) The Logic Symbology shows the "on" condition.
   (b) LGS indicates glideslope capture.
   (c) LGS 45 indicates 45 seconds after LGS.

2. The gain shcedule is a function of time from middle marker capture.

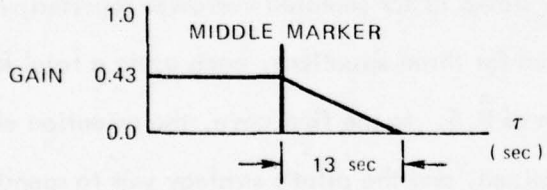

3. The gains and time constants are:

   $K_{I_{\dot{h}}}$ = Altitude Rate Synchronizer Gain = 2.0 sec^{-1}

   $K_{\dot{h}}$ = Altitude Rate Gain = 0.1 deg/fps

   $T_{\dot{h}}$ = Altitude Rate Lag T.C. = 0.5 sec

   T_{θ} = Pitch Washout (Lag) T.C. = 15 sec

   K_{ϵ} = Glideslope Deviation Gain = 16

Figure 29. Collins FD-109 Pitch Axis Flight Director.

Table 27. Display Variable Equations for C-135B Simulation.

ADI

$$\theta_A = 57.3\,\theta$$

$$\dot{\theta}_A = 57.3\,q$$

GLIDE SLOPE

$$\gamma = 0.0109\,z$$

$$\dot{\gamma} = 0.0109\,w$$

ALTIMETER

$$h = -z$$

$$\dot{h} = -0.025\,u - 0.9997\,w$$

IVSI

$$V_D = 1.5\,u + 59.98\,w$$

$$\dot{V}_D = 15.318\,u_g + 37.64\,w_g - 13980\,q_g - 15.318\,u - 37.64\,w + 48.408\,\theta + 13980\,q - 436.14\,\delta_e$$

FLIGHT DIRECTOR

$$\theta_c = 0.0525\,z + \theta_2 - \theta_h + 57.3\,\theta$$

$$\dot{\theta}_c = 0.00355\,u + 0.2525\,w + 3.82\,\theta + 57.3\,q + 2.0667\,\delta_h - 0.0667\,\theta_2$$

VESTIBULAR SYSTEM

$$y_{scc} = 0.00001289\,SCC_1 + 0.3479\,SCC_2 + 0.0139\,q - 0.0139\,q_s$$

$$y_{oto_1} = -1.024\,OTO_1 - 0.944\,q + 2.0229\,\theta_s + 0.944\,q_s$$

$$y_{oto_2} = -1.024\,OTO_2 + 0.2095\,w - 0.2095\,w_s - 7.8\,q - 0.0508\,\theta_s + 7.8\,q_s$$

Table 28. Display Variables - Weights and Thresholds.

Display Element	Maximum Value	Cost Weight	Threshold
θ	5°	0.04	2°
$\dot{\theta}$	2.5°/sec	0.16	1°/sec
γ	1/2 scale	4	0.1
$\dot{\gamma}$	1/2 scale/7 sec	196	0.05
h	50 ft	0.0004	20 ft
$\dot{h}$	7 ft/sec	0.0204	3 ft/sec
V_D	200 ft/min	0.000025	50 ft/min
$\dot{V}_D$	30 ft/min/sec	0.0011	7 ft/min/sec
θ_c	4°	0.0625	1°
$\dot{\theta}_c$	2°/sec	0.25	0.2°/sec
y_{scc}	-	0	0.57 rad/sec^2
y_{oto_1}	-	0	0.015 g's
y_{oto_2}	-	0	0.015 g's

Table 29. RMS Errors for Low-Visibility Approach.

Display Variable (Units)	Model			Experiment (Ref. 59)		
	IMC Opt. Attention	IMC =Attention	VMC =Attention	CAVU	400/1600	100/1200
θ (deg)	0.73	0.79	0.80	0.77	0.94	0.83
q (deg/sec)	0.28	0.29	0.29	0.84	0.70	0.66
γ (%)	10.65	10.86	10.81			
h (ft)	9.77	9.96	9.92	9.58	8.94	9.36
$\dot{h}$ (fpm)	90.29	93.12	93.05			
θ_c (deg)	0.79	0.85	0.85			
δ_e (deg)	0.49	0.47	0.47	1.23	1.26	1.26

Independent research performed in-house at AFFDL by Pollard (Reference 61) and by Harrington (yet to be published) yielded similar results to those shown in Table 29. These two models plus the model of this report, in three independent studies, showed the same trends for pitch rate, q, and elevator control, δ_e. It is theorized that an incorrect gain on the order of 2.25 was inadvertently recorded when the experimental simulation was documented.

SECTION VI

SUMMARY, CONCLUSIONS, AND RECOMMENDATIONS

6.1 SUMMARY AND CONCLUSIONS

This section presents a summary of the principle accomplishments achieved during this effort and a review of the most significant results, followed by some suggestions for additional research and experimental investigations based on the study results.

A comprehensive literature survey was conducted to determine the current state-of-the-art of pilot modeling and to identify data sources for developing and validating the pilot model with motion cues. Section 2 presents an overview of the literature survey and Appendix A contains a complete compilation of all pertinent citations obtained during the study.

An extended pilot model was formulated to predict closed loop pilot behavior in a multi-variable, multi-loop aircraft control task with multiple inputs and outputs. The optimal control model of the human operator was selected as the foundation for the extended model. The conventional optimal control pilot model was extended to incorporate effects of scanning and attention allocation, motion cues sensed by the vestibular system, and VMC/IMC (visual meteorological conditions/instrument meteorological conditions) cues.

There are two dimensions to the approach of developing a pilot model incorporating visual and motion cues (indeed, for most model developments): one dimension is the number of data sources, ranging from raw data in one well-controlled set of experiments to several sources published in the open literature; the other dimension is that of finely tuning the model parameters to provide excellent fits to the data versus minimal, heuristically-pleasing changes to the existing IMC models. The

method we selected was based on pragmatic considerations of available resources and philosophical grounds. We developed the components of the model on data published by one investigator and validated it on data published by another in a purely predictive fashion. There are many difficulties inherent in the use of data published in the literature, but we feel that the robustness of a model developed in this fashion will compensate for any resulting lack of perfect fit. By the same token we elected to incorporate the components of motion and visual cues by modeling their physical properties and by minimizing the changes and additions to the rules and guidelines for specification of the model parameters. This was done because the limited number of published data sources would not allow both a complete revision of parameter selection rules and a validation of these numerous revisions. The important parameters of the optimal control model of the pilot are described, and guidelines are presented for specifying these parameters to represent a particular simulation situation. The guidelines we have proposed for choosing the weighting coefficients and thresholds removed much of the unnecessary freedom in the model, and appear to give excellent results. The guidelines are to choose the weights on the display variables inversely proportional to the square of the maximum allowable deviation, and to choose the maximum display rate by assuming the ratio between maximum rate and maximum position is the reciprocal of an equivalent time constant of the desired response. The thresholds on display position are those derived from psychophysical or indifference considerations, and the threshold on the display rate is that for position divided by the equivalent time constant of the response.

Motion cues may be effectively incorporated as additional measurement sources from the vestibular system in the optimal control model of the pilot. We have accomplished this by modeling motion cues as being sensed by an equivalent set of vestibular sensors fixed in body axes whose output is proportional to the afferent

firing rate, with the dynamics of the vestibular system incorporated within the controlled element dynamics. These vestibular signals are treated as additional measurements and are not included in the cost functional. Based on the data used in this study, we tentatively assign a noise/signal ratio of -18 dB to the vestibular measurements. The sensitivity of the model predictions to these results should be verified by a more exhaustive investigation before this value becomes an accepted constant in the use of the model.

VMC cues seem to be most appropriately modeled by different behavioral objectives based on the data used in this investigation. In the attitude control task, we ascertained that the maximum roll rate used in the weighting coefficients for the cost functional can be increased by a factor of 10 to describe the behavior of a pilot using VMC cues. No data were available for investigating the effects of VMC cues in a position control task. We suspect that these cues may be accounted for by increasing the maximum attitude angle (threfore decreasing its weight in quadratic cost functional). An alternative is to consider an increase in the maximum linear velocity, or a decrease in penalty on the velocity terminal functional.

During the model development phase three sets of experimental data were utilized to determine appropriate values for the model parameters to incorporate motion cues and VMC cues. The noise/signal ratio for the vestibular measurements was selected from using the data base compiled by Shirley (Reference 17). Five controlled plants of Shirley's were analyzed for motion only (no visual) inputs. It was found that three of the five controlled elements gave a consistent noise/signal ratio of approximately -18 dB for agreement between the model and the experimental data. The single integrator (1/s) gave higher RMS predictions using this value while the neutrally stable plant $10/(s^2 + 10)$ gave lower RMS predictions. These results might be explained by the effect of different levels of motor noise induced by motion effects.

The optimal control model of the pilot was applied to the VTOL hovering task described by Ringland, Stapleford and Magdaleno (Reference 23). These data permitted the investigation of fixed-base experiments in comparison with moving-base with angular motion only, and moving-base experiments containing both linear and angular cues. Data were used for simultaneous longitudinal, lateral and vertical tracking tasks, with experimental results for both "good" and "bad" dynamics corresponding to the degree of aerodynamic damping. The extended pilot model was used to predict RMS tracking performance for each task for different levels of control workload. It was found that motion cues reduced the RMS error as expected, and that bad dynamics generally exhibit more sensitivity to changes in workload than good dynamics. The optimum allocation of control attention between position display and attitude display was determined. Bad dynamics were found to require more attention to the attitude display to derive the necessary information for stabilization, whereas with good dynamics the attention can be devoted to the ultimate position control task. The results of the total task performance predictions showed excellent agreement between the model predictions and the observed range of subject means, both on a relative basis and on an absolute basis. The optimal attention allocations were compared with the measured dwell fraction averaged over all motion conditions. The fraction of attention derived from the model was found to vary in the same manner as the observed dwell fraction, although there is a difference in the attitude and position displays. A closer correspondence between the fraction of attention and dwell fraction might be obtained by artificially imposing a minimum constraint on the fraction of attention for the attitude instrument to account for pilot scanning habits.

The experimental data compiled by Newell and Smith (Reference 25) were used to examine the effects of VMC/IMC cues in the model predictions. For this

roll-control tracking task, the effect of a wide view contact analog display (an approximation to VMC conditions) seems to be well represented by an increase in the maximum roll rate, rather than a decrease in roll rate thresholds. Comparison of the IMC and VMC predictions with the experimental data obtained in flight shows good agreement in the mid to high frequency range. In the low frequency range the forward loop transfer function behaves as a gain instead of an integrator as implied by the experimental data. This low frequency behavior of the describing function apparently cannot be resolved by simply adjusting visual/vestibular weightings, but appears to be a characteristic of the model as it is formulated. (An alternative explanation is the rational approximation to the shelf spectrum input. The optimal control model of the pilot appears to be quite sensitive to the input spectrum shape, even for the same RMS level.) In spite of this discrepancy the agreement between the model and the analytical predictions is quite good over the frequency range of most interest.

With the parameters determined from the model development phase, the model was applied to two problems for which experimental data exist with motion cues. The first experiment was conducted by Stapleford, Peters and Alex (Reference 15) and consisted of a two degree-of-freedom roll-control task in the NASA six degree-of-freedom VTOL simulator. The second set of experiments consisted of data recorded during a simulated C-135B approach to landing, in which both VMC and IMC cues were available, but in which the predominant cues were obtained from the instruments. In both cases the model provided a very reasonable prediction of the experimentally observed results. The closed-loop describing function both fixed-base and moving-base agreed very well with the experimental results, with the exception of the above-mentioned fall off in gain at low frequencies. The RMS error predictions for the C-135B approach also matched the experimental results for pitch and altitude very closely.

A digital computer program (Program PIREP) has been developed to implement the extended optimal control model of the pilot. The user's guide for program PIREP has been written as a separate volume for the convenience of the user. This program has been installed and is operating on the Wright-Patterson digital computer facility. This is a flexible and useful program that can predict closed loop pilot behavior in a multi-variable, multi-loop aircraft task with multiple inputs and outputs. Program PIREP can be a useful tool to improve simulation analysis and planning, increase simulation efficiency, and lower simulator operating costs. Furthermore, aircraft display and control system design, which depends heavily on pilot models, can benefit from this program.

6.2 RECOMMENDATIONS FOR ADDITIONAL RESEARCH

The main thrust of the recommendations may be summarized by the necessity for validating and improving the optimal control model of the pilot under a wider variety of motion and visual cue conditions. The specific needs are as follows:

1. More experimental data are required to confirm the noise/signal ratio of -18 dB which we have tentatively established using the data in this study.

2. Experimental data from VTOL position control under VMC conditions are required to determine the effects of VMC cues in this task, and whether the change in pilot performance can be represented by a decrease in the quadratic functional rates.

3. A careful study on the behavior of the optimal control model to more fully understand its low frequency predictions and the sensitivity to the input spectrum seems necessary. It appears as though this behavior is a characteristic of the model as it is currently used, and is not a result of the incorporation of the motion cues used here.

4. The investigation of simpler representations of the vestibular sensor signals should be undertaken to reduce the complexity and computation requirements of the model.

5. Perhaps the most extensive effort should be expended in the development of quantitative models of subjective simulator fidelity. It is apparent from the many data bases we examined in the course of the study that the control performance and describing function are not the most sensitive indicators of pilot interaction with the simulation. Although the with/without motion cue effects are reflected in the describing function, the motion system fidelity as represented by the various washout circuits may lead to very strong pilot opinion regarding the simulation without changing his control performance or describing functions. Ideally, such a simulation evaluation scheme should be able to predict when the pilots feel that the simulation is "good", when it feels "different", and when the simulation is unnatural, disorienting, or leads to debilatory response.

APPENDIX A

LITERATURE SURVEY ON PILOT MODELING FOR MANNED SIMULATION

In accordance with the contract requirements a literature search was conducted. This included four computer-aided literature retrieval searches in the area of pilot modeling for manned simulation. A Defense Documentation Center (DDC) bibliography of reports was searched for a ten-year period (1965-75) and in the NASA Scientific and Technical Information Facility retrieval of information listed in STAR was similarly searched for both limited distribution and open reports. The descriptive terms used for both of these searches are listed below:

Aircraft piloting tasks
Control theory pilot models
Human pilot dynamics
Manned aircraft simulations
Manned simulation of aerospace vehicles
Manual vehicular control
Mathematical models of human pilot behavior
Pilot behavior
Pilot models
Pilot modeling techniques

Although the STAR list of open literature revealed little that was not already known to us, a number of government and industrial reports and theses not appearing in open literature journals were uncovered by the DDC search.

An interactive computer retrieval search of the Compendex listing of Engineering Index citations was performed on the MIT NASIC system using as key words: human engineering, pilots, simulators, and man-machine systems. Only ten citations of interest were brought forth from the open literature. However, using the MIT NASIC system on the NTIS government report data base a large number of new reports which seem appropriate to us were revealed. For the NTIS data base, the following descriptors were used: pilot performance, simulators, motion stability, vestibular tests, and display

devices. We printed all information on vestibular tests as well as items having pilot performance and any of the other descriptors listed. The four literature searches were then culled for the titles and abstracts deemed most relevant to this contract, and were divided into the following main subject headings:

Simulators or simulation
Pilot performance
Pilot models
Vestibular system
Motion
Displays
Scanning
Workload

A.1 SIMULATORS OR SIMULATION

Alex, F. R.; Peters, R. A.; and Stapleford, R. L.: Experiments and a Model for Pilot Dynamics with Visual and Motion Inputs. Report No. NASA-CR-1325, May 1969.

Armstrong, B. D.: Flight Trials to Discover Whether Peripheral Vision is Needed for Landing. Royal Aircraft Establishment, Farnborough, England, Report No. RAE-TH-7025, November 1970.

Arnold, J. D.: Improved Method of Predicting Longitudinal Handling Qualities. Jt. Autom. Control Conf. of the Am. Autom. Control Counc., June 20-22, 1973.

Baron, S.; and Kleinman, D. L.: Prediction and Analysis of Human Performance. NASA Spec. Publ. SP-281, pp. 247-256, June 1971.

Benjamin, P.: A Hierarchical Model of a Helicopter Pilot. Human Factors, Vol. 12, pp. 361-374, August 1970.

Berthoz, A.; Pavard, B.; and Young, L.: The Role of Peripheral Vision and Visual Vestibular Interactions in the Exocentric Perception of Linear Movement in Humans. Report No. NASA-TT-P-15737, August 1974.

Bray, R. S.: Vertical Motion Requirements for Landing Simulation. Report No. NASA-TM-X-62236, February 1973.

Dierke, R.; and Erdmann, F.: The Effect of Impressions of Motion on Guidance Errors at Simulated ILS Approaches. (In German) Deutsche Gesellschaft fver Luet - Und Raumeahrt Jahrestagung 3rd, December 3-4, 1970.

Franklin, J. A.; and Innis, R. C.: Pitch Attitude, Flight Path, and Airspeed Control During Approach and Landing of a Powered Lift STOL Aircraft. Report No. NASA-TM-X-62203, December 1972.

Frick, R. K.: Quantitative Effects in the Use of Simulators for Training Fighter Pilots. AIAA Paper 72-161, January 1972.

Klier, S.; and Gage, H.: Motion Factors in Flight Simulation. Grumman Aerospace Corp., Bethpage, N. Y., Report No. NAVTRADEVCEN-7890-2, December 1970.

Lew, D. W.; and Dyda, K. J.: Ground-Based Simulation Techniques. North American Aviation, Inc., Los Angeles, California, Los Angeles Division, Report No. DA-1F125901A142, October 1967.

Mathery, W. G.: A Model for Predicting Man's Control Behavior in a Man-Machine System, The Simulation of Human Behavior, NATO Symposium, July 17-21, 1967.

Mission Analysis Study Group: Mission Analysis on Future Undergraduate Pilot Training: 1975 through 1990. Volume 1, Final Report. Randolph Air Force Base, Texas, January 1972.

Newell, F. D.; and Smith, H. J.: Human Transfer Characteristics in Flight and Ground Simulation for a Roll Tracking Task. Report No. NASA-TN-D-5007, February 1969.

Onstott, E. D.; and Salmon, E. P.: Airplane Flying Characteristics in Turbulence. Northrop Corp., Hawthorne, California, Aircraft Division, Report No. NOR-70-139, February 1971.

Palmer, R. G.: A Survey of Selected Visual Stimulation Systems, Naval Training Equipment Center, Orlando, Florida, Report No. NAVTRAEQUIPCEN-IH-192, January 1973.

Rasmussen, P. G.; and Hasbrook, A. H.: Pilot Tracking Performance During Successive In-Flight Simulated Instrument Approaches. Civil Aeromedical Inst., Oklahoma City, Oklahoma, Report, February 1972.

Reeves, P. M.; Campbell, G. S.; Ganzer, V. M.; and Joppa, R. G.: Development and Application of a Non-Gaussian Atmospheric Turbulence Model for Use in Flight Simulators. Report No. NASA-CR-2451, September 1974.

Report on the DGLR Symposium on Flight Mechanical Simulation - Ground Based or In-Flight, December 4, 1970.

Ringland, R. F.; and Stapleford, R. L.: Experimental Measurements of Motion Cue Effects on STOL Approach Tasks. Report No. NASA-CR-114458, April 1972.

Ringland, R. F.; Stapleford, R. L.; and Magdaleno, R. E.: Motion Effects on an IFR Hovering Task Analytical Predictions and Experimental Results. Report No. NASA-CR-1933, November 1971.

Ruocco, J.; Klier, S.; Gage, H.; and Vitale, P.: Design Factors in Environmental Simulation, Grumman Aircraft Engineering Corp., Bethpage, New York, Report No. NAVTRADEVCEN-7890-1, December 1970.

Simulation AGARD Conference Proceedings, Report No. AGARD-CP-79-70, January 1971.

Smith, H. J.: Human Describing Functions Measured in Flight and on Simulators. IEEE Transactions on Human Factors in Electronics, Vol. HEE-8, December 1967.

Snyder, C. T.; Fry, E. B.; Drinkwater, F. J. III; Forrest, R. D.; and Scott, B. C.: Motion Simulator Study of Longitudinal Stability Requirements for Large Delta Wing Transport Airplanes During Approach and Landing with Stability Augmentation Systems Failed. Report No. NASA-TN-X-62200, December 1972.

Stone, J. R.; and Gerken, G. J.: Prediction of Pilot Acceptance for a Large Aircraft. Jt. Autom. Control Conf. of the Am. Autom. Control Counc., June 20-22, 1973.

Szalai, K. J.: Motion Cue and Simulation Fidelity Aspects of the Validation of a General Purpose Airborne Simulator. Report No. NASA-TN-D6432, October 1971.

Thomas, J.; and Kchnen, E.: Evaluation of Man-Machine System Experiments. (In German) Dtsch. luft Raumfahrt, Mitt n 74-03, 1974.

Weener, E. F.: The Effect of Simulator Dynamics on Pilot Response. Report No. NASA-CR-132459, October 1974.

Weir, D. H.; and McRuer, D. T.: Pilot Dynamics for Instrument Approach Tasks Full Panel Multiloop and Flight Director Operations. Report No. NASA-CR-2019, May 1972.

A.2 PILOT PERFORMANCE

Connelly, E. A.; Knoop, P. A.; and Schuler, A. R.: Study of Adaptive Mathematical Models for Deriving Automated Pilot Performance Measurement Techniques, Volume 1 - Model Development. AFHRL-TR-69-7-VOL-1, October 1969.

Kraus, E. F.: A Parametric Study of Pilot Performance with Modified Aircraft Control Dynamics, Varying Navigational Task Complexity and Induced Stress. Illinois University Savoy Aviation Research Lab. Report No. ARL-73-10/AFOSR-73-6/FAA-73-3, May 1973.

Pap, Behavioral Models for Pilots. (In German) Dtsch Luft Raumfahrt, Mitt n 74-42, 1974.

Prophet, W. W.: Performance Measurement in Helicopter Training and Operations. Human Resources Research Organization, Alexandria, Virginia, Report No. HUMRRO Professional Paper-10-72, April 1972.

Wanner, J.-C.: Presentation of the Data Required for Takeoff and Landing - Pilot Performance Model for Cockpit Display Development. (In French) NATO, AGARD Symposium on Take-Off and Landing, April 1-5, 1974.

Wells, W. R.: Application of Nonlinear Estimation Theory to Pilot Modeling. Symposium on Nonlinear Estimation Theory and its Applications, September 10-12, 1973.

A.3 PILOT MODELS

Allen, R. W.; and Jex, H. R.: An Experimental Investigation of Compensatory and Pursuit Tracking Displays with Rate and Acceleration Control Dynamics and a Disturbance Input. Report No. NASA-CR-1082, June 1968.

Connelly, E. M.; Schuler, A. R.; Bourne, F. J.; Knoop, P. A.: Application of Adaptive Mathematical Models to a T-37 Pilot Performance Measurement Problem, Melpar, Falls Church, Virginia, Report No. 9050, January 1971.

Denero, R. P.; and Greenleaf, G. L.: Selection of Optimal Stability Augmentation System Parameters for a High Performance Aircraft Using Pitch Paper Pilot. Master's Thesis, Air Force Institute of Technology, Wright-Patterson AFB, Ohio, October 1972.

Elkind, J. I.; Levinson, W. H.; and Ward, J. L.: Studies of Multivariable Manual Control Systems - A Model for Task Interference. Report No. NASA-CR-1746, May 1971.

Frostell, C. E.: A Comparison of Pilot Describing Function Measurement Techniques. Toronto University Institute for Aerospace Studies, Report No. UTIAS-TN-167, October 1971.

Heifferon, J. C.: The Effects of Input Power Spectra on Human Operator Compensatory Tracking. Master's Thesis, Air Force Institute of Technology, Wright-Patterson AFB, Ohio, March 1970.

Hill, J. W.; and Goebel, R. A.: Development of Automated GAT-1 Performance Measures. Stanford Research Institute, Melno Park, California, Report No. AF-1123, May 1971.

Jones, J. G.: On the Measurement of Human Operator Describing Functions in Flight Experiments, Royal Aircraft Establishment, Farnborough, England, Report No. RAE-TM-AERO-967, December 1966.

Klein, R. H.; and Weir, D. R.: The Measurement and Analysis of Pilot Scanning and Control Behavior During Simulated Instrument Approaches. Report No. NASA-CR-1535, June 1970.

Magdaleno, R.; McRuer, D. T.; and Stapleford, R. L.: Pilot Describing Function Measurements in a Multiloop Task. Report No. NASA-CR-542, August 1966.

McRuer, D. T.: Human Pilot Dynamics in Compensatory Systems. Systems Technology, Inc., Hawthorne, California, Project No. AF-8219, July 1965.

McRuer, D. T.; Hofmann, L. G.; Jex, H. R.; Moore, G. P.; and Phatak, A. V.: New Approaches to Human-Pilot/Vehicle Dynamic Analysis, Systems Technology, Inc., Hawthorne, California, Report No. STI-TR-164-2, February 1968.

McRuer, D. T.; and Krendel, E. S.: Mathematical Models of Human Pilot Behavior. Report No. AGARD-AG-188, January 1974.

Thielges, J. R.; and Matheny, W. G.: Analysis of Visual Discriminations in Helicopter Control. Human Resources Research Organization, Alexandria, Virginia, Report No. HUMRRO-TR-71-13, June 1971.

Walker, S. A.: Pilot Parameter Identification via the Extended Kalman Filter. Master's Thesis, Air Force Institute of Technology, Wright-Patterson AFB, Ohio, June 1973.

Warren, R. D.: A Hybrid Computer Technique for Measuring Human Describing Functions and Remnant in Closed-Loop Tracking Tasks. Master's Thesis, Naval Postgraduate School, Monetery, California, June 1972.

Willen, T. B.: The Human Pilot as a Dynamic Element in Aircraft Control Systems. Aeronautical Systems Division, Wright-Patterson AFB, Ohio. Report No. ASD-TR-73-47, April 1974.

A.4 VESTIBULAR SYSTEM

Benson, A. J.; Reason, J. T.; Diaz, E.: Testing Predictions Derived from a Model of Progressive Adaptation to Coriolis Accelerations. Flying Personnel Research Committee, London, England, Report No. FPRC/1311, July 1971.

Dowd, P. J.; Moore, E. W.; and Cramer, R. L.: Effects of Flying Experience on the Vestibular System: A Comparison Between Pilots and Non-Pilots to Coriolis Stimulation. School of Aerospace Medicine, Brooks AFB, Texas, Report No. SAM-TR-66, 210, January 1966.

Gazenko, O. G.; and Chekhonadskiy, N. A.: Some Properties of a Mathematical Analog of the Central Portion of a Vestibular Analyzer. Report No. NASA-TT-P-15130, September 1973.

Malcik, V.: Pilot Orientation in Complicated Meteorological Conditions. Foreign Technology Division, Wright-Patterson AFB, Ohio, Report No. FTD-HT-23-372-68, July 1968.

Ormsby, C. C.: Model of Human Dynamic Orientation. Ph.D. Thesis, Massachusetts Institute of Technology, 1974.

Peters, R. A.: Dynamics of the Vestibular System and Their Relation to Motion Perception, Spatial Disorientation, and Illusions. Report No. NASA-CR-1309, April 1969.

Sinacori, J. B.: Validation of Ground Based Simulation. J. Amer. Helicopter Soc., Vol. 15, No. 13, 3 July 1970.

Toppinga, M. L.: The IW-TNO Simulator - An Investigation of Rotation Sensation. (In Dutch) Institute for Perception, RVO-TNO, Soesterberg, Netherlands, Report No. IZF-1974-16, 1974.

Young, L. R.: Research on Biophysical Evaluation of the Human Vestibular System. Report No. NASA-CR-140063, August 1974.

A.5 MOTION

Besco, R. O.: The Effects of Cockpit Vertical Accelerations on a Simple Piloted Tracking Task. North American Aviation, Inc., Los Angeles, California, Report No. NA-61-47, April 1961.

Caiger, B.: Some Effects of Vertical Vibration on a Pilot's Head Motion and His Instrument Reading Capability. National Aeronautical Establishment, Ottawa, Canada, Report, August 1966.

Cramer, R. L.; and Wolfe, J. W.: Effects of Pitch and Coriolis Illusions Upon Adjustment of Pitch Angle. School of Aerospace Medicine, Brooks AFB, Texas, Report No. SAM-TR-70-249, 1970.

Gibino, D. J.: Effects of Presence or Absence of Cockpit Motion in Instrument Flight Trainers and Flight Simulators. Aeronautical Systems Div., Wright-Patterson AFB, Ohio, Report No. ASD-TR-68-24, June 1968.

Hutton, G. B.: Vertical Cockpit Accelerations Measured on an Operational Jet Transport Aircraft. Royal Aircraft Establishment, Farnborough, England, Report No. RAE-TR-69214, 1971.

Jacobs, R. S.; Williges, R. C.; and Roscoe, S. N.: Simulator Motion as a Factor in Flight-Director Display Evaluation. Report No. ARL-72-1/ONR-72-1/AFOSR-72-1, February 1972.

Koonce, J. M.: Effects of Ground-Based Aircraft Simulator Motion Conditions Upon Prediction of Pilot Proficiency, Parts I and II. Report No. ARL-74-5/AFOSR-74-3-PT-1,2, April 1974.

Newell, F. D.; and Pietrzak, P. E.: In-Flight Measurement of Human Response Characteristics, Cornell Aeronautical Lab., Inc., Buffalo, New York, Report, 1967.

Piranian, A. G.: The Influences of Buffet, Sustained Normal Accelerations, and Basic Aircraft Flying Qualities on Tracking Performance in Air Combat Maneuvering. Naval Air Development Center, Warminster, Pennsylvania, Report No. NADC-73257-30, July 1974.

Ringland, R. B.; and Stapleford, R. L.: Motion Cue Effects on Pilot Tracking. NASA Spec. Publ. SP-281, June 1971.

Smiles, K. A.: Human Performance Capability in the Aircraft Acceleration Environment of Aerial Combat. Aerospace Medical Research Lab, Wright-Patterson AFB, Ohio, Report No. AMRL-TR-72-60, 1972.

A.6 DISPLAYS

Ehrhardt, L. E.; Cavallero, F. R.; and Kennedy, R. S.: Effect of a Predictor Display on Carrier Landing Performance, Part II. Laboratory Mechanization, Dunlap and Associates, Inc., Inglewood, California, Project NR-196-106, June 1973.

Pangburn, R. C.; Metzler, T. R.; and Kline, J. M.: Pilot Performance as a Function of Three Types of Altitude Displays. Aeronautical Systems Div., Wright-Patterson AFB, Ohio, Report No. ASD-TR-72-63, August 1972.

Wilson, C. A.: The Simulation and Analysis of Carrier Landings Using a Nonlinear Pilot Model. Master's Thesis, Naval Postgraduate School, Monterey, California, June 1973.

Wulfeck, J. W.; Prosin, D. J.; and Burger, W. J.: Effect of a Predictor Display on Carrier Landing Performance, Part I, Experimental Evaluation. Dunlap and Associates, Inc., Inglewood, California, Project NR-196-106, June 1973.

A.7 SCANNING

Carbonell, J. R.; Senders, J. W.; and Ward, J. L.: A Queueing Model of Visual Sampling Experimental Validation. IEEE Transactions on Man-Machine Systems, Vol. MMS-9, September 1968.

Clement, W. F.; Graham, D.; and Best, J. J.: A Reexamination of Eye Movement Data. Systems Technology, Inc., Hawthorne, California, Report No. STI-TM-163-A, February 1967.

Machuca, L. A.; and Lind, J. M.: Verification and Extension of Display Scanning and Remnant Models Using Aircraft Lateral and Longitudinal Dynamics as Controlled Elements. Master's Thesis, Air Force Institute of Technology, Wright-Patterson AFB, Ohio, May 1971.

Senders, J. W.: A Re-Analysis of the Pilot Eye-Movement Data. IEEE Transactions on Human Factors in Electronics, Vol. HFE-7, June 1966.

Stern, J. A.: The Effect of Fatigue on Visual Search Activity in Helicopter Pilots. Washington University, St. Louis, Missouri, Annual Summary Report, 1970.

Wanamaker, J. E.; and Sower, W. A.: Extension of Pilot Describing Functions to Multiple Compensatory Tracking Tasks. Master's Thesis, Air Force Institute of Technology, Wright-Patterson AFB, Ohio, March 1969.

A.8 WORKLOAD

Soliday, S. M.: Effects of Task Loading on Pilot Performance During Simulated Low-Altitude Highspeed Flight. North American Aviation, Inc., Columbus, Ohio, Project ID1312010159, February 1965.

APPENDIX B

OPTIMAL CONTROL MODEL OF THE PILOT

The overall closed-loop pilot/vehicle/display system is shown in Figure B-1. The equalization network represents the means by which the pilot attempts to optimize his control strategy for a given situation.

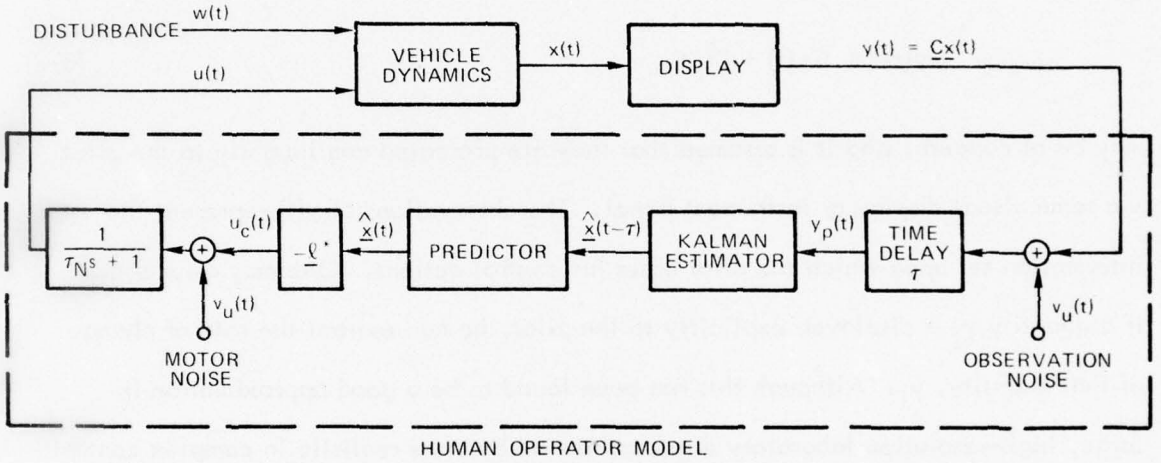

Figure B-1. Optimal Control Model of Human Operator.

B.1 BASIC FORMULATION

To simplify the discussion the important elements of the optimal-control model will be reviewed for a single system control input (model output). Note, however, that this distinction between single-loop and multi-loop tasks is not restrictive, since both are subsumed in this formulation. The multi-control input (multi-axis) case is a straightforward extension of these results and will be described later.

It is assumed that the vehicle dynamics, which may include actuator, sensor, and display dynamics, are represented by the linear time-invariant equations of motion:

$$\dot{x}(t) = Ax(t) + bu(t)\ Ew(t) \tag{B-1}$$

where the n-vector x(t) represents the vehicle state, u(t) is the pilot's control input to the system, and w(t) represents random external disturbances (e.g., turbulence, wind gusts). Shaping filters states are incorporated in x(t) to provide correlation. Without loss of generality, w(t) is a vector of independent zero-mean normalized Gaussian white noises.

Several system outputs

$$y(t) = Cx(t) + Du(t) \tag{B-2}$$

may be of concern, and it is assumed that they are presented continuously to the pilot via some visual display or instrument panel. The observations of y(t) represent the information set upon which the pilot bases his control actions. One may assume that if a quantity y_i is displayed explicitly to the pilot, he can extract the rate of change of that quantity, $\dot{y}_i$. Although this has been found to be a good approximation in large, high-resolution laboratory displays, it may be more realistic in complex control and monitoring tasks to have y consist of explicitly displayed variables only.

In the model of Figure B-1 an "equivalent" observation noise vector is added to y(t). A single noise $v_{y_i}(t)$ is associated with each displayed output $y_i(t)$. Studies of controller remnant (Reference B-1) have suggested that over a wide range of tracking tasks, the injected noises $v_{y_i}(t)$ are sufficiently wide-band so as to be approximated by independent Gaussian white-noise processes with auto-covariances

$$E\{v_{y_i}(t)\, v_{y_i}(\sigma)\} = V_{y_i} \cdot \delta(t-\sigma), \quad i = 1, 2, \ldots, r$$

or

$$E\{v_y(t)\, v_y'(\sigma)\} = \text{diag}\,(V_y) \cdot \delta(t-\sigma) \tag{B-3}$$

This has been found to be an excellent assumption.

In general, a numerical determination of the noise covariance matrix V_y will depend, among other things, on the relevant features (quality, type, and form) of the display and on where the human is fixating, i.e., whether he is viewing a display directly (foveally) or peripherally.

The pilot perceives

$$y_p(t) = y(t - \tau) + v_y(t - \tau)$$

$$= Cx(t - \tau) + Du(t - \tau) + v_y(t - \tau) \qquad \text{(B-4)}$$

a delayed noisy replica of the system outputs. $y_p(t)$ is "processed" by the pilot (through some equalization network and motor dynamics) to yield a "commanded" control input $u_c(t)$.

A motor noise $u_m(t)$, which could represent random errors in executing the intended control movements, or the fact that the human does not have perfect knowledge of the system input $u(t)$, is added to $u_c(t)$. Thus,

$$u(t) = u_c(t) + u_m(t) \qquad \text{(B-5)}$$

$u_m(t)$ is assumed to be a (wide-band) first-order noise process generated by

$$\dot{u}_m(t) + \gamma u_m(t) = u_m(t) \qquad \text{(B-6)}$$

where

$u_m(t)$ is a Gaussian white noise level with autocovariance V_m.

It is assumed that the control task is adequately reflected in the pilot's choice of a feedback control $u_c(\cdot)$ which, in the steady state, minimizes the cost functional

$$J(u) = E\left\{\sum_{i=1}^{r}\right\} q_i y_i^2 + g\dot{u}_c^2 \qquad \text{(B-7)}$$

conditioned on the perceived information $y_p(\cdot)$;

The cost functional weightings $q_i \geq 0$, and $g > 0$ in Equation B-7 may be either objective (specified by the experimenter or designer) or subjective (adopted by the human in performing and relating to the task). Clearly, the selection of any subjective cost weightings is a nontrivial matter and is tantamount to mathematically quantifying the pilot's control objectives. In some cases this can be accomplished a priori, since the actual weightings may often correspond to the objective weightings. Furthermore, since the pilot will adapt a strategy to obtain "good" performance, and since a control system designer would be able to choose weighting to give "good" performance in a linear-system quadratic-cost design procedure, the choise of weights is relatively straightforward. Thus, the pilot's control characteristics are determined by the solution of a well-defined optimal linear regulator problem with time delay and observation noise. It can be shown (Reference B-2) that the control $u_c(t)$ that minimizes $J(u)$, conditioned on the observations $y_p(\cdot)$, is generated by the linear (separable) feedback law

$$\tau_N \dot{u}_c(t) + u_c(t) = -L^* \hat{x}(t) - L_m^* \hat{u}_m(t) \qquad \text{(B-8)}$$

where $\hat{x}(t)$ is the best estimate of the system state $x(t)$ based on the observed data $y_p(\sigma)$, $\sigma < t$, and $\hat{u}_m(t)$ is the best estimate of $u_m(t)$. Note that $\hat{u}_c(t) = u_c(t)$.

The time constant τ_N and the optimal gains L^* are given by

$$\tau_N = \lambda_{n+1}^{-1} \quad L_i^* = \tau_N \lambda_i, \quad i = 1, \ldots, n \qquad \text{(B-9)}$$

where

$\lambda = [\lambda_1, \lambda_2, \ldots, \lambda_{n+1}]$ is obtained from

$$\lambda = b_0' K_0 / g \tag{B-10}$$

K_0 is the unique positive definite solution of the n + 1 dimensional Riccati equation

$$A_0' K_0 + K_0 A_0 + C_0' Q C_0 - K_0 b_0 b_0' K_0 / g = 0 \tag{B-11}$$

with $Q_0 = \text{diag}\,[q_1, q_2, \ldots, q_r]$; $b_0 = \text{col}\,[0, 0, \ldots, 0, 1]$ and

$$A_0 = \left[\begin{array}{c|c} A & b \\ \hline 0 & 0 \end{array}\right] \qquad C_0 = [\,C \,|\, D\,] \tag{B-12}$$

The gain L_m^* on $\hat{u}_m$ may be determined from

$$L_m^* = \tau_N [(\gamma I - A_0 + b_0 \lambda)^{-1} b_0]' (C_0' Q_d + K_0 \bar{b}) / g \tag{B-13}$$

where

$\bar{b} = \text{col}\,[b, 0]$.

Two physically reasonable assumptions are

$$\gamma \approx \tau_N^{-1} \tag{B-14}$$

which means that the bandwidths of $u_c(t)$ and $u_m(t)$ are approximately equal, and

$$L_m^* u_m(t) << L^* x(t) \quad \text{or} \quad u_m(t) \simeq 0$$

With these assumptions, Equations (B-6) and (B-8) may be added to give

$$\tau_N \dot{u}(t) + u(t) = m(t) + v_m(t)$$

$$m(t) = -L^* \hat{x}(t) \tag{B-15}$$

The state estimate $\hat{x}(t)$ is generated from $y_p(\cdot)$ by the cascade combination of a Kalman filter and a least-mean-squared predictor, both of which are linear dynamic elements. The Kalman filter generates a least-mean-squared estimate $\hat{x}(t - \tau)$ of the delayed state $x(t - \tau)$ by

$$\dot{\hat{x}}(t - \tau) = A_1 \hat{x}(t - \tau) + \Sigma C_0' V_y^{-1} [y_p(t) - C_0 \hat{x}(t - \tau)]$$

$$+ b_0 \tau_N^{-1} m(t - \tau) \tag{B-16}$$

where $x(t) = \text{col}\,[x(t), u(t)]$. Σ is the error covariance matrix and is the unique positive definite solution of the variance equation

$$0 = A_1 \Sigma + \Sigma A_1' + W - \Sigma C_0' V_y^{-1} C_0 \Sigma \tag{B-17}$$

with

$$A_1 = \left[\begin{array}{c|c} A & b \\ \hline 0 & -\tau_N^{-1} \end{array}\right] \qquad W = \left[\begin{array}{c|c} EE' & 0 \\ \hline 0 & V_m \tau_N^{-2} \end{array}\right]$$

The predictor generates the best estimate $\hat{x}(t) = \text{col}\,[x(t), u(t)]$ from the Kalman filter output $p(t) = \hat{x}(t - \tau)$ according to

$$\hat{x}(t) = \bar{\xi}(t) + e^{A_1 \tau} [p(t) - \xi(t - \tau)]$$

$$\dot{\xi}(t) = A_1 \xi(t) + b_0 \tau_N^{-1} m(t) \tag{B-18}$$

Finally, using the techniques of Reference B-3, it is possible to obtain a closed-form expression for the covariance of $\hat{x}(t)$,

$$E\{\hat{x}(t)\hat{x}'(t)\} = e^{A_1\tau}\Sigma e^{A_1\tau} + \int_0^{\tau} e^{A_1\sigma} W e^{A_1'\sigma} d\sigma$$

$$+ \int_0^{\infty} e^{\bar{A}} e^{A_1} \Sigma C_0' V_v^{-1} C_0 \Sigma_e A_1'^{\tau} e^{\bar{A}'\sigma} d\sigma \qquad \text{(B-19)}$$

where $\bar{A} = A_0 - b_0\tau$. Thus,

$$E\{\hat{x}_i^2(t)\} = X_{ii}, \qquad i = 1, 2, \ldots, n$$

$$E\{y_i^2(t)\} = (C_0 X C_0')_{ii}, \qquad i = 1, 2, \ldots, r$$

$$E\{u^2(t)\} = X_{n+1,\, n+1} \qquad \text{(B-20)}$$

B.2 MULTI-AXIS TASKS

The description of the optimal control model of the pilot above is concerned with single-output (single system input) models appropriate to multi-group tracking tasks. The extension to more than one pilot output, i.e., *multi-access tracking tasks*, is a straightforward extension of the above results (Reference B-4). Specifically, the engine state Equation (B-1) is modified to reflect multiple inputs. The measurement Equation (B-2) is not modified. The cost function (Equation (B-7)) is augmented to include control rate ratings on each of the pilot outputs. The control vector minimizes the quadratic functions. This is analagous to Equation (B-8):

$$T_N \dot{\underline{u}} + \underline{u} = \underline{L}\,\hat{\underline{x}}(t) \qquad \text{(B-21)}$$

where T_N is a matrix of coefficients, u is a vector control variable, L is a matrix of feedback gains derived from the deterministic solution of the matrix Riccati equation (Reference B-4) and $\hat{x}$ is the output of the Kalman filter/predictor in the pilot model. When the statistics of the noise are stationary, and when the vehicle dynamics are stationary, Equation (B-21) reduces to the matrix of transfer functions.

$$\underline{u}(s) = [T_N s + 1]^{-1} L \hat{x}(s) \qquad \text{(B-22)}$$

B.3 ATTENTION ALLOCATION USING THE OPTIMAL CONTROL MODEL

The basic approach that we follow in applying the optimal control pilot model to predict attention allocation among a set of display indicators is to optimize a quadratic cost functional with respect to pilot attentional constraints. In order for the entire scheme to be computationally attractive, the following must be accomplished (Reference B-5):

- Relate attentional model parameters (f_i) to pilot model parameters.
- Obtain an expression for J^* = minimum J that shows explicitly how the f_i affect the various cost functional terms.
- Obtain an expression for the gradient terms $\frac{\partial J^*}{\partial f_i}$ that will be needed in subsequent optimization algorithms.
- Develop an algorithm to minimize J^* with respect to the f_i, subject to total workload constraints on f_i.

In this appendix the discussion is directed toward a pilot control task, although the concepts can be applied to a pilot monitoring situation as well.

In the optimal control model, a fractional allocation of attention f_i to the informational variable y_i modifies the "observation" noise $V_{y_i}(t)$ associated with that variable (Reference B-5). Thus, the noise covariance associated with y_i is

$$V_{y_i} = \frac{\rho_i^o}{f_i} \hat{\sigma}_i^2 \tag{B-23}$$

where

$$\hat{\sigma}_i = \sigma_i / N(\sigma_i) \tag{B-24}$$

σ_i = RMS value of y_i

$N(\sigma_i)$ = describing function gain of threshold

$$= \text{erfc}\left(\frac{a_i}{\sigma_i\sqrt{2}}\right) \tag{B-25}$$

The noise/signal ratio ρ_i^o is the "full attention" noise ratio, which typically is 0.01π or -20dB. Note that Equation (B-1) represents an implicit relationship for the actual noise variance V_{y_i} since $\hat{\sigma}_i^2$ is itself a function of V_y. For a given ρ_i^o/f_i, the requisite V_y is solved for via an iterative procedure. The quantity $\rho_i^o/f_i = \rho_i$ is called the modified noise/signal ratio.

The method that is used to determine how a pilot allocates attention among the various y_i is to minimize the optimal control cost with respect to f_i subject to constraints. This step will require an iterative process to arrive at the optimal f_i, where successive iterates f_i^n result in lower values for the cost functional. The cost functional that is used to determine the f_i is

$$J^* = \min_u J(u) \tag{B-26}$$

where J(u) is the basic cost functional in the optimal control pilot model.

In lieu of attempting to minimize the entire expression for J* numerically with respect to f_i, it is more efficient to isolate those terms in J* that are affected by f_i. Since changes in f_i are reflected as changes in observation noise V_y, we first obtain an expression for J* that shows the V_y dependence. In Reference B-5 it is shown that the

only term of interest is called the "scanning cost":

$$J_0 = \text{part of } J^* \text{ dependent on } V_y$$

$$= \text{tr}\{L_e \Sigma L_e'\} \tag{B-27}$$

where

$$L_e = \text{"Equivalent" gains}$$

$$= Q_r^{1/2} [T_N^{-1} L \vdots 0] e^{\tilde{A}\tau} \tag{B-28}$$

and Σ satisfies the variance equation

$$0 = \tilde{A}\Sigma + \Sigma\tilde{A}' + \tilde{W} - \tilde{\Sigma}\tilde{C}' V_y^{-1} \tilde{C}\Sigma \tag{B-29}$$

Minimizing J_0 (and hence J^*) with respect to f_i represents a difficult nonlinear optimization problem. The difficulty is two-fold. First, f_i affects V_y in an implicit manner, second V_y affects J_0 through the Riccati solution Σ. As it is unlikely that a closed-form solution for the optimum f_i can be found, the optimization process will be carried out numerically via some form of gradient algorithm.

In order that the numerical process be reasonably efficient, it is desired to obtain closed-form expressions for the gradients $\frac{\partial J_0}{\partial f_i}$ or $\frac{\partial J_0}{\partial V_{y_i}}$. Thus, the time-consuming process of numerically evaluating these derivatives can be avoided.

We wish to obtain the gradient vector

$$g_f = \frac{\partial J_0}{\partial f} = \Gamma' \frac{\partial J_0}{\partial V_y} \tag{B-30}$$

where $\frac{\partial J_0}{\partial V_y}$ is the gradient vector of J_0 with respect to V_{y_i}, $i = 1, 2, \ldots m$, and Γ is a "transformation" matrix where

$$(\Gamma)_{ij} = \frac{\partial V_{y_i}}{\partial f_j} \tag{B-31}$$

The gradient vector $\frac{\partial J_0}{\partial V_y}$ can be evaluated using a technique for derivatives of trace functionals (Reference B-5):

$$\frac{\partial J_0}{\partial V_y} = \text{diag}\,(G' M G) \tag{B-32}$$

where the term $G = \Sigma \tilde{C}' V_y^{-1}$ is the Kalman filter optimal gain matrix, and M is easily computed by solving the linear (Lyapunov) equation

$$\hat{A}'M + M\hat{A} + L_e' L_e = 0 \tag{B-33}$$

The elements of the matrix Γ must be computed. Since $V_{y_i} = \frac{\rho_i^o}{f_i} \hat{\sigma}_i^2$, we obtain

$$\Gamma_{ij} = \frac{\partial V_{yi}}{\partial f_j} = \frac{V_{yi}}{f_i} \left[\frac{\hat{\sigma}_i^2}{S_{f_i}} - \delta ij \right] = \frac{V_{y_i}}{f_i} S_{fj}^{V_{y_i}} \tag{B-34}$$

where S_y^x is a sensitivity coefficient, defined as

$$S_y^x = \frac{\partial x/x}{\partial y/y} \tag{B-35}$$

If the terms $S_{f_i}^{\hat{\sigma}_i^2}$ happen to be $\ll 1$, then Γ is approximately a diagonal matrix

$$\Gamma \cong \Gamma_{ii} = -\frac{V_{y_j}}{f_i} = -\frac{\rho_i \hat{\sigma}_i^2}{f_i} \tag{B-36}$$

More precise algorithms for determining the matrix Γ, including threshold effects and additive as well as multiplicative observation noise, are contained in Reference B-5.

The above algorithm is used to obtain $g_f = \frac{\partial J_0}{\partial f}$ which is the unconstrained gradient vector. However, the attentional allocations f_i are not free but are constrained by

$$\sum_{i=1}^{m} f_i = f^* = \text{total attention} \quad \text{and} \quad f_i \geq 0 \tag{B-37}$$

The constraint (Equation (B-37) describes a portion of a hyperplane,

$$< c, f > = f^* \tag{B-38}$$

with $c = \text{col}[1, 1, \ldots, 1]$. Thus, in order to determine the feasible direction for cost reduction, it is necessary to find the projection of g_f on the hyperplane (Equation (B-38)). This is given by

$$g_f^p = g_f - \frac{< g_f, c >}{< c, c >} c \tag{B-39}$$

or,

$$g_f^p = g_f - \left(\frac{1}{m} \sum_{i=1}^{m} g_{f_i} \right) c \tag{B-40}$$

In other words, g_f^p is obtained by subtracting the average of the g_{f_i} from each element of the vector. The angle between g_f and g_f^p is

$$\cos\theta = \frac{< g_f, g_f^p >}{\| g_f \| \cdot \| g_f^p \|} \tag{B-41}$$

In order to develop a projected gradient optimization scheme, assume we are at iteration n, with attention vector f^n. A small change Δf^n such that $f_i^n + \Delta f^n$ still satisfies the constraints (Equation (B-37)) will cause a corresponding small change in J_0^n. Thus, at iteration n,

$$J_0^{n+1} \cong J_0^n + \langle g_f^p , \Delta f^n \rangle \tag{B-42}$$

If Δf^n is selected as

$$\Delta f^n = - \varepsilon J_0^n g_f^p / \| g_f^p \|^2 \quad \varepsilon < 1 \tag{B-43}$$

then,

$$J_0^{n+1} \sim (1 - \varepsilon) J_0^n \tag{B-44}$$

Thus, each successive iteration will result in a lower cost (to first order terms only) of $100\varepsilon\%$.

Equation (B-44) serves as the basis for a gradient optimization scheme. We set

$$\varepsilon = \beta \cos \theta \tag{B-45}$$

and pick $\beta < 1/2$ and sufficiently small such that $f^{n+1} = f^n + \Delta f^n$ satisfies $f_i^{n+1} > 0$ and also $J_0^{n+1} < J_0^n$. Convergence occurs when J_0^{n+1} is arbitrarily close to J_0^n. If $J_0^{n+1} > J_0^n$, a smaller step is taken by reducing β. Note that since Δf^n is in the direction of g_f^p, the resulting f^{n+1} must necessarily continue to satisfy the constraints imposed on f^n.

REFERENCES

B-1. Levison, W. H.; Baron, S.; and Kleinman, D. K.: A Model for Human Controller Remnant. IEEE Trans. Man-Mach. Syst., 1969, MMS-10, pp. 101-108.

B-2. Baron, S.; et al.: Application of Optimal Control Theory to the Prediction of Human Performance in a Complex Task. AFFDL TR-69-81, March 1970.

B-3. Kleinman, D. L.: Optimal Control of Linear Systems with Time-Delay and Observation Noise. IEEE Trans. Auto. Control. Vol. AC-14, Oct. 1969, pp. 524-527.

B-4. Kleinman, D. L.; Baron, S.; and Levison, W. H.: An Optimal Control Model of Human Response, Part I: Theory and Validation. Automatica, 1970, Vol. 6, pp. 357-369.

B-5. Hoffman, W. C.; Curry, R. E.; Kleinman, D. L.; and Hollister, W. M.: Display/Control Requirements for VTOL Aircraft. ASI-TR-75-26, August 1975.

REFERENCES

1. McRuer, D.T.; and Krendel, E.S.: Mathematical Models of Human Pilot Behavior. AGARDOGRAPH Report, AGARD-AG-188, January 1974.

2. Kleinman, D.L.; Baron, S.; and Levison, W.H.: An Optimal Control Model of Human Response, Part I: Theory and Validation. Automatica, Vol. 6, pp. 357-369, 1970.

3. Young, L.R.: Vestibular System and Posture Control. Chapter 27 in Medical Physiology, V. Mountcastle, ed. Mosby, St. Louis, 1974.

4. Allen, R.W.; Clement, W.F.; and Jex, H.R.: Research on Display Scanning, Sampling, and Reconstruction Using Separate Main and Secondary Tracking Tasks. NASA CR-1569, July 1970.

5. Hoffman, W.C.; Curry, R.E.; Kleinman, D.L.; and Hollister, W.M.: Display/Control Requirements for VTOL Aircraft. Final Report, ASI-TR-75-26, Aerospace Systems, Inc., Burlington, Mass., August 1975.

6. Levison, W.H.: Elkind, J.I.; and Ward, J.L.; Studies of Multivariable Manual Control Systems: A Model for Task Interference. NASA CR-1746, May 1971.

7. Levison, W.H.; Baron, S.; and Kleinman, D.L.: A Model for Human Controller Remnant. IEE Trans. Man-Mach. Syst., MMS-10, pp. 101-108, 1969.

8. Levison, W.H.: The Effects of Display Gain and Signal Bandwidth on Human Controller Remnant. Report No. AMRL-TR-70-93, Aerospace Medical Research Laboratory, Wright-Patterson Air Force Base, Dayton, Ohio, March 1971.

9. Ashkenas, I.L.; McRuer, D.T.: A Theory of Handling Qualities Derived from Pilot-Vehicle System Considerations. Aerospace Eng., Vol. 21, No. 2, pp-60,61, 83-102, 1962.

10. McRuer, D.T.; and Jex, H.R.: A Review of Quasi-linear Pilot Models. IEEE Trans. Hum. Factors Electronics, HFE-8, pp. 231-249, 1967.

11. Weir, D.H.; and Johnson, W.A.: Pilot Dynamic Response to Sudden Flight Control System Failures and Implications for Design. NASA CR-1087, 1968.

12. Harper, R.P., Jr.: Flight Evaluations of Various Longitudinal Handling Qualities in a Variable-Stability Jet Fighter. WADC Tech. Rep. 55-299, 1955.

13. Young, L.R.: Some Effects of Motion Cues on Manual Tracking. J. Spacecraft and Rockets, pp. 1300-1303, October 1967.

14. Shirley, R.S.; and Young, L.R.: Motion Cues in Man-Vehicle Control: Effects of Roll-Motion on Human Operator's Behavior in Compensatory Systems with Disturbance Inputs. IEEE Trans. on Man-Machine Systems, Vol. MMS-9, No. 4, December 1968.

15. Stapleford, R.L.; Peters, R.A.; Alex, F.R.: Experiments and a Model for Pilot Dynamics with Visual and Motion Inputs. NASA CR-1325, May 1969.

16. Ormsby, C.C.: Model of Human Dynamic Orientation. Ph.D. Dissertation, MIT, January 1974.

17. Shirley, R.S.: Motion Cues in Man-Vehicle Control. Sc.D. Dissertation, MIT, Man-Vehicle Lab., Report MVT-68-1, January 1968.

18. Young, L.R.; and Meiry, J.L.: Manual Control of an Unstable System with Visual and Motion Cues. IEEE International Convention Record, Vol. 13, Part 6, pp. 123-127, 1965.

19. Meiry, J.L.: The Vestibular System and Human Dynamic Space Orientation. MIT Man-Vehicle Control Lab. Report T-65-1, June 1965 (Sc.D. Thesis, MIT).

20. Vuorikari, V.O.: Human Role in the Control Loop of the Automatic Landing Aircraft (S.M. Thesis, MIT, 1965).

21. Benjamin, P.: Visual and Motion Cues in Helicopter Flight. MIT Man-Vehicle Control Lab. Report T-66-1, January 1966.

22. Dinsdale, P.B.: Relative Effects of Roll and Yaw Motion Cues in Manual Control. MIT Manned Vehicle Laboratory Report MVT-68-4, September 1968.

23. Ringland, R.F.; Stapleford, R.L.; and Magdaleno, R.E.: Motion Effects on IFR Hovering Task — Analytical Predictions and Experimental Results. NASA CR-1933, 1971.

24. Newell, F.D.: Human Transfer Characteristics in Flight and Ground Simulation for the Roll Tracking Task. Technical Report AFFDL-TR-67-30, April 1968.

25. Newell, F.D.; and Smith, H. J.: Human Transfer Characersitics in Flight and Ground Simulation for a Roll Tracking Task. NASA TN D-5007, 1969.

26. Smith, H.J.: Human Describing Functions Measured in Flight and on Simulators. NASA SP-128, Second Annual NASA-University Conference on Manual Control, MIT, February 28-March 2, 1966.

27. Newell, F.D.; and Pietrzak, P.E.: In-Flight Measurement of Human Response Characteristics. AIAA Journal of Aircraft, Vol. 5, No. 3, May-June 1968.

28. Sinacori, J.B.: A Study of VSTOL Ground Based Simulation Techniques. USAAVLABS TR-70-16. See also USAAVLABS TR-67-55.

29. Rolfe, J.M.; Hammerton-Frazier, A.M.; Poulter, R.F; and Smith, E.M.B: Pilot Response in Flight and Simulated Flight. Ergonomics, Vol. 13, pp. 761-786, 1970.

30. Rangland, S.; Chambers, R.M.; Crosbie, R.J.; and Hiscock, L.: Simulation and Effects of Severe Turbulence on Jet Airline Pilots. NADC ML-6411, 1964.

31. Douvillier, J.G.; Turner, H.L.; McClain, J.D.; Heinle, D.R.: Effects of Flight Simulator Motion on Pilots Performance Over Tracking Tests. NASA TN-D 143, 1960.

32. Flaxman, R.: Man In Motion — The Connecting Link. GPI, Binghamton, 1966.

33 Huddleston, H.F.: Cockpit Motion Requirements for Flight Simulation. RAF Institute of Aviation Report, IAM 363, 1966.

34. Bergeron, H.P.: The Effects of Motion Cues on Compensatory Tracking Tasks. AIAA Visual and Motional Simulation Technology Conference, Cocoa Beach, Florida, March 1970. Fifth Annual NASA-University Conference on Manual Control, 1969.

35. Bergeron, H.P.; and Adams, J.J.: Measured Transfer Functions of Pilots During Two Axis Tasks with Motion. NASA TN-D-2177, 1964.

36. Dillow, J.D.; Picha, D.C.; and Anderson, R.O.: Slushy Weightings for the Optimal Pilot Model. NASA TMX 62464, May 1975.

37. Junker, A.M.; Repperger, D.W.; and Neff, J.A.: A Multiloop Approach to Modeling Motion Sensor Response. NASA TMX 62464, May 1975.

38. Repperger, D.W.; and Junker, A.M.: Performance Evaluation of Tracking Based on a Low Pass Filter Model, NASA TMX 62464, May 1975.

39. Junker, A.M.; and Replogle, C.R.: Motion Effects on the Human Operator in a Roll Axis Tracking Task. Aviation, Space and Environmental Medicine, 1976.

40. Matheny, W.G.; Lowes, A.L.; Baker, G.; and Bynum, J.A.: An Investigation of Visual, Aural, Motion, and Control Movement Cues. Naval Training Devices Center, Technical Report 69-C-03040-1, 1971.

41. Klier, S.; and Gage, H.: Motion Factors in Flight Simulation. Naval Training Devices Center, Technical Report 68-C-0007-1, 1970.

42. Jacobs, R.S.; Williges, R.C.; and Roscoe, S.N.: Simulator Motion as a Factor in Flight Director Display Evaluation. Human Factors, Vol. 15, pp. 569-582, 1973.

43. Staples, K.J.: Motion, Visual, and Aural Cues in Piloted Flight Simulation. AGARD Conference Proceedings, CP-79, pp. 4.19-4.21, 1970.

44. Bray, R.S.: Discussion of Paper by Staples. AGARD Conference Proceedings, CP-70-9, pp. 4.19-4.21, 1970.

45. Lew, D.M.; and Dyda, K.J.: Ground Based Simulation Techniques. AV Labs, TR-67-56, 1967.

46. Sinacori, J.: Validation of Ground-Based Simulation. Journal of the American Helicopter Society, Vol. 15, pp. 10-21, 1970.

47. Sadoff, M.; and Dolkas, C.B.: Acceleration Stress Effects on Pilot Performance and Dynamic Response. Second Annual NASA-University Conference on Manual Control, NASA-SP-128, pp. 241-258, 1966.

48. Allen, R.W.; Jex, H.R.: Vertical Vibration Interference on a Pitch Attitude Control Task. Proc. of the Tenth Annual Conference on Manual Control, 1974.

49. Levison, W.H.: Analysis of Vibration Induced Pilot Remnants, Proc. of the Tenth Annual Conference on Manual Control, 1974.

50. Benson, A.J.; Guedry, F.E., Jr.: Comparison of Tracking Task Performance and Nystagmus During Sinusoidal Oscillation in Yaw and Pitch. Naval Aero. Med. Lab. NAMRL-1123, 1970.

51. Gilson, R.D.; Benson, A.J.; and Guedry, F.E., Jr.: Influence Vestibular Stimulation and Display Luminants on the Performance of a Compensatory Tracking Task. Naval Aero. Med. Inst. 1097, 1970.

52. Clement, W.F.; and Hofman, L.G.: A System Analysis of Manual Control Techniques and Display Arrangements for Instrument Landing Approaches in Helicopters. Vol. I: Speed and Height Regulation. JANAIR Report 690718, Systems Technology, Inc., Tech. Report 183-1, July 1969.

53. Hofman, L.G.; Clement, W.F.; and Blodgett, R.E.: Further Examination of Pilot Instrument Scanning Data and Development of a New Link Value Estimator. Proceedings of 9th Annual Conference on Manual Control, pp. 379-388, May 1963.

54. Clement, W.F.; Hofman, L.G.; and Graham, D.: A Direct Procedure for Partioning Scanning Workload in Control Display System Design. Proceedings of 9th Annual Conference on Manual Control, pp. 389-400, May 1973.

55. Kleinman, D.L.: Optimal Control of Linear Systems with Time-Delay and Observation Noise. IEEE Trans. Auto. Control. Vol. AC-14, pp. 524-527, October 1969.

56. Baron, S.; and Levison, W. H.: A Display Evaluation Methodology Applied to Vertical Situation Displays. Proceedings of 9th Annual Conference on Manual Control, pp. 121-132, May 1973.

57. Baron, S.: Analysis of Response to Wind-Shears Using the Optimal Control Model of the Human Operator. Proceedings of the 9th Annual Conference on Manual Control, pp. 419-428, May 1973.

58. Gressang, R.V.; et al: Low Visibility Landing Pilot Modeling Experiment and Data. AFFDL TR-75-41, November 1974.

59. Gressang, R.V.: Low Visibility Landing Pilot Modeling Experiment and Data, Phase II. AFFDL-TR-75-57, August 1975.

60. Brunnell, J.W.; and Eicher, J.A.: A Low Visibility Landing Simulation of the Boeing 707/C-135B. AFFDL TM 75-60-FGD, June 1975

61. Pollard, J.J.: All-Digital Simulation for Manned Flight in Turbulence. AFFDL-TR-75-82, March 1975.

☆ U. S. GOVERNMENT PRINTING OFFICE: 1977 — 757-001/240